

People's Democratic Republic of Algeria
وزارة التعليم العالي والبحث العلمي
Ministry of Higher Education and Scientific Research

Mohamed Khider University - Biskra
Faculty of Science and Technology
Department: Civil and Hydraulic Engineering



جامعة محمد خيضر بسكرة
كلية العلوم والتكنولوجيا
قسم: الهندسة المدنية والري
المرجع:

Ref:

Thesis presented with a view to obtaining
LMD Doctorate in Civil Engineering

Option: Numerical modeling in civil engineering

**3D numerical modeling of the behavior of piled raft
foundations in the case of clay soils**

**Modélisation numérique 3D du comportement des
fondations composites radier-pieux dans le cas des sols
argileux**

Presented by:

FERCHAT Abdelkrim

Publicly supported on: 23/09/2021

before the jury composed of:

Dr. Naima BENMEBAREK	Professor	Chair	University of Biskra
Dr. Sadok BENMEBAREK	Professor	Supervisor	University of Biskra
Dr. Mohamed KHEMISSA	Professor	Examiner	University of M'Sila
Dr. Mohamed saddek Remadna	Professor	Examiner	University of Biskra

ACKNOWLEDGMENTS

First of all, all praise is due to “Allah” almighty.

I would like to sincerely thank Pr. Sadok BENMEBAREK from the University of Biskra, my supervisor and thesis director for providing the scientific supervision of this thesis. I must admit that he knew well, first during the work of my master's thesis, and then during this thesis, to point me in the right way in times of confusion. His availability, his experience, and his thoroughness allowed this thesis to succeed. It was also a great pleasure for me to work under his direction.

I would also like to thank Pr. Naima BENMEBAREK from the University of Biskra for having done me a great honor by accepting to chair the jury for this thesis. I also thank Pr. Mohamed KHEMISSA (University of M'SILA) and Dr. Mohamed Saddek REMADNA (University of Biskra), for the time and their interest in this research by agreeing to review this work.

I would also like to sincerely thank Dr. Mohamed Nabil HOUHOU from the University of Biskra, his availability, experience, and thoroughness allowed this thesis to succeed. It was also a great pleasure for me to work with him.

I would like to express my special gratefulness to Dr. Ahmed ALOUI from the University of Biskra for their support and information during the progress of this research.

Finally, I would like to thank all my family for supporting me during all these years of preparing this thesis, my father, my mother, my wife, my son Farouk, and my daughters Alae and Illef. Special thanks are reserved for those who encouraged me to complete this thesis.

To the memory of my dear friend
ABDELMADJID AROUADOU

ABSTRACT

Piled raft foundations are increasingly recommended as an economical and efficient foundation system for high-rise buildings. However, there is a reluctance to use them in the case of soft clays due to concerns about excessive settlement and insufficient bearing capacity. Despite these reasons, the use of piled raft foundations in the case of soft clays is increasing swiftly. The behavior of the piled raft foundations is affected by various parameters such as the raft thickness, number, length, and spacing of the piles. Therefore, economical and efficient design requires integrating all these parameters into the design approach. However, the current analysis methods for piled raft foundation on soft clay are not sufficient, especially for the prediction of the overall bearing capacity. In this context, this research work is interested, on the one hand, in a literature review on the results of field auscultation and model tests, and on the other hand, in the numerical modeling of the behavior of piled raft foundations with a thorough parametric study of the various influencing factors.

The finite-difference code FLAC^{3D} was used in this thesis to investigate the behavior of piled raft foundation in soft clay conditions. The overall objective of the present study focuses on the load response and the effects of multiple interactions of the piled raft foundation subjected to vertical loading. For this purpose, several types of foundations were considered, including piled raft, pile group, unpiled raft, and single pile. For optimization purposes, the interaction behavior of the piled raft foundation was also investigated by varying some parameters as piles number and pile spacing. The obtained numerical results are validated by comparing them to those of similar subgrade structures and in the comparable geological conditions provided within the literature. The results prove that even for soft clays, the piled raft components interact with each other producing a fully different behavior from that of the unpiled raft and pile group. Therefore, neglecting these interaction effects could lead to an overestimation of the ultimate bearing capacity of piled raft foundations, essentially for cases of large piles number. The concluded observations from the parametric study provide further insight into the mechanical response of piled raft and aim at helping the engineers in taking a logical path in an iterative design process for a piled raft foundation. A predicted model for the efficiency factor of the pile group is also proposed which is validated with the obtained numerical results to better goodness of fit.

Keywords Numerical modeling; Piled raft foundation; Settlement; Interaction factors; Clay; Pile group; bearing capacity

ملخص

يوصى بشكل متزايد بالأساسات المركبة (أساس مساحي "طوف"-خوازيق "ركائز") كنظام أساس اقتصادي وفعال للمباني الشاهقة. ومع ذلك، هناك إجماع حول استخدامها في حالة الطين اللين بسبب مخاوف بشأن الهبوط المفرط والقدرة غير الكافية على التحمل. رغم هذه الأسباب، فإن استخدام الأساسات المركبة في حالة الطين اللين في توسع مستمر. يتأثر سلوك الأساسات المركبة بمعلمات مختلفة مثل سمك الطوف وعدد وطول وتباعد الركائز. لذلك، يتطلب التصميم الاقتصادي والفعال دمج كل هذه المعلمات في نهج التصميم. ومع ذلك، فإن طرق التحليل الحالية لأساس المركب في الاتربة الطينية اللينة ليست كافية، لا سيما لحساب قدرة التحمل الإجمالية. في هذا السياق، فإن هذا العمل البحثي يهتم من ناحية استعراض للنتائج الميدانية بالحجم الحقيقي والنماذج الفيزيائية المصغرة ومن ناحية أخرى بالمحاكاة العددية لسلوك أساسات المركبة مع دراسة حدودية لتأثير المعلمات الرئيسية المختلفة.

تم استخدام كود الفروق المتناهية $FLAC^{3D}$ في هذه الرسالة لأجل دراسة سلوك الأساسات المركبة في ظل ظروف الطين اللين. يركز الهدف العام لهذه الدراسة على استجابة الحمل وتأثيرات التفاعلات المتعددة للأساس المركب المعرض للتحميل العمودي. لهذا الغرض، تم النظر في عدة أنواع من الأساسات، بما في ذلك الأساس المركب، مجموعة الركائز، الطوف، والركيزة المنفردة. لغرض التحسين، تمت أيضاً دراسة السلوك التفاعل للأساس المركب من خلال تغيير بعض المعلمات مثل عدد الركائز وتباعدها. تم التحقق من صحة النتائج العددية التي تم الحصول عليها من خلال مقارنتها مع تلك الهياكل الأساسية المماثلة وتحت ظروف جيولوجية مماثلة. تثبت النتائج المتحصل عليها أنه حتى بالنسبة للطين اللين، تتفاعل مركبات الأساس المركب مع بعضها البعض، مما ينتج عنه سلوكاً مختلفاً تماماً عن سلوك الطوف ومجموعة الركائز. لذلك، فإن إهمال هذه التأثيرات التفاعلية يمكن أن يبالغ بشكل كبير في تقدير قدرة التحمل النهائية للأساسات المركبة، بشكل أساسي لحالات العدد الكبير من الركائز. ومع ذلك، فإن الملاحظات النهائية للدراسة الحدودية توفر نظرة ثاقبة إضافية للاستجابة الميكانيكية للأساس المركب وتهدف إلى مساعدة المهندسين على اتباع مسار منطقي في عملية تصميم تكرارية لأساس مركب. تم أيضاً اقتراح نموذج تنبؤ لعامل الكفاءة لمجموعة الركائز والتحقق من صحته من خلال النتائج العددية التي تم الحصول عليها للحصول على جودة أفضل للملاءمة.

كلمات مفتاحية: محاكاة عددية، أساس مركب، هبوط، معامل التفاعل، طين، مجموعة ركائز

TABLE OF CONTENTS

LIST OF SYMBOLS	i
LIST OF FIGURES	iv
LIST OF TABLES.....	ix
INTRODUCTION.....	1
CHAPTER 1	
LITERATURE REVIEW ON ANALYSIS METHODS OF PILED RAFTS	
1.1 Introduction	5
1.2 Design concepts.....	6
1.2.1 Design philosophy	6
1.2.2 Design considerations	7
1.2.3 Favorable and unfavorable condition	9
1.3 Classification of analysis methods	9
1.3.1 Simplified calculation methods	10
1.3.1.1 Load-settlement behavior	11
1.3.1.2 Vertical load capacity	14
1.3.1.3 Load Transfer Mechanism	18
1.3.2 Approximate numerical analysis method	25
1.3.3 More rigorous numerical analysis method	27
1.4 A brief review of studies on piled raft foundations.....	29
1.4.1 Experimental studies	29

Table of contents

1.4.2 Analytical and numerical studies	35
1.5 Summary.....	43

CHAPTER 2

OVERVIEW OF THE NUMERICAL TOOL USED AND THE CONSTITUTIVE MODELS

2.1 Introduction.....	44
2.2 Constitutive models.....	44
2.2.1 Elastic model group	44
2.2.2 Elastoplastic constitutive law	47
2.2.3 Mohr-Coulomb Model (linear elastic perfectly plastic model)	52
2.3 Description of the FLAC code.....	56
2.3.1 Overview	56
2.3.2 Finite difference method	56
2.3.3 3D discretization	57
2.3.4 Explicit solving scheme	62
2.3.5 Modeling methodology	63
2.3.6 Interfaces	64
2.1 Summary.....	66

CHAPTER 3

NUMERICAL INVESTIGATION ON PILE GROUP EFFICIENCY EMBEDDED IN SOFT CLAY

3.1 Introduction.....	67
-----------------------	----

Table of contents

3.2	Numerical analysis.....	68
3.2.1	Mesh and constitutive modeling	68
3.2.2	Validation	70
3.2.3	Parametric study	72
3.3	Results and discussion.....	73
3.1	Summary.....	82

CHAPTER 4

3D NUMERICAL STUDY OF THE BEHAVIOR OF PILED RAFT FOUNDATIONS IN THE SOFT CLAY

4.1	Introduction	84
4.2	3D numerical modeling.....	85
4.2.1	Modeling procedure and post analysis	85
4.2.2	Validation of numerical model	89
4.3	3D numerical analysis of piled raft interaction in drained soft clay conditions....	91
4.3.1	Parametric study	92
4.3.2	Computed results	94
4.4	3D numerical investigation of piled raft interaction factors in soft clay conditions.....	104
4.4.1	Parametric Study	104
4.4.2	Assessment of piled raft interaction effects from the computed results	107
4.5	Summary.....	116
	CONCLUSIONS AND RECOMMENDATIONS.....	118

Table of contents

REFERENCES..... 122

ANNEX..... 133

PRACTICAL ENGINEERING EXAMPLES (CASE STUDIES)..... 133

LIST OF SYMBOLS

PR	Piled raft
UR	Unpiled raft
GP	Group of piles
SP	Single piled or individual pile
Ppr	Piles of piled raft foundation
Rpr	Raft of piled raft foundation
W_r	raft settlement
W_e	Elastic compression of the piles above the equivalent raft level, which are treated as free-standing columns.
q_t	Average pressure applied to the raft, (Poulos, 1993)
I_ϵ	Influence factor from which the vertical strain may be calculated, (Poulos, 1993)
H_i	Thickness of the i^{th} layer, (Poulos, 1993)
E_s	Young's modulus of the i^{th} layer, (Poulos, 1993)
F_D	Correction factor, (Poulos, 1993)
n_s	Number of soil layers
S_p	Pile spacing
n	Number of piles
α_p	Load sharing ratio
L	Length of pile
d	Diameter of pile
B_r	Width of the raft
t	Thickness of the raft
C_g	Efficiency factor of a pile group

List of Symbols

n_r	Pile-Raft interaction factor
n_p	Raft-Pile interaction factor
E_r	Young's modulus of the raft
E_s	Young's modulus of the soil
ν_r	Poisson's ratio of the raft
ν_s	Poisson's ratio of the soil
E_p	Young's modulus of the pile
ν_p	Poisson's ratio of the pile
B_r	Width of the raft
L_r	Length of the raft
t_r	Thickness of the raft
σ_i	Vertical stress along the pile head at cylindrical solid element i
S_i	Segment cross section area of element i
P_p	Axial pile load
E	Young's modulus
ν	Poisson's ratio
γ	Density
C_u	Undrained shear strength
c	Cohesion
φ	Friction angle
ψ	Dilation angle
s	Settlement
σ_n	Normal stress
τ	Shear stress
ε^e	Elastic strains
ε^p	Plastic strains

List of Symbols

Q_{pr}	Bearing capacity of the piled raft foundation
Q_{gp}	Bearing capacity of the pile group
Q_{ur}	Bearing capacity of the unpiled raft
Q_r	Load carried by the raft
Q_p	Load carried by the piles
Q_t	Total applied load
A_g	Diameter of the equivalent pier
E_{eq}	Young's modulus of the equivalent pier
A_{pg}	Total cross-sectional area of the piles in the group
A	Cross-sectional area of the raft
R	overall aspect ratio, Randolph (1994)
K_r and K_p	Raft and pile group stiffness, respectively.
Q_l	Load capacity of the piled raft foundation
Q_{st}	Load capacity of the raft
Q_{pl}	Load capacity of the single pile
F_{pl}	Shaft capacity of the single pile
μ	Reduction factor
S_p and S_s	Cross-sectional area of the pile and raft, respectively,
k_p and k_s	Bearing factors
P_{le}^*	Equivalent net limit pressure
τ_z	Unit shaft friction of layer
z	Thickness of the layer z

LIST OF FIGURES

CHAPTER 1

Figure 1.1 Schematic design of (a) Shallow foundation, (b) Piled raft foundation, and (c) Deep foundation (Borel 2001).....	6
Figure 1.2 Interactions of piled raft foundations adopted from Katzenbach and Choudhury (2013).....	9
Figure 1.3 Adopted depth of the equivalent raft. (A) Piles work mainly by friction, (b) combination of friction and end bearing piles (c) end bearing piles.....	11
Figure 1.4 Schematic view of the equivalent pier method, adopted from Sönmez, (2013).....	12
Figure 1.5 Equivalent pier design (Poulos and Davis, 1980).....	13
Figure 1.6 Burland’s simplified design concept, adapted from Poulos (2001).....	15
Figure 1.7 Simplified representation of a pile-raft unit, adopted from Poulos (2001).....	16
Figure 1.8 Simplified load-settlement curve for preliminary analysis, adopted from Poulos (2001).....	17
Figure 1.9 Fundamental Piled raft interactions.....	20
Figure 1.10 Schematic description of piled strip problem via GASP approach (Poulos, 1991).....	27
Figure 1.11 Simulation approaches of piled raft foundation, (a) plane deformations (b) axisymmetric, and (c) three-dimensional, adopted from Nguyen (2008).....	29
Figure 1.12 Failure zone of the piled raft foundation (a) equivalent pile failure (b) individual pile failure. (Kishida and Meyerhof, 1965).....	29
Figure 1.13 General section of centrifuge package (Horikoshi and Randolph,1996)....	31
Figure 1.14 Diagram of the test setup (Lee et Chung, 2005).....	32
Figure 1.15 schematic view of the centrifuge test and model foundations adopted by Park and Lee (2014).....	33

List of figures

Figure 1.16 Schematic view of pile-pile, raft-pile, and pile-raft interactions for piled raft foundation (Park and Lee, 2014).....	34
Figure 1.17 Piled raft configurations considered in these experimental tests (Patil et al., 2015) (unity: mm).....	35
Figure 1.18 Comparison of different load-settlement analysis methods (Poulos 2001).	36
Figure 1.19 3D Parametric study (a) piled raft configurations (b) finite element mesh around the pile (de Sanctis and Mandolini, 2006).....	37
Figure 1.20 Typical mesh and boundary condition (Lee et al., 2010).....	38
Figure 1.21 Pile configurations foundation types are considered in the numerical analysis carried out by Park et al. (2016).....	40

CHAPTER 2

Figure 2.1 Load surface concept.....	48
Figure 2.2 Uniaxial compression (or tensile) test of a material.....	49
Figure 2.3 Description of isotropic hardening in projection: (a) in the deviatoric plane; (b) in the plane $\sigma_{axial} - \varepsilon_{axial}$ in simple traction-compression.....	50
Figure 2.4 Description of kinematic hardening in projection: (a) in the deviatoric plane; (b) in the plane $\sigma_{axial} - \varepsilon_{axial}$ in simple traction-compression.....	51
Figure 2.5 Representation of the Mohr-Coulomb criterion in the Mohr plane.....	53
Figure 2.6 Mohr-Coulomb and Tresca yield surfaces in principal stresses space, (Itasca 2013).....	54
Figure 2.7 Modeling of dilation ψ from the triaxial test (Vermeer and de Borst, 1984)...	55
Figure 2.8 Deformation mode for which mixed discretization should be most efficient, (Itasca, 2013)	60
Figure 2.9 An 8-node zone with 2 overlays of 5 tetrahedral in each overlay, (Itasca, 2013).....	61
Figure 2.10 FLAC calculation sequence, (Itasca, 2013).....	62
Figure 2.11 Components of the bonded interface constitutive model, (Itasca, 2013).....	64

List of figures

Figure 2.12 Zone dimension used in stiffness calculation, (Itasca, 2013)..... 65

CHAPTER 3

Figure 3.1 Grid used in FLAC^{3D} simulations..... 69

Figure 3.2 Comparison between results of present study and those of the centrifuge test conducted by Horikoshi et al (2003)..... 72

Figure 3.3 Load-settlement curves of piles group for different n and S_p 75

Figure 3.4 Maximum shear strain development for group of 16 piles with different pile spacing..... 76

Figure 3.5 Soil displacement for groups of 16 and 9 piles with different pile spacing..... 77

Figure 3.6 Comparison of C_g values calculated from the present study and different formulas available in the literature for different n and S_p 79

Figure 3.7 Plastic zone for group of 16 piles with different pile spacing..... 80

Figure 3.8 Comparison of C_g values calculated from: the proposed formula, the obtained results of FLAC^{3D}, and the popular formulas available in the literature..... 82

CHAPTER 4

Figure 4.1 Detail of FLAC^{3D} grid used in numerical analyses..... 86

Figure 4.2 FLAC^{3D} meshes used for several foundation types considered in numerical analyses..... 89

Figure 4.3 Comparison between results of present study and previous numerical works of load-settlements behavior of piled raft..... 90

Figure 4.4 Pile configurations considered for parametric analysis..... 93

Figure 4.5 Load-normalized settlement curves of PR, UR and GP for $n = 16$ and $S_p = 4d$ 95

Figure 4.6 Load-normalized settlement curves of PR, Ppr and Rpr for $n = 16$ and $S_p = 4d$ 95

Figure 4.7 Load-normalized settlement curves for $n = 9$ and $S_p = 4d$, PR, UR and GP... 96

Figure 4.8 Load-normalized settlement curves for $n = 9$ and $S_p = 4d$, PR, Ppr and Rpr... 97

List of figures

Figure 4.9 Evolution of load capacities of PR and the sum of UR and GP in the case of 16 piles with $S_p = 3d$ and $6d$	98
Figure 4.10 Load-normalized settlement curves of UR and PR for different values of n and S_p	99
Figure 4.11 Load-normalized settlement curves of PR for different values of S_p for given values of n	100
Figure 4.12 Evolution of the load sharing ratio according to the settlement level for different values of pile spacing and piles number.....	101
Figure 4.13 Load distributions between piles of PR for different values of pile spacing S_p and settlement level s in the case of 16 piles.....	103
Figure 4.14 Load distributions between piles of PR for different values of pile spacing S_p and settlement level s in the case of 9 piles.....	103
Figure 4.15 Various types of foundations used for 3D numerical parametric study.....	105
Figure 4.16 Various configurations of piled raft considered for parametric analysis.....	106
Figure 4.17 Load-normalized settlement curves of GP for different n and S_p and using n times SP load responses.....	108
Figure 4.18 Distribution of maximum shear strain for GP with 16 piles and different pile spacing.....	109
Figure 4.19 Load-normalized settlement curves of GP and Ppr, for the case of $n = 25$ piles, (a) $S_p = 3d$ and (b) $S_p = 4d$	111
Figure 4.20 Load-normalized settlement curves of GP and Ppr, for the case of $n = 16$ piles with different S_p	112
Figure 4.21 Load-normalized settlement curves of UR and Rpr, for different n and S_p ...	115

ANNEX

Figure A.1 La Azteca building, Mexico (Poulos, 2016).....	133
Figure A.2 Details La Azteca foundation (Zeevaert, 1957).....	134
Figure A.3 Burj Khalifa building (Poulos, 2016).....	135

List of figures

Figure A.4 Contours of the maximum axial load obtained from the numerical analysis (Poulos, 2016).....	136
Figure A.5 Incheon tower, South Korea.....	137
Figure A.6 Plan view of piles arrangement (Poulos et al., 2011).....	137
Figure A.7 Architectural rendering of the Jeddah tower, Saudi Arabia (Poulos, 2016)..	138
Figure A.8 Plan view of pile configuration (Poulos, 2016).....	139
Figure A.9 Messeturm tower of Frankfurt city, Germany (Katzenbach and Leppla, 2015).....	140
Figure A.10 Pile arrangement (Katzenbach et Leppla, 2015).....	140
Figure A.11 3D architectural rendering of Mirax Plaza in Kyiv, Ukraine.....	141
Figure A.12 Project cross-section (Katzenbach et al., 2013).....	142
Figure A.13 Hyde Park Barracks building, London.....	143
Figure A.14 Hyde Park Barracks Foundation Details (Hooper, 1973).....	143
Figure A.15 Soil profile, foundation plan and elevation of nineteen story residential tower (Yamashita et al., 2011).....	144
Figure A.16 Schematic view of the building with the soil profile (Yamashita et al., 2011).....	145
Figure A.17 Pile arrangement (Yamashita et al., 2011).....	146
Figure A.18 Schematic view of the hospital construction with soil profile (Yamashita et al., 2011)	147
Figure A.19 Pile arrangement (Yamashita et al., 2011).....	148
Figure A.20 Detail view of the building (a) Schematic view with soil profile (b) Pile arrangement (Yamashita et al., 2011).....	149

LIST OF TABLES

CHAPTER 1

Table 1.1 Conceptions of interaction factors of piled raft system by several researchers..	24
--	----

CHAPTER 2

Table 2.1 Summary of primitive mesh shapes, (Itasca, 2013).....	57
---	----

CHAPTER 3

Table 3.1 Comparison of results	71
Table 3.2 Input parameters of soil and interface properties (Alnuiam et al., 2013).....	71
Table 3.3 Material parameters used in the analyses (Nguyen, 2008).....	73

CHAPTER 4

Table 4.1 Material parameters used in the analyses (Sinha and Hanna 2016).....	90
Table 4.2 Material properties, adopted from Horikoshi and Randolph (1996).....	91
Table 4.3 Comparison of the results.....	91
Table 4.4 Material parameters used in the parametric study.....	94
Table 4.5 Material parameters used in the analyses, adopted from Jeong et al. (2004)....	106
Table 4.6 Values of χ_g for different n and S_p	110
Table 4.7 η_r and η_p values at ultimate state.....	114

INTRODUCTION

The establishment of structures resting on the foundations in soft clays implies a good adaptation of the reconnaissance techniques of the soils in place, a study of the mechanical behavior of these soils, as well as adapted foundation solutions. Besides, high-rise buildings and the offshore oil industry also face similar difficulties because of the extreme applied load and the inappropriate soil conditions. The foundations in these soils eventually pose the problem of their insufficient bearing capacity, their significant settlement (total and differential settlement), and negative friction along with the pile's shaft. This, therefore, leads to choosing foundations adapted to these types of structures, such as piled raft foundations.

The raft foundation is regarded as an alternative design approach when appropriate load-bearing soil layers do not exist. In inappropriate soil conditions, installing a limited number of piles to the raft not only helps to avoid the excessive settlement of the foundation but also enhances the bearing capacity of the foundation and also may improve the required thickness of the raft (Poulos 2001; Ghalesari and Choobbasti 2018). This combination of the shallow and deep foundation has become an alternative foundation mode which is known as a piled raft foundation. This system of the foundation has proved to be an economical and effective foundation type compared to conventional foundations (Poulos 2001).

The piled raft system was developed to use the load-carrying capacities of both raft and piles as an optimized foundation type and design concept (Randolph, 1994). In the design of piled rafts, the piles are used up to a load level that can be of the same order of magnitude as the bearing capacity of a comparable single pile or even greater (Reul and Randolph, 2003). The overall load response of piled raft is related to a complex soil-structure interaction scheme, including the pile-soil, pile-pile, raft-soil, and pile-raft interactions (Katzenbach et al., 2000; de Sanctis and Russo, 2008; Katzenbach and Choudhury, 2013; Park and Lee, 2015). Therefore, evaluation of the bearing capacity for the piled raft is rather complicated and requires the consideration of various design parameters, such as dimensions of each foundation component, pile number, pile spacing, and soil conditions. According to Eurocode

7, this system of the foundation is classified in the category of complex geotechnical constructions (Geotechnical Category 3).

Both the bearing capacity and the settlements of piled raft have been commonly estimated based on empirical formulas and analytical relationships inspired by simplified theories (Poulos and Davis, 1980; Clancy and Randolph, 1993; Randolph, 1994; Burland, 1995; van Impe and Clerq 1995; Poulos, 1994; Viggiani, 1998). In the light of the intrinsic complexity of the raft-soil-pile interaction, the traditional design methods for piled raft foundations are in many cases inaccurate and unlikely to result in optimum design. To design such subgrade-structure, it is essential to identify the different mechanisms of piles interaction via the connections to the raft but especially through the soil.

The behavior of piled raft foundations continues to be the subject of many important studies/researches, using various experimental, analytical, and numerical methods (Horikoshi and Randolph, 1996; Poulos, 2000; Katzenbach et al., 2000; Conte et al., 2003; de Sanctis and Mandolini, 2006; Lee et al., 2010; Park and Lee, 2014-2015; Lee et al., 2014; Alshenawy et al., 2016; Sinha and Hanna, 2016; Kumar and Choudhury, 2018; Deb and Pal, 2019). Some of these studies have considered the interaction effects of piled raft systems and modified the design approaches (e.g. de Sanctis and Mandolini, 2006; lee et al., 2015; Kumar and Choudhury, 2018; or Deb and Pal, 2019). However, the evaluation of interaction factors for piled raft foundations is very complex and there is no simplified methodology to predict the interaction effects. Moreover, the interaction behavior and the load sharing mechanism are not sufficiently identified so, the design of bearing capacity of the piled raft foundation depends on the interaction factors is not yet developed.

To consider more complex cases compared to field and model tests, numerical methods have been widely developed in the last three decades. Although the two-dimensional equivalents (axisymmetric equivalent model, equivalent two-dimensional model, plane strain local model) are still frequently used because they lead to smaller numerical models in terms of number of nodes and elements, they involve many conservative assumptions and have serious limitations. However, resorting to 3D finite difference or finite element analyses seem to be the most reliable option, since complex geometries and multiple interactions can be explicitly considered.

In this context, this research is interested in the use of FLAC^{3D} code to respond to the concerns of practitioners by proposing, from the results of numerical modeling, tables, and

charts for several forms of foundations, including piled rafts, pile groups, unpiled raft, and single pile.

The main objectives of this work are (i) to investigate the effects of the raft-soil-pile interactions on the load response of piled raft subjected to vertical loading in the case of soft clay conditions by varying some parameters as pile number and piling configuration. (ii) to assess the pile group efficiency based on the load-settlement response in the case of soft clays, considering several pile configurations using a variable number of piles and pile spacing. The pertinence of the 3D numerical results of the efficiency coefficient is judged by comparison with those obtained from the most popular formulas available in the literature.

The present thesis consists of the following five chapters:

The first chapter reviewed and summarized the design techniques and analysis methods available in the literature of piled raft foundations. The different design philosophies regarding the piled raft foundations and the classification of the analysis methods of piled raft foundations are outlined in this chapter. Also an updated review of experimental, analytical, and numerical studies on piled raft foundations are presented and discussed in this chapter.

In the second chapter, the constitutive laws used in this thesis, in particular the perfectly plastic elastic model of Mohr-Coulomb as well as the numerical tool used, namely the FLAC^{3D} code are described in detail.

The third chapter presents our first contribution, concerning numerical investigation on pile group efficiency embedded in soft clay. This chapter focuses on the evaluation of pile group efficiency based on the load-settlement response, considering several pile configurations. After validating the developed numerical model by comparing the obtained results to those of similar subgrade-structure and in a comparable geological condition provided within the literature, this study aims to perform a full 3D numerical analysis, using the FLAC^{3D} code, of the overall load response of the pile group and to determine the effects of piles number and pile spacing on the freestanding pile group performance embedded in soft clay conditions.

The second contribution in this thesis is presented in the fourth chapter. A full 3D numerical analysis, using the FLAC^{3D} code, of the overall load response, load sharing behavior, pile load distribution, and effects of the interactions of piled raft foundation subjected to vertical static loading in soft clays are performed. Several types of foundations

Introduction

are considered including piled raft, group of piles, unpiled raft, and single pile. The study results are also validated by comparing them to those of similar subgrade-structure and in a comparable geological condition provided within the literature.

For design optimization purposes, the interactions behavior and the performance of the piled raft foundation is also investigated by varying some parameters as piles number and pile configuration. The change in these settings produces a wide variety of cases to be studied. The concluded observations from the parametric study provide further insight into the mechanical response of piled raft and aim at helping the engineers in taking a logical path in an iterative design process for a piled raft foundation.

A summary of the main results obtained from the present work and necessary recommendations are presented in section of conclusions and recommendations. References are added at the end.

CHAPTER 1

LITERATURE REVIEW ON ANALYSIS METHODS OF PILED RAFTS

1.1 Introduction

In geotechnical engineering, the choice of a foundation type for whichever structure must not only be capable of transmitting the total structural load to the ground, but also achieve this goal satisfactorily. It must be adequately designed to satisfy strength, serviceability, constructability, and economic conditions. When the shallow foundation (Figure 1.1a) is not sufficient to carry all the structural load, installing a limited number of piles below the foundation not only prevents excessive settlement but also improves the bearing capacity of the foundation (Poulos, 2001). This foundation system is called the piled raft foundation (Figure 1.1b), which has proven to be an economical type of foundation compared to conventional foundations. In other words, piled rafts are foundations in which the pile heads are connected by a raft in contact with the ground surface located between the piles which therefore contribute to the distribution of loads.

The concept of piled raft foundations was originally described by Sievert (1957) for compressible volcanic clay in Mexico City, and their advantages encouraged designers to adopt this approach for foundations of high-rise buildings. Several efforts are in progress to combine the two types of foundations (shallow and deep foundations), to achieve a cost-effective design process. The main objective is not only the load sharing between these two components, or to limit the total and differential settlement within an acceptable limit, but also to develop a simple analytical method that can be used by engineers, based on numerical and/or experimental methods, to estimate the ultimate load of the piled raft foundations.

In this chapter, after describing the different design philosophies regarding piled raft foundations, a literature review on analysis methods of piled raft foundations will be presented in detail. Also an updated brief review of experimental, analytical, and numerical methods regarding the analysis and design techniques of piled raft foundations is presented in this chapter.

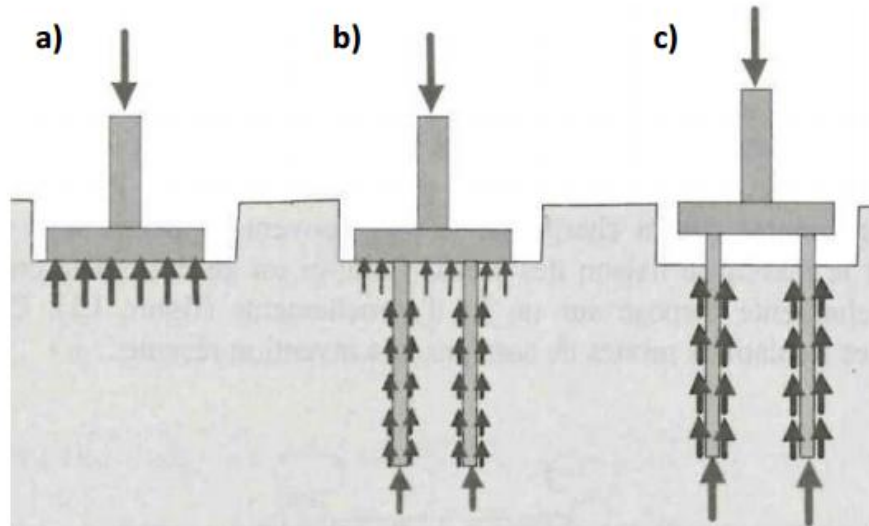


Figure 1.1 Schematic design of (a) Shallow foundation, (b) Piled raft foundation, and (c) Deep foundation (Borel 2001).

1.2 Design concepts

1.2.1 Design philosophy

Many research studies were done and others still in progress to develop a practical design strategy for the piled raft foundation based on several design philosophies. Randolph (1994) defined three different design philosophies regarding piled raft foundation:

- a. The conventional approach, in which the foundation is designed as a group of piles with regular spacing over the entire surface of the raft to carry most part of the total structural load and taking into account the contribution of the raft to transmit a certain load directly on the ground, primarily to ultimate load capacity.

As reported by Sinha (2013), every design by the conventional approach philosophy will necessarily remain in the elastic domain, where the piles are loaded below their bearing capacity and uniformly distributed over the entire raft surface. The shaft capacity of the group pile is “extremely difficult and has not been resolved yet” (Das 2015). Furthermore, the allowance of the raft contribution is not identified in this approach, which they let for engineering judgment.

- b. The Creep Piling approach, where the piles are designed to operate at a working load at which significant creep begins to occur (usually 70-80% of the bearing capacity). The net contact pressure between the raft and the surface soil has been reduced by adding sufficient piles to reduce the pre-consolidation pressure of the soil.

In this approach, the piles are designed to operate at a working load below the creep load in this approach, while the capacity of the pile group is extremely difficult which is under development.

- c. The differential settlement control approach, in which the piles in piled raft foundation are strategically located beneath the raft to minimize the differential settlement, rather than to reduce the average settlement.

According to Poulos (2001), the latter approach should be the most economical, since the piles are strategically located to reduce differential settlement. Fewer piles will be needed, compared to the two other approaches.

Based on the design requirements, Russo and Viggiani (1998) classified piled raft foundations into two broad categories.

- The first group is the "small" piled raft foundation, in which the bearing capacity of the raft foundation is insufficient, and therefore the main reason for adding piles is to achieve an appropriate safety factor. In this group, the raft stiffness is normally high and the differential settlement could be limited. This typically involves rafts with widths between 5 and 15 m.
- The second group is the "large" piled raft foundation, in which the bearing capacity of the raft is sufficient to carry the total structural load with an acceptable safety margin, so the installation of piles beneath the raft is normally designed to reduce settlement or differential settlement. In such cases, the raft width is larger compared to the length of the piles.

These two categories described widely the conventional and creep piling approaches defined by Randolph (1994).

1.2.2 Design considerations

Poulos (2001) reported that the design of a piled raft foundation requires the consideration of some issues, as well as:

- Ultimate load capacity for vertical, lateral and moment loadings;
- Maximum settlement;
- Differential settlement;
- Raft moments and shears for the structural design of the raft;
- Pile loads and moments, for the structural design of the piles.

Katzenbach et al. (2005) termed the piled raft foundation as the Combined Piled Raft Foundations (CPRF), which constitutes of three supporting elements: piles, raft, and subsoil. The raft and pile stiffness, the soil properties, the pile dimensions, and the pile configuration all play an important role in the design of a piled raft foundation. Therefore, to develop an optimum piled raft foundation, the following issues should be considered.

- Ultimate geotechnical capacity under vertical, lateral and moment loadings
- Maximum and total settlements
- Differential settlement and angular rotation
- Lateral movement and stiffness
- Load shearing between the piles and the raft
- Raft moment and shear for the structural design of the raft and its stiffness
- Pile loads and moments for the structural design of the piles and its stiffness.

The behavior of a piled raft foundation implies a complete interaction between the piles, the raft, and the subsoil. Therefore, to develop a design method for a piled raft foundation, the following factors should be also taken into consideration.

- The raft characteristics (stiffness, flexibility, rigidity, shape, and dimension);
- Piles' characteristics (number, configuration, length, diameter, stiffness);
- Applied load characteristics (concentrated or distributed load and its level related to the ultimate capacity);
- Soil characteristics (soil profile, layers and their stiffness, the ultimate soil bearing capacity).

The broad study of piled raft foundations requires taking into account the full interactions between the different elements of the system. Katzenbach et al. (2000) categorized these interactions into (1) pile-pile, (2) raft-pile, and (3) pile-raft interactions. In 2013, Katzenbach and Choudhury reclassified the piled raft interactions into, (1) the raft-soil interaction and (2) the pile-soil interaction corresponding to the behavior of conventional raft and pile foundations, (3) the pile-pile interaction corresponding to the group effect, and (4) the pile-raft interaction, representing the effect of soil loading on the pile's load-settlement response behavior (Figure 1.2).

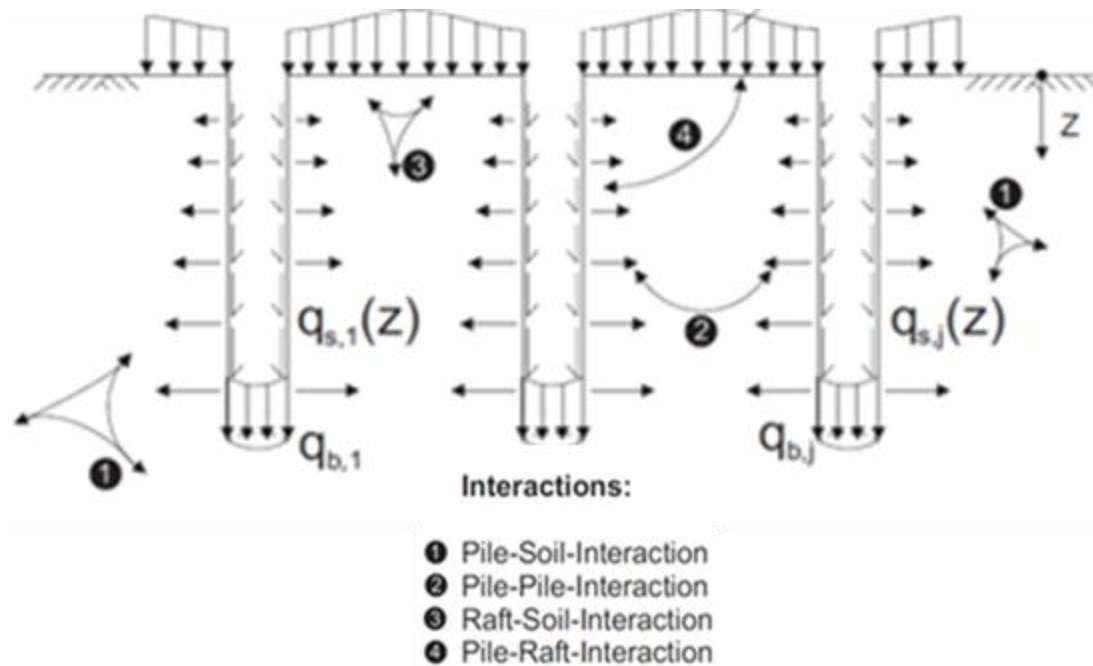


Figure 1.2 Interactions of piled raft foundations adopted from Katzenbach and Choudhury (2013).

1.2.3 Favorable and unfavorable condition

Poulos (1991) reported that the following conditions can be favorable, after investigating a number of idealized soil profiles for piled raft foundations:

- A uniform soil layer of relatively stiff clay;
- A uniform soil profile of relatively dense sand.

Consequently, the following situation may be unfavorable for applying a piled raft foundation

- Presence of relatively soft clay in the soil profile near the surface;
- Presence of relatively loose sand in soil profile near the surface;
- Presence of soft compressive layer in a soil profile at relatively shallow depth;
- Soil profiles, which are likely to undergo consolidation settlement due to external causes;
- Soil profiles, which are likely to undergo swelling movement due to external causes.

1.3 Classification of analysis methods

Since the research work of research of Zeevaert (1957), researchers and designers have been adopting of the piled raft system for the foundation of high-rise buildings. Several design methods have been developed based on various approaches. To carry out a critical review, these works have been categorized under three major group, namely:

- Simplified calculation methods, which involves several simplifications concerning the modeling of the soil profile and the loading conditions on the raft. These methods are those of Poulos and Davis (1980), Randolph (1983, 1994), van Impe and Clerq (1995), and Burland (1995);
- Approximate numerical analysis methods, such as the "strip-on-springs" approach, in which the raft is represented by a series of strip footings, and the piles are represented by springs of appropriate rigidity (Poulos, 1991), or the "plate-on-springs" approach, in which the raft is represented by a plate and the piles as springs (e.g. Clancy and Randolph 1993, Poulos 1994, Viggiani 1998,);
- More rigorous numerical analysis methods, like the boundary element methods, in which the raft and piles of the system are discretized with boundary elements, using an elastic theory (eg. Brown and Wiesner 1975, and Sinha 1997); methods combining boundary elements for piles and finite element analysis for the raft (eg Ta and Small 1996, and Russo and Viggiani, 1998); simplified finite element analysis, which generally involve the representation of the foundation system in the form of a plane strain problem or an axisymmetric problem; three-dimensional finite element analyses and corresponding finite difference analysis via the commercial program FLAC^{3D} (Poulos 2001).

1.3.1 Simplified calculation methods

The simplified methods found in the literature are those of Poulos and Davis (1980), Randolph (1983, 1994) van Impe and Clerq (1995), and Burland (1995). They are based on simplifications in terms of the soil profile and loading conditions on the raft. The simple analytical methods aim to solve the complicated analysis of settlement of pile groups. So, some approximations have been made to make the calculation procedure intended to handle piled raft foundations. A method involving the combination of Poulos and Davis (1980) and Randolph (1994) methods has been identified as the Poulos-Davis-Randolph (PDR) method. This simplified method examines the interaction between piles in a pile group and piles with a raft, as described in detail by Poulos (2001). Combarieu and Evrard (1979) also proposed an analytical method based on pressuremeter methods to calculate the bearing load of a piled raft foundation. However, the full interaction effects of the foundation system are not taken into consideration in this method. To this day, much research and efforts are underway to develop a simple method to evaluate the ultimate load capacity of the piled raft foundation as a function of its component capacities, which can be simply assessed by the standard theories.

1.3.1.1 Load-settlement behavior

A. Equivalent raft method

The foundation is considered as a union and the settlement of the piled raft foundation is evaluated by considering an equivalent raft located at two-thirds (2/3) of the way down the piles that penetrate the main foundation layer, or at the level of the bases of piles for end-bearing piles (Tomlinson, 1986; Bowles, 1988). The adopted depth of the equivalent raft, given by Tomlinson (1986) in Figure 1.3, depends on the nature of the soil.

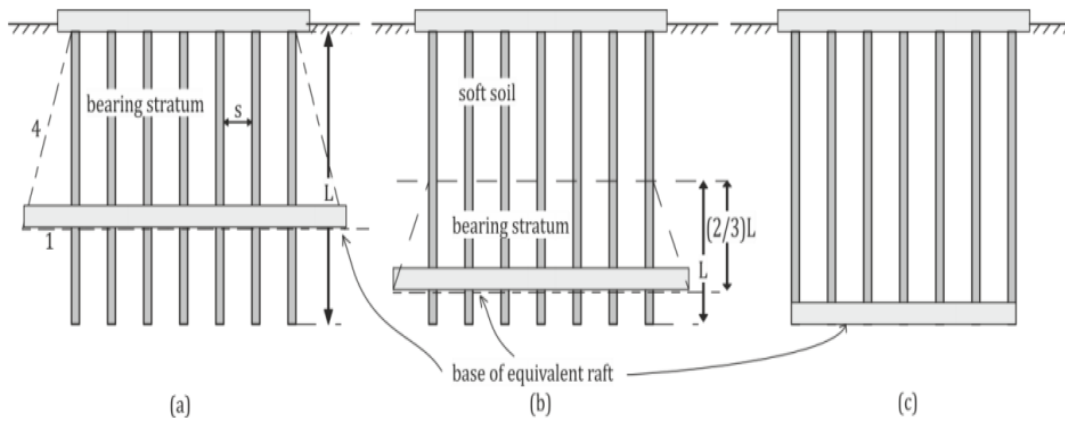


Figure 1.3 Adopted depth of the equivalent raft. (A) Piles work mainly by friction, (b) combination of friction and end bearing piles (c) end bearing piles

The average settlement at soil level is calculated as follows:

$$W_{avr} = W_r + W_e \quad (1.1)$$

where

W_r is the raft settlement; W_e is the elastic compression of the piles above the equivalent raft level, which are treated as free-standing columns.

A practical calculation method for W_r is based on the integration of vertical strains under the equivalent raft, taking into account variations in soil modulus and correcting the embedment of the raft below the soil surface (Poulos, 1993), as follows:

$$W_r = F_D q_t \sum_{i=1}^{n_s} \left(\frac{l_\varepsilon}{E_s} \right)_i H_i \quad (1.2)$$

where

q_t is the average pressure applied to the raft; I_ε is the influence factor from which the vertical strain may be calculated; H_i and E_s are the thickness and the Young's modulus of the i^{th} layer; F_D is the correction factor; n_s is the number of soil layers.

Poulos (1993) performed comparison results of a parametric study using the equivalent raft method with those of a finite difference analysis and found that, for groups containing more than 16 piles, the equivalent raft method can be a useful approach for prediction of settlement, while it considerably overestimates the settlement for a relatively small number of piles.

B. Equivalent pier method

In practice, the equivalent pier method is often used to estimate the settlement of a pile group. The basic principle of this method is that the region of the soil in which the piles are embedded is considered as a continuum and the pile group is replaced by an equivalent pier as shown in Figure 1.4.

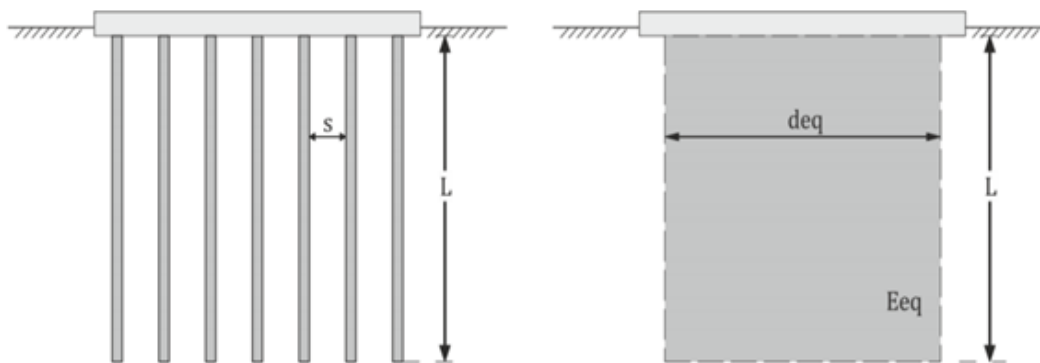


Figure 1.4 Schematic view of the equivalent pier method, adopted from Sönmez, (2013)

This method has been firstly proposed by Poulos and Davis (1980). The authors presented two approaches; (1) A single equivalent pier of the same plane area of the group, as a rectangle, and equivalent length L_e (the equivalent pier type I in Figure 1.5). (2) A single equivalent pier of the same length L as the piles but having an equivalent circular area of diameter d_{eq} , (the equivalent pier type II in Figure 1.5). However, the second technique is good at calculating the overall mean settlement, while, it does not offer a solution for the differential settlement. Poulos and Davis (1980) reported that the latter approach is more appropriate in layered and nonhomogeneous soils.

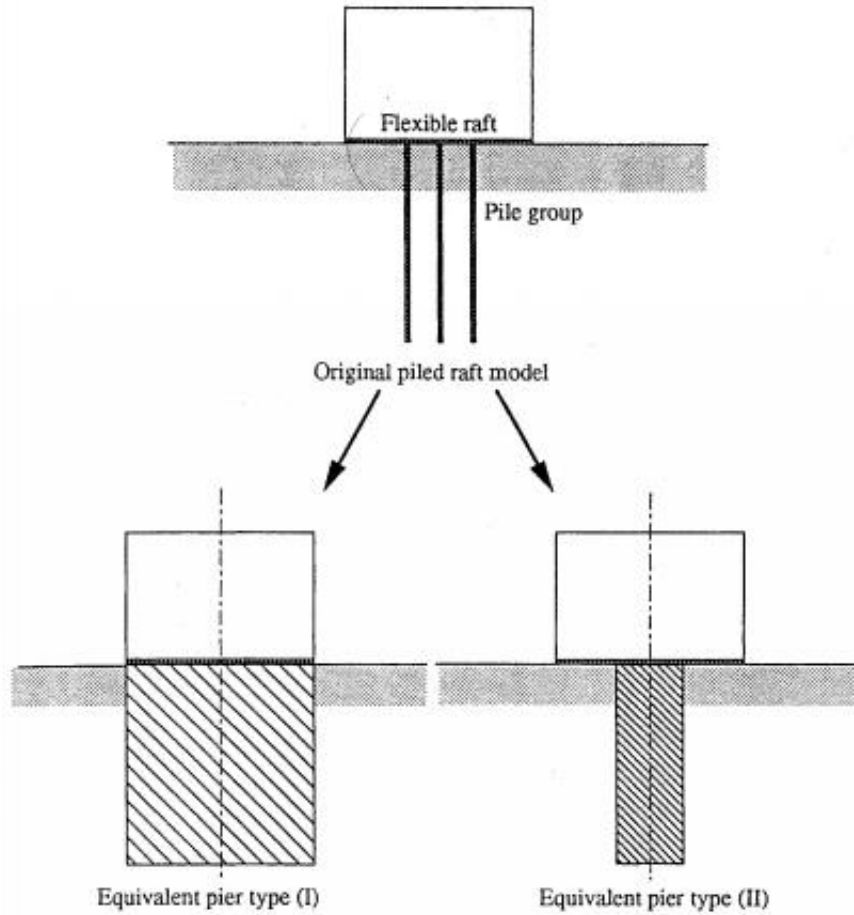


Figure 1.5 Equivalent pier design (Poulos and Davis, 1980)

Poulos and Davis (1980) assumed, by a pure geometric analogy, that the diameter of the equivalent pier subjected to lateral friction and end-bearing is given by the following expression:

$$d_{eq} = \sqrt{\frac{4}{\pi}} A_g = 1.13 \sqrt{A_g} \quad (1.3)$$

where

A_g is the diameter of the equivalent pier.

The Young's modulus of the equivalent pier is defined by the following relation:

$$E_{eq} = E_s + (E_p - E_s) \frac{A_{pg}}{A_g} \quad (1.4)$$

where

E_s is the average Young's modulus of the soil penetrated by the piles, E_p is the Young's modulus of the piles, and A_{pg} is the total cross-sectional area of the piles in the group.

The advantage of this method is that it can show the group effect with total soil clamping between the piles. So, the equivalent pier can be calculated as a single pile.

Poulos (1993) presented the results of a parametric study comparing the equivalent pier method to more rigorous numerical analysis. He found that the equivalent pier method tends to underestimate settlement in the case of a large number of piles. In contrast, the simplified method can be employed with more confidence for groups including a relatively small number of piles. Randolph and Clancy (1993) extended the equivalent pier method by replacing the large pile group with smaller subgroups. This method makes it possible to simplify the calculation of the group and to determine the settlement of each of the subgroups.

Randolph and Clancy (1993), and Randolph (1994) reported that the distinction between the equivalent raft and the equivalent pier method is made by an overall aspect ratio "R" expressed as follows:

$$R = \sqrt{\frac{n \times S_p}{L}} \quad (1.5)$$

where

n , S_p , and L are the number, spacing, and length of piles, respectively.

The equivalent raft method is more appropriate for values of R greater than 4 and the equivalent pier method is more logical for smaller values of R (Randolph, 1994).

Viggiani et al. (2012) suggested that the equivalent raft method is more appropriate for large pile groups, where the width of the group is greater than the length of the piles, and the equivalent pile method is recommended for small pile groups.

1.3.1.2 Vertical load capacity

A. Burland's approach

Burland (1995) developed the following simplified design process, for the case where the piles are planned to act as settlement reducers and to develop their full bearing capacity at the design load:

- Estimate the total long-term load-settlement response for the raft alone (see Figure 1.6). The design load Q_0 gives a total settlement w_0 ;
- Evaluate an adequate design settlement S_d , including a margin of safety;
- P_1 is the load carried by the raft corresponding to S_d ;

- The overload $P_0 - P_1$ is considered to be taken by piles. Burland suggests that a “mobilization factor” of about 0.9 can be applied to the ‘conservative best estimate’ of the ultimate shaft capacity of these piles, Q_{su} . However, Poulos (2001) reported that the shaft resistance of these piles will be fully mobilized and therefore no factor of safety is applied;
- If the piles are located below columns that carry a load in excess of Q_{su} , the piled raft foundation may be analyzed as a raft subjected to decreased column loads. At such columns, the reduced load Q_r is:

$$Q_r = Q - 0.9Q_{su} \quad (1.6)$$

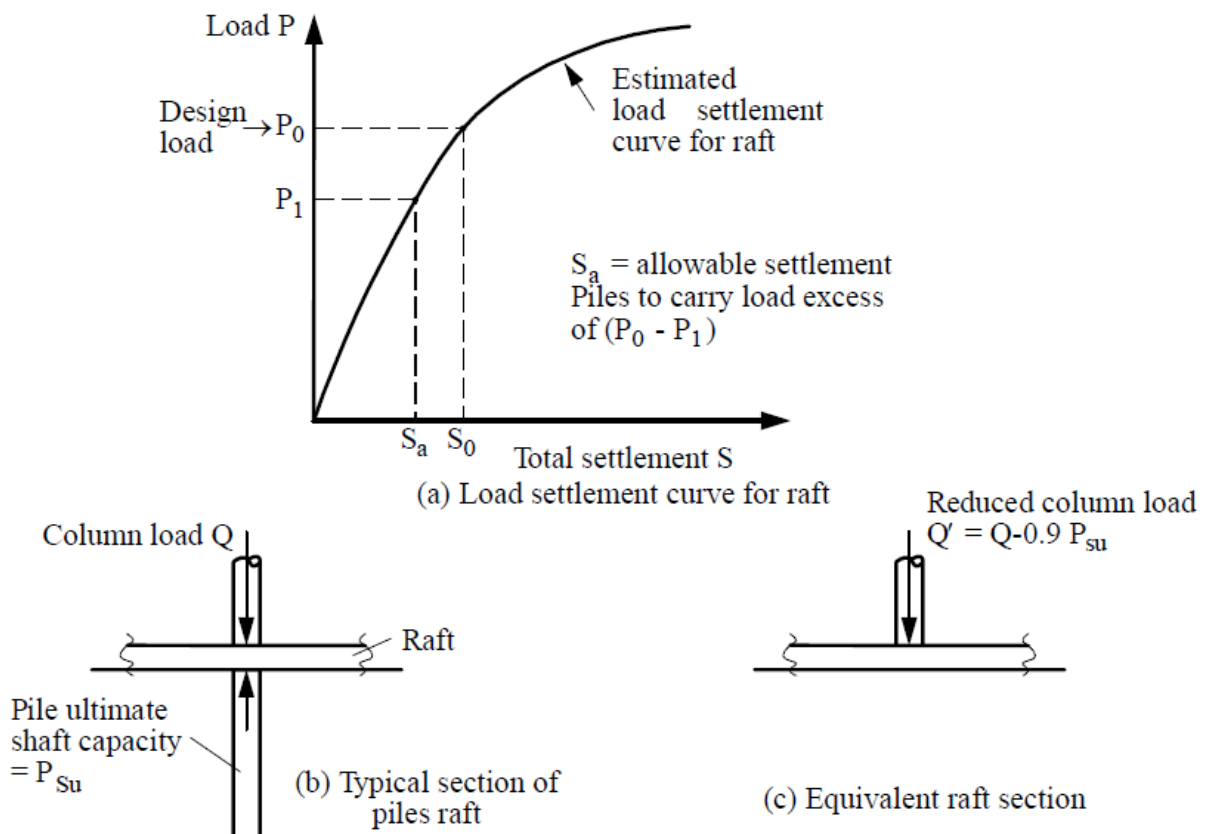


Figure 1.6 Burland’s simplified design concept, adapted from Poulos (2001).

The bending moments in the raft can therefore be obtained by analyzing the piled raft foundation as a raft subjected to reduced loads Q_r . Burland did not provide a process for estimating the settlement of piled raft foundations; Poulos (2001) suggests adopting the approximate approach of Randolph (1994), in which:

$$S_{pr} = \frac{S_r k_r}{k_{pr}} \quad (1.7)$$

where

S_{pr} is the piled raft settlement, S_r is the raft settlement subjected to the total applied loading, K_r is the raft stiffness, and K_{pr} is the piled raft stiffness.

B. PDR method

A simple analysis approach mainly based on elasticity is often used in practice with formulas or charts proposed by Poulos and Davis (1980); Randolph (1983, 1994) named the Poulos–Davis–Randolph (PDR) method. In this method, the ultimate load capacity of a piled raft foundation is considered as the smallest of the following two values:

- The sum of the ultimate capacities of the raft plus all the piles;
- The ultimate capacity of a block containing the piles and the raft, plus that of the portion of the raft outside the periphery of the piles.

The approach described by Randolph (1994) can be adopted in order to estimate the behavior of load-settlement. The definition of the pile problem is shown in Figure 1.7. The stiffness of the piled raft foundation is estimated as follows:

$$k_{pr} = \frac{k_p + k_r(1 - 2\alpha_{rp})}{1 - \alpha_{rp}^2 \left(\frac{k_r}{k_p} \right)} \quad (1.8)$$

where

K_p is the pile group stiffness, K_r is the raft stiffness, and α_{rp} is the raft-pile interaction factor.

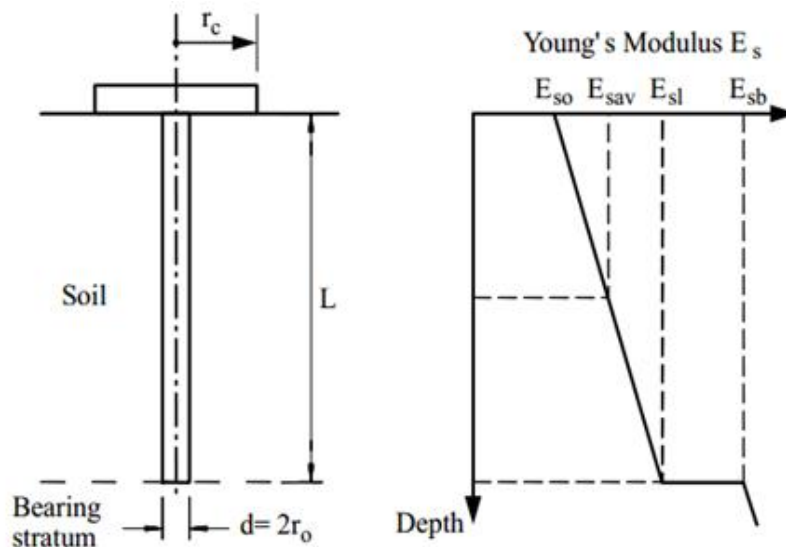


Figure 1.7 Simplified representation of a pile-raft unit, adopted from Poulos (2001).

The proportion of the total applied load carried by the raft is expressed as follows:

$$\frac{Q_r}{Q_t} = \frac{k_r(1-\alpha_{rp})}{k_p + k_r(1-2\alpha_{rp})} \quad (1.9)$$

where

Q_r is the load carried by the raft, and Q_t is the total applied load.

The raft and pile group stiffness, K_r and K_p respectively, can be estimated through elastic theory, using for example, the solutions of Mayne and Poulos (1999) for K_r and Poulos and Davis (1980) or Fleming et al (1992) or Poulos (1989) for K_p .

Eqs. 1.8 and 1.9 are used to develop a tri-linear load-settlement curve, as shown in Figure 1.8. The piled raft stiffness is computed from Eq. 1.8 for a given number of piles. This stiffness will continue to operate until the pile capacity is fully mobilized (point A). After this point, the stiffness of the foundation is that of the raft (K_r) until the ultimate load capacity of the piled raft foundation is reached (Point B). At this stage, the load-settlement response becomes horizontal.

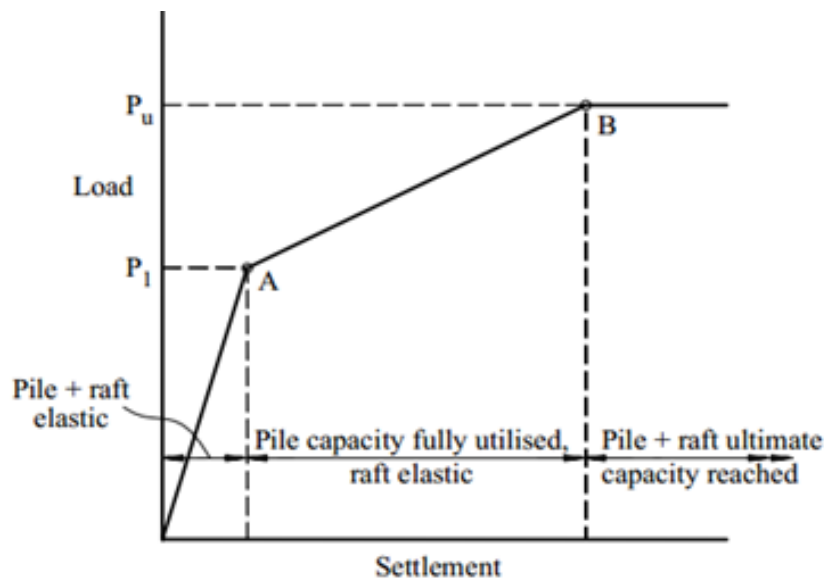


Figure 1.8 Simplified load-settlement curve for preliminary analysis, adopted from Poulos (2001).

The load-settlement behavior of the piled raft foundation calculated using the PDR approach tends to be in good agreement with the one obtained from more rigorous numerical methods (Poulos, 2001). Additionally, Nguyen et al. (2013b) reported that in this simplified approach, only the interaction between the piles and the raft is taken into account with the factor α_p and the interaction between the piles in the pile group is not considered.

C. Pressiometric method

Combarieu and Evrard (1979) proposed the following calculation method of a piled raft foundation based on the pressiometric methods commonly used for the traditional foundation, shallow or deep foundations. It has the advantage of being applicable from geotechnical tests which are now very widespread.

$$Q_l = Q_{sl} + n \times Q_{pl} + n \times (\mu * F_{pl}) \quad (1.10)$$

$$Q_{sl} = (S_s - n \times S_p) \times k_s \times (P_{le}^* - q_0) \quad (1.11)$$

$$Q_{pl} = S_p \times k_p \times P_{le}^* \quad (1.12)$$

$$F_{pl} = 2\pi R_p \sum \tau_z \times dz \quad (1.13)$$

where

Q_l is the load capacity of the piled raft foundation, Q_{sl} is the load capacity of the raft, Q_{pl} is the load capacity of single pile, F_{pl} is the shaft capacity of the single pile, n is the number of piles, μ is the reduction factor, S_p and S_s are the cross-sectional areas of the pile and raft, respectively, k_p and k_s are the bearing factors, P_{le}^* is the equivalent net limit pressure, τ_z is the unit shaft friction of layer z , and z is the thickness of layer z .

In this method, the ultimate load capacity of a piled raft foundation is considered as the sum of the ultimate capacities of all piles plus that of the portion of a reduced raft (reduced raft has a cross-sectional area equal to the cross-sectional area of the raft minus those of all piles). However, this calculation method neglects all interactions between the pile, raft, and soil in the piled raft foundations.

1.3.1.3 Load Transfer Mechanism

As the piled rafts are a combined foundation system, they were developed to use the load-carrying capabilities of both rafts and piles. Therefore, the ultimate load capacity of the piled raft is composed of the load-carrying capacities of the raft and piles components. The load distribution at failure in the piled raft system can be expressed as follows:

$$Q_{pr,ult} = Q_r + Q_p \quad (1.14)$$

where

$Q_{pr,ult}$ is the ultimate load capacity of piled raft, Q_r and Q_p are the load-carrying capacities of the raft and piles components respectively.

The ultimate load capacity of the piled rafts was expressed in terms of ultimate load capacities of unpiled raft and group of piles as it is proposed by Liu et al. (1985), and also Poulos (2000) as follows:

$$Q_{pr,ult} = Q_{ur,ult} + Q_{gp,ult} \quad (1.15)$$

where

$Q_{ur,ult}$ and $Q_{gp,ult}$ are the ultimate load capacities of unpiled raft and group of piles respectively.

The mobilized stress and the displacement fields of raft overlap with those of piles within the soil, which creates complex load-carrying mechanisms and different types of interaction effects. Moreover, the performance of piles in the piled raft is influenced not only by the vicinity interaction between piles but also by the raft pressure. Due to the interactions between the raft and piles when they are combined into a piled raft foundation Q_r and Q_p in Eq. (1.14) differ from $Q_{ur,ult}$ and $Q_{gp,ult}$ in Eq. (1.15), respectively. To address this, Eq. (1.15) can be modified as it was described by Park and Lee (2014):

$$Q_{pr,ult} = \eta_r \times Q_{ur,ult} + \eta_p \times Q_{gp,ult} = \eta_r \times Q_{ur,ult} + \eta_p \times C_g \times \sum Q_{sp,ult} \quad (1.16)$$

where

η_r and η_p are pile-raft and raft-pile interaction factors respectively; C_g is pile-pile interaction factor referring to the efficiency of the group of piles. C_g is usually used to assess the load capacity of the group; $Q_{sp,ult}$ is the ultimate load capacity of single pile.

1.3.1 Piled Raft Interaction

Because of the overlapped stress and displacement fields of the raft and piles in piled raft systems, inevitable complex interactions inevitably occur. Consequently, these interactions affect the behavior of the foundation in different aspects depending on the variation of interaction factors. The piled raft interaction effects should be identified and need to be considered in foundation design. The fundamental interactions are pile-pile interaction (P-P), pile-raft interaction (P-R), and raft-pile interaction (R-P) according to (Katzenbach et al., 2000), which represent the pile group effect and the interactive effects between rafts and piles as shown in Figure 1.9

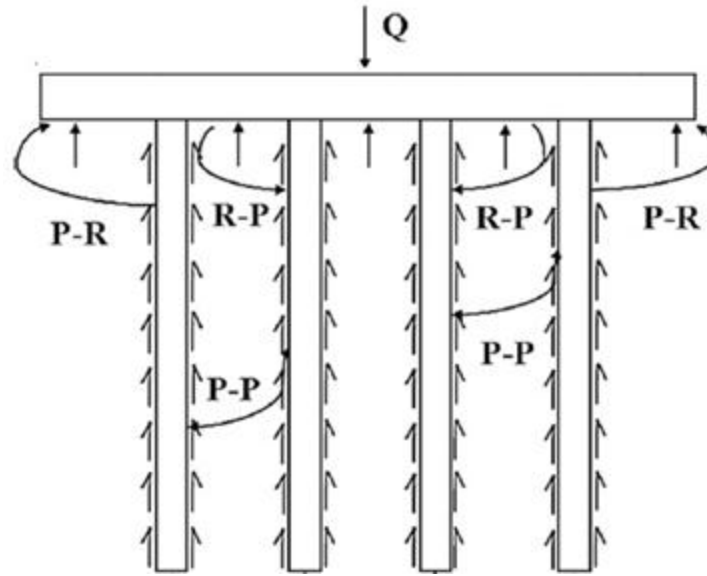


Figure 1.9 Fundamental Piled raft interactions.

- **Interaction effect of pile group**

The vicinity of the piles affects the load capacity of each pile in the group and on the settlement of the foundation system. The behavior of a pile group may be different from that of single pile and the axial load capacity of a group of n piles ($Q_{gp,ult}$) may be less than n times the axial load capacity of single pile ($Q_{sp,ult}$). The pile group interaction effect is characterized through the pile-pile interaction factor (C_g) which is defined as a ratio of the ultimate load capacity of a group of n piles to n times the bearing capacity of single pile, as follows:

$$C_g = \frac{Q_{gp,ult}}{n \times Q_{sp,ult}} \quad (1.17)$$

In the last century some investigations have been carried out to define the value of the efficiency coefficient C_g such as the research works of Feld (1943), Whitaker (1957), Saffery and Tate (1961), De Mello (1969), Barden and Monckton (1970), Brand et al. (1972), O'Neill et al. (1982) Briaud et al. (1989). Most experimental evaluations of C_g are applied depending only on soil conditions and the pile installation method. In conditions of loose to medium dense sand, $C_g = 1$ for driven piles and for bored friction piles C_g tends to lower values. However, in clay soils, C_g is often lower than unity (de Sanctis and Mandolini, 2006). Nevertheless, the efficiency coefficient also depends on the number of piles and pile spacing (Cooke, 1986; Frank, 1999). Empirical formulas have also been developed for the evaluation of the efficiency factor of the pile group such as the Converse-Labarre method (Bolin, 1941) or the Los Angeles group action method (Das, 2015). Unlike the other methods, these empirical formulas only consider the plan geometry of the foundation.

Several efficiency conceptions have been proposed to relate the behavior of a pile group to that of an individual pile. The most conventional and popular formulas for group of piles in clay are briefly summarized as follows:

1. Converse-Labarre method (Bolin, 1941):

On the regulatory plan, the formula of Converse-Labarre (Bolin, 1941) was recommended for identical, vertical and regularly spaced piles. In this formula C_g is given as a function of the geometric parameters of the group, as follows:

$$C_g = 1 - \frac{\arctg\left(\frac{d}{S_p}\right)}{90^\circ} \times \left[\frac{(n_2-1) \times n_1 + (n_1-1) \times n_2}{n_1 \times n_2} \right] \quad (1.18)$$

where n_1 and n_2 are the number of rows and the number of piles per row, respectively; d is the pile diameter and S_p is the pile spacing.

2. Seiler and Keeney method:

For defining the coefficient C_g , Seiler and Keeney (1944) proposed the following formula:

$$C_g = \left\{ 1 - \left[\frac{11 \times S_p}{7 \times (S_p^2 - 1)} \right] \times \left[\frac{n_1 + n_2 - 2}{n_1 + n_2 - 1} \right] \right\} + \left[\frac{0.3}{n_1 + n_2} \right] \quad (1.19)$$

where

S_p is in ft.

This equation tends to minimize the effect of the number of piles compared to the effect of pile spacing.

3. Sayed and Bakeer method:

Sayed and Bakeer (1992) proposed a new formula to evaluate the efficiency of pile group subjected to axial load. It should be applicable for a pile group in both cohesive and cohesionless soils. The formula of C_g in this method accounts for the three dimensional geometry of the pile group as follows:

$$C_g = 2 \times \left\{ \frac{[(n_2-1) \times S_p + d] + [(n_1-1) \times S_p + d]}{\pi \times n_1 \times n_2 \times d} \right\} \quad (1.20)$$

4. Code "Fascicule 62-V,":

The Code of Practice, called "Fascicule 62 –Titre V," was approved and officially adopted in France by the Ministry of Equipment, Housing and Transport in March 1993 (MELT, 1993).

This code is very directive on the values of the coefficient of efficiency to adopt. For cohesive soils, the group effect is neglected if the pile spacing S_p is greater than $3d$. Otherwise, the coefficient of efficiency can be evaluated by the following equation:

$$C_g = 0.25 \times \left(1 + \frac{S_p}{d}\right) \quad (1.21)$$

According to this formula, it can be seen that the effect of the number of piles is neglected.

5. Das method:

Das (2015) developed another formula for the coefficient of efficiency C_g :

$$C_g = \frac{2 \times (n_1 + n_2 - 2) \times S_p + 4d}{p \times n_1 \times n_2} \quad (1.22)$$

where

p is the perimeter of the cross section of pile.

In this formula, C_g somehow represents the ratio between the perimeter of the cross section of the pile block and the sum of the perimeter of all piles.

6. Los Angeles group action method (Das,2015):

$$C_g = 1 - \frac{d}{\pi \times S_p \times n_1 \times n_2} \left[n_1(n_2 - 1) + n_2(n_1 - 1) + \sqrt{2}(n_1 - 1)(n_2 - 1) \right] \quad (1.23)$$

7. McCabe and Lehane method:

McCabe and Lehane (2006) also suggested a conception for C_g as a function of the geometric parameters of the group of piles as follows:

$$C_g = \frac{\left(\frac{B_g}{B_p}\right)^{0.66}}{n} \quad (1.24)$$

where

B_g and B_p are the diameter of pile envelope of the pile group and diameter of the pile, respectively; n is the number of piles.

Other methods, e.g., those of Feld (1943) and Whitaker (1957) were also developed for the efficiency of a group of piles. In the method of Feld, the coefficient of efficiency C_g takes values between 0.72 and 0.94 depending on the number of piles. Based on the results of the experimental models, Whitaker (1957) established design charts for determining the pile group efficiency. These charts are adopted in the design manuals of the U.S. Army Corps of Engineers and the U.S. Navy.

- **Interaction effects between rafts and piles**

For building projects, the group of piles is often connected by a concrete raft cast on the ground; the presence of the raft can modify the behavior of the group of piles which is expressed by the raft-pile interaction. On the other hand, the pile-raft interaction presents an effect on the raft performance due to the existence of piles underneath the raft. These interaction mechanisms are expressed by the pile-raft and raft-pile interaction factors representing the ratios of load-carrying capacities of piled raft components Q_r and Q_p to the ultimate load capacities of unpiled raft and group of piles as written in Eqs. 5 and 6, respectively.

$$\eta_r = \frac{Q_r}{Q_{ur,ult}} \quad (1.25)$$

$$\eta_p = \frac{Q_p}{Q_{gp,ult}} \quad (1.26)$$

The presence of the raft on the piles' head affects the performance of these piles in two different aspects, positive and negative impacts, regarding load-carrying capacity (Katzenbach et al. 2000). The increased pile skin friction is caused by an increase of confining stress in the soil surrounding the piles by raft pressure (Katzenbach et al. 2000), which is the positive effect. The effect of increasing confining stress can vary depending on the loading rate and the pile configuration. In contrast, the negative effect, as reported by Han and Ye (2006), represents less mobilization of pile friction because of the decreased relative displacement between the piles and the surrounding soil, as the subsoil is forced to move down upon loading.

The P-R interaction represents changes in the raft performance caused by the bearing mechanism of the piles. According to Park and Lee (2014), the mobilization of the pile

friction produces downward displacements of the surrounding soil, which causes a decrease in the contact pressure between the raft and the underlying soil with less load-carrying capacity.

Recently, various research studies have been performed to investigate the interaction behavior in the piled raft systems, several conceptions are proposed to estimate the interaction factors. Recent studies are summarized in Table 1.1.

Table 1.1 Conceptions of interaction factors of piled raft system by several researchers

Interaction	Conception	Reference	Consideration
Pile-Raft	$\alpha = 1 - \frac{\ln(r_r/r_p)}{\ln(r_m/r_p)}$	Randolph (1994)	The pile and raft sizes
Pile-Raft	$\alpha = \frac{k_p}{P_p} \left(w_{pr} - \frac{P_r}{k_r} \right)$	Clancy and Randolph (1996)	The stiffness of raft and piles
Pile-Raft	$\alpha_{pr} = 1 - 3 \frac{\left(\frac{A_g}{A} \right)}{\left(\frac{S_p}{B_p} \right)}$	de Sanctis and Mandolini (2006)	The pile layout and geometry.
Pile-Pile	$\alpha_{kj} = \frac{\Delta w_k}{w_{1j} Q_j}$	Nguyen et al. (2013b)	The effect of adjacent pile on single pile
Pile-Raft	$\beta = \frac{\Delta W}{n}$		The change in settlement and the piles number in the piled raft
Pile-Raft	$\alpha_{pr} = 1 - e^{\left[-10.55(w/B_r)^{0.26} \right]}$	Kumar and Choudhury (2018)	The settlement dependence
Raft-Pile	$\alpha_{rp} = (\eta - \alpha_{pr}) \frac{Q_{PG}}{Q_{UR}}$		The efficiency factors
Pile-Raft	$\beta_{pr} = 1.6 \left(w/B_r \right)^{0.25}$	Deb and Pal (2019)	The settlement dependence
Raft-Pile	$\beta_{rp} = \frac{1}{1 - \alpha_{PR}} - \frac{\beta_{pr}}{\left(Q_{UR}/Q_{GP} \right)}$		The efficiency factors

Nomenclature: r_r is the raft diameter; r_p is the pile diameter; k_p is the pile group stiffness; k_p is the raft stiffness; P_p is the load carried by piles in the piled raft foundation; P_r is the load carried by raft in piled raft foundation; w_{pr} is the settlement of piled raft foundation; A_g is the area defined by perimeter line of piles; A is the raft area; S_p is the pile spacing; B_p and B_r are the pile diameter and the raft width, respectively; Δw_k is the change in settlement of pile; w_{1j} is the settlement due to unit load of pile; Q_j is the load on pile; ΔW is the additional settlement caused by a pile for the raft; n is the piles number; Q_{PG} is the load carrying capacity of pile group; Q_{SP} is the load carrying capacity of single pile; w is the settlement; η is the piled raft efficiency factor; α_{PR} is the load sharing ratio; Q_{UR} is the load carrying capacity of unpiled raft.

2.3.1 Load sharing behavior

The piled raft foundation is a combination of piles and raft based on the concept of load sharing between their components. Referring to the PDR and Burland approaches in the above sections, the sharing of the applied load mainly depends on the settlement levels (Figures 1.6 and 1.8). At the initial settlement range, the total load is carried by piles. After this settlement range, for a settlement large enough to mobilize the full capacity of piles, a considerable part of the applied load will be taken by the raft.

The load sharing behavior can be defined using the load sharing ratio which represents the ratio of the load carried by piles to the total applied load on the piled raft foundation, this load sharing ratio is given as follows:

$$\alpha_p = \frac{Q_p}{Q_{pr}} = 1 - \frac{Q_r}{Q_{pr}} \quad (1.27)$$

Clancy and Randolph (1996) proposed an expression for the load sharing ratio α_p in terms of the pile and raft stiffness as follows:

$$\alpha_p = 1 - \frac{(1-i_{rp})\left(\frac{k_r}{k_p}\right)}{1+(1-2i_{rp})\left(\frac{k_r}{k_p}\right)} \quad (1.28)$$

where

i_{rp} is the R-P interaction factor.

Lee et al (2014) proposed an expression of the load sharing ratio based on the hyperbolic load settlement relation. This proposed expression depends on the normalized settlement and geometry of the piled raft components as follows:

$$\alpha_p = \frac{1}{(\beta\xi) \left[\frac{a_p \lambda_B + b_p (s/B_r)}{a_r + b_r (s/B_r)} \right] + 1} \quad (1.29)$$

where

$$\xi = \frac{Q_{ur}}{Q_{gp}} \quad (1.30)$$

$$\beta = \frac{\eta_r}{\eta_p} \quad (1.31)$$

λ_B is the foundation size ratio = B_p/B_r ; β is the load capacity interaction factor; a_r , b_r , a_p and b_p are the model parameters for normalized relationship = 0.02, 0.8, 0.01 and 0.9 respectively; s is the settlement.

Lee et al. (2014) suggested a value of unity for the load capacity interaction factor ($\beta = 1$). They reported that in clay, the interaction effects of piled raft foundation are not very significant. However, the interaction effects are probably not very significant but may produce a different load-carrying behavior from that of the unpiled raft and group of piles. Lee et al. (2015) investigated the load sharing mechanism of the piled raft system in the sand. They found that the interaction effects are significant in the sand, and they proposed an expression for the load capacity interaction factor β as a function of settlement:

$$\beta = 0.09 \left(\frac{S}{B_r} \right)^{-0.32} \quad (1.32)$$

1.3.2 Approximate numerical analysis method

A. Strip-on-springs approach (GASP)

Poulos (1991) presented an example of the "strip on springs" approach to investigate the performance of the piled strip foundation, considering the strip as beams of identical length, and piles as springs of similar stiffness in an elastic continuum of soil volume as shown in Figure 1.10. An approximate contribution is made for all interaction components. The effects of the raft parts outside the strip section are considered by calculating the free field soil settlements from these parts. These settlements are then included in the analysis, and the strip section is examined to get the settlements and moments from the applied load on the strip section and to the soil settlements due to the sections outside the raft.

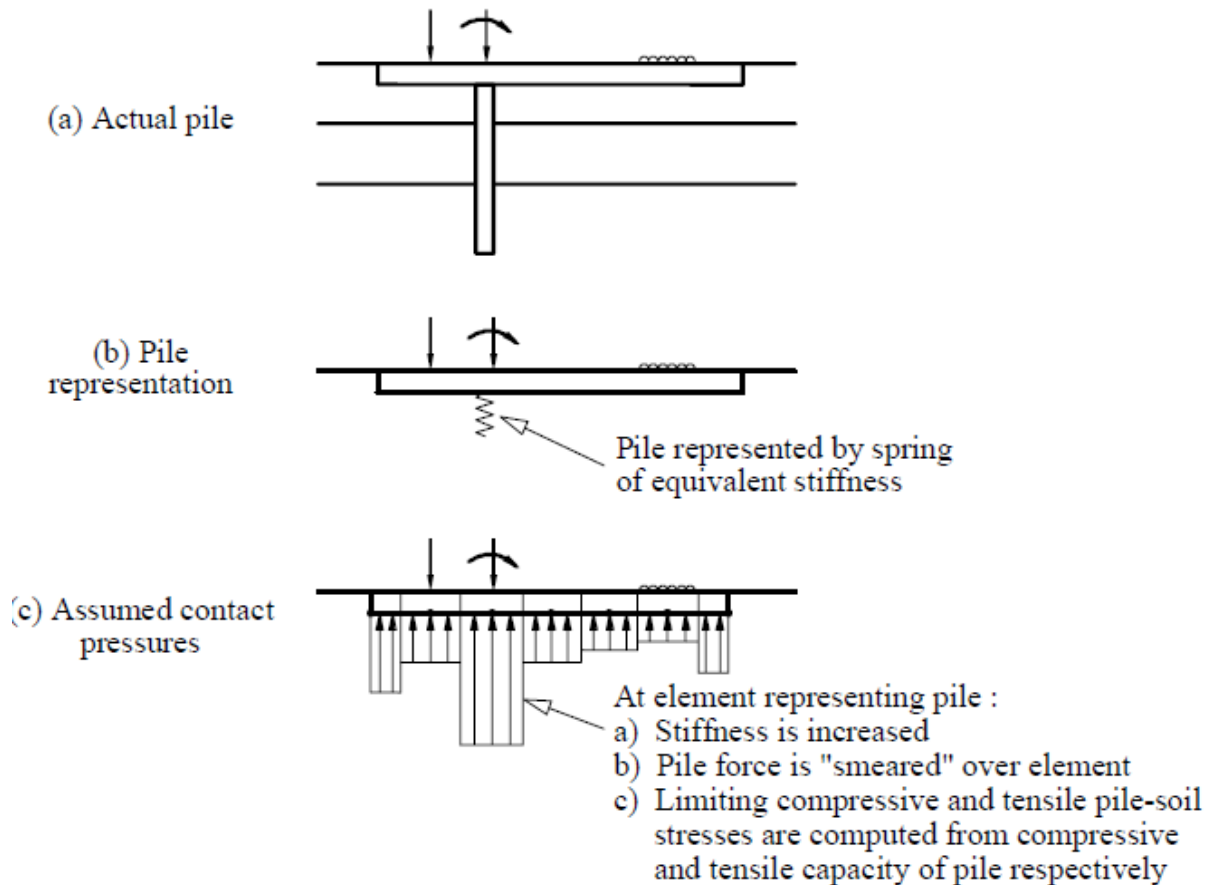


Figure 1.10 Schematic description of piled strip problem via GASP approach (Poulos, 1991)

The non-linearity of the soil is considered approximately via limiting the strip-soil contact pressures to not overestimate the bearing capacity, in compression and the raft uplift capability, in tension. Moreover, the approximate allowance also results in a limitation of the pile-soil contact to not exceed the compressive and uplift capacities of the piles. However, the bearing capacities of piles should be pre-defined and are often considered to be the same as those for separated piles. In the comparative study between the different analysis methods of piled raft foundation conducted by Poulos (2001), the results obtained from the "strip on spring" approach were in good agreement with those obtained from the more rigorous numerical method. Nevertheless, as mentioned in the above sections, the raft pressures on the soil surrounding the piles can have a positive effect on the piles' performance, as reported by Katzenbach et al. (2000). Thus, the assumptions required in modeling the piles in the GASP approach can be conservative.

B. Plate-on-Springs approach

In this method, the raft is represented by an elastic plate, and the piles are modeled as interacting springs in an elastic continuum of a soil volume (Clancy and Randolph, 1993,

Randolph, 1994). Poulos (1994) used the finite-difference analysis for the plate and allowing for multiple interactions via elastic solutions. Allowance is made for layering of the soil, the effects of piles attaining their ultimate capacity, the development of bearing capacity collapse beneath the raft, and the presence of free-field soil settlements acting on the piled raft system. The involved approximations are similar to those used in the previous approach mentioned above for piled strips.

Sales et al. (2000) replaced the finite difference analysis for the raft with a finite element analysis and used a modified approach to take into account the development of the bearing capacity in the piles.

1.3.3 More rigorous numerical analysis method

Since the overall load response of piled raft is related to a complex soil-structure interaction scheme. This model of the foundation is classified in the category of complex geotechnical constructions in Eurocode 7 (Geotechnical Category 3), and therefore, the more rigorous numerical methods seem to be the most reliable options. The most common numerical methods used to simulate the piled raft foundations are mainly the finite element method (FEM), the boundary element method (BEM), and the finite difference method (FDM), or a combination of two or more of these methods. Although the two-dimensional equivalents (axisymmetric equivalent model, equivalent two-dimensional model, plane strain local model) are still frequently used because they lead to smaller numerical models in terms of the number of nodes and elements, they involve many conservative assumptions and have serious limitations (especially concerning ground motions within the pile group). Figure 1.11 shows the geometric modeling of a piled raft foundation in; plane deformations, axisymmetric, and three-dimensional. As shown in Figure 1.11a, the piles in the numerical modeling using 2D plane deformations, are assimilated to a continuous wall. Thus, they must be assigned an equivalent rigidity equals to that of a whole row of piles (Desai, 1974). The second method is illustrated in Figure 1-11b, where the pile configurations are likened to concentric rings. Studies using this method show that the load transfer mechanisms within the platform are found to be imperfectly modeled. However, resorting to 3D finite difference or finite element analyses seems to be the most reliable option, since complex geometries and multiple interactions can be explicitly considered. However, these numerical methods imply a greater discretization of the elements and require a large computation memory with high-speed processors.

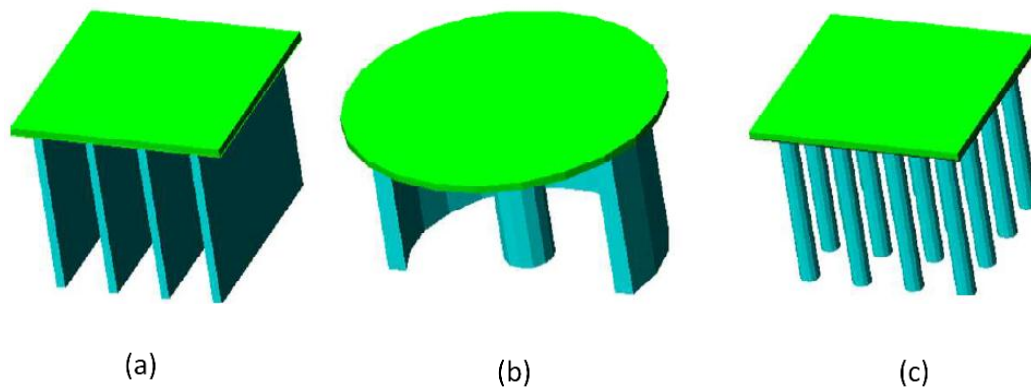


Figure 1.11 Simulation approaches of piled raft foundation, (a) plane deformations (b) axisymmetric, and (c) three-dimensional, adopted from Nguyen (2008)

1.4 A brief review of studies on piled raft foundations

This part summarizes various studies published in peer reviewed journals. These studies are classified into experimental and analytical studies.

1.4.1 Experimental studies

Kishida and Meyerhof (1965) analyzed model tests on pile groups and piled raft foundations with different configurations under central and eccentric loads in sands. They reported that the total bearing capacity of piled raft foundations can be estimated from the bearing capacity of the pile group taking into account the raft effect. This effect includes the bearing capacity of the raft and its overloading effect on the end bearing of the piles, using the entire raft for individual pile failure for groups with large spacing (Figure 1.12b). Or using the outside edge of the raft outside the equivalent area of the piles for bloc failure for groups with close spacing. (Figure 1.12a).

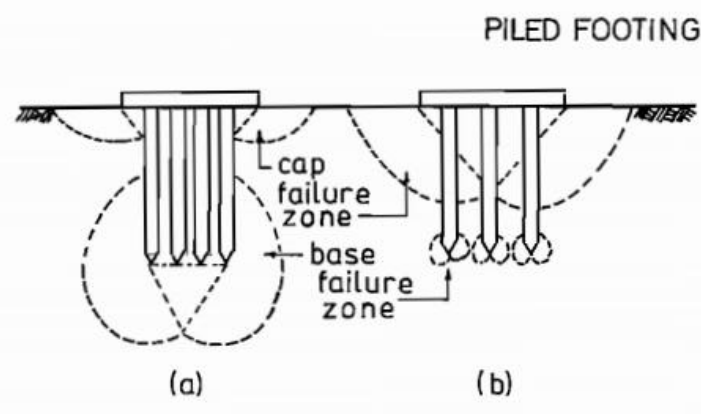


Figure 1.12 Failure zone of the piled raft foundation (a) equivalent pile failure (b) individual pile failure. (Kishida and Meyerhof 1965).

Akinmusuru (1980) carried out laboratory tests on a piled raft, pile group, and unpiled raft in dry sand and showed that the bearing capacity of the piled raft foundation exceeds the sum of the bearing capacity of the pile group and the unpiled raft. This is because the bearing capacity of the piles is increased by the raft pressure on the soil between piles (the pile-raft interaction effect). Besides, the author observed that the load-carrying capacity of the raft in the piled raft was similar to that of the unpiled raft. Based on these observations, the author proposed a formula (Eq. 1.33) for the bearing capacity of piled raft foundations:

$$Q_{pr} = \alpha \times Q_{gp} + Q_r \quad (1.33)$$

where Q_{pr} is the bearing capacity of the piled raft foundation, Q_{gp} is the bearing capacity of the pile group, Q_r is the bearing capacity of the unpiled raft, and α is the ratio of the load-carrying capacity of piles in the piled raft on the bearing capacity of the pile group (the pile-raft interaction effect). The author stated that α is always greater than unity. Where, α is influenced by pile length, pile spacing, soil conditions, and pile installation method.

Cooke (1986) performed an experimental study on different types of foundations such as unpiled raft, pile group, and piled raft foundations with different sizes in stiff clay. He found that the stiffness of the piled raft foundation increase by 30% to that of the pile group. He also observed that in the case of a rigid raft, the load distribution between piles under the rigid raft depends on their number and their spacing. The author stated that the corner piles and side piles support at least twice and 1.5 times the load carried by the inner piles, respectively.

Phung (1993) carried out field tests for different types of foundations, single pile, pile group, and piled raft in sandy soils. He found that the piled raft behavior is mainly governed by the raft-pile interaction, which causes an increase in the frictional resistance of the pile shaft due to the pressure of the raft on the ground. He concluded that the load sharing between the piles and the raft in the piled raft system generally depends on the construction procedure. This influence can be significant only at the initial loading process. He also reported that as soon as the raft comes into good contact with the piles and the soil surface, the load sharing will be governed by the settlement. For very low settlement, the piles take a large part of the load. For a settlement large enough to mobilize the full capacity of the piles, a considerable part of the applied load will be transferred to the raft. Subsequently, the load sharing between the components of the piled raft system becomes almost constant. However, the portion of the load carried by the raft and that taken by the piles also both increased. For the load distribution between the elements of a pile group or a piled raft foundation in the sandy soils,

the author showed that the inner piles often have a greater capacity compared to the corner pile and the edge pile. Phung also stated that the existing calculation methods, based on the theory of elasticity are inaccurate and unlikely to result in optimum design when predicting the behavior of the piled raft foundation in which the piles are close or in failure. So, the analysis methods based on the elastoplastic soil model are strongly needed.

It can be noted that there is a contrast between the results of the above studies regarding the load distribution between piles in the piled raft foundation. This can be attributed to the fact that the authors compared the load carried by each pile at a different level of the settlement where the load distribution between piles can depend on the settlement level.

Horikoshi and Randolph (1996) reported results of centrifuge tests on models of a flexible circular raft set on a group of piles embedded in clay. The authors focused on the differential settlement across the raft and the load transferred to the pile group. The general section of the centrifuge package is shown in Figure 1.13. They concluded that even a small group of piles can significantly reduce the differential settlement of the raft and they also showed that a small raft on piles could significantly increase the bearing capacity of the system, because of the direct transfer of load to the soil through the raft.

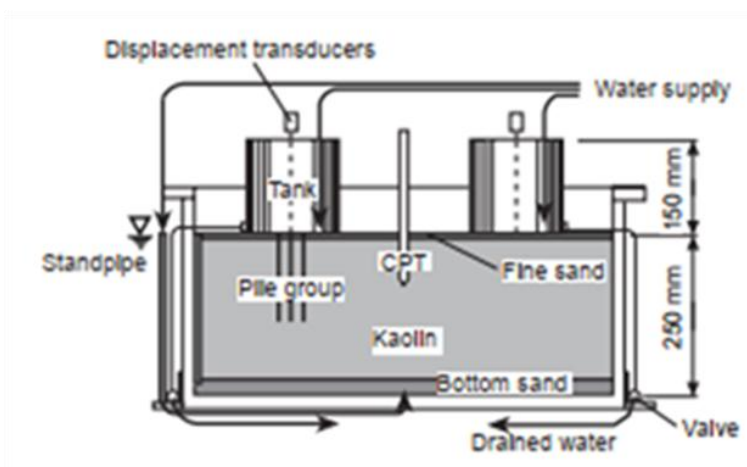


Figure 1.13 General section of centrifuge package (Horikoshi and Randolph,1996)

Conte et al. (2003) extended the experimental work of Horikoshi and Randolph (1996) and performed centrifuge tests on models of square pile groups and piled raft foundations in clay soil. They found that the central piles below the raft can be loaded near full capacity without compromising the stability of the foundation. They also found that the stiffness of piled raft foundation R_M increases with increasing factor parameters. and can be given as follows:

$$R_M = \frac{A_R}{A_g} \times \sqrt{\frac{n \times s}{L}} \quad (2.2)$$

where A_R is the raft surface, A_g is the planner section of the pile group, n is piles number, s is pile spacing, and L is pile length.

Lee and Chung (2005) performed model tests on pile group and piled raft foundations to assess the influence of the raft on pile group behavior. All the pile groups in this study consist of nine piles (3 x 3) driven into dense sand (Figure 1.14). They found that the pressure of the raft on the soil surface causes an increase in the frictional resistance of the pile shaft and this effect depends on the pile spacing and their positions.

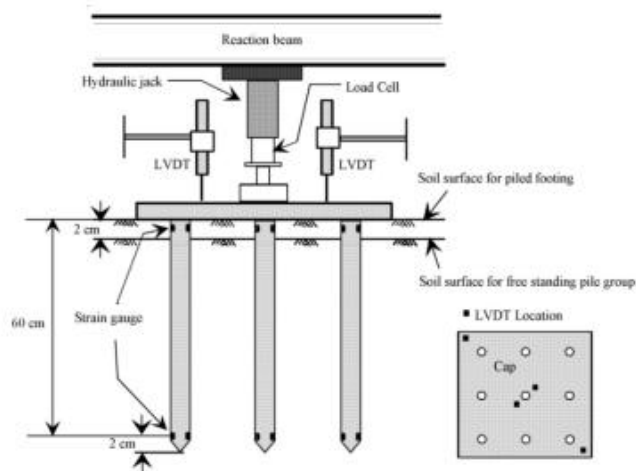


Figure 1.14 Diagram of the test setup (Lee et Chung, 2005)

Fioravante et al. (2008) carried out a centrifuge test on a circular raft set on piles embedded in an over-consolidated clay. They found that the load distribution between the piles below the raft is not uniform and the pile load transfer mechanism under a raft differed from that of a single pile. They also found that the contribution of the raft begins when the piles approach their ultimate capacity state. Moreover, the authors observed that raft settlement decreases with the increase in the number of piles.

The uniformity of the load distribution between piles beneath a raft should depend on the uniformity of the configuration of piles and can also depend on the raft shape and their rigidity.

Nguyen et al. (2013a) carried out an experimental study using a centrifuge test on models of piled raft foundations in dry sand. The same flexible raft was considered for two models of piled raft foundations set on the same number of piles in different piles arrangement, a uniform, and a concentrated pile arrangement. another model with a rigid raft set on

concentrated pile arrangement was also examined in this experimental test by the authors. To verify the reliability of these tests, they carried out numerical simulations using the Plaxis 3D software. Nguyen et al. (2013a) concluded that the concentrated pile arrangement case can lead to a decrease in total and differential settlements of about 30-40% compared to the uniform arrangement case. Besides, this case also makes it possible to reduce the bending moment and to limit the development of the maximum bending moment of the raft.

It should be mentioned that Cooke (1986) found that the corner piles and side piles support at least twice and 1.5 times the load carried by the inner piles, respectively. Therefore, the pile arrangement effect on the performance of the foundation should be identified as a function of settlement level, working state, and ultimate state.

Park and Lee (2014) performed a centrifuge test using different types of the foundation model in the sand of different densities. Single pile, pile group, unpiled raft, and piled raft foundations were adopted in the test to analyze the different interaction effects of the piled raft foundation. Figure 1.15 shows the schematic view of the conducted centrifuge test and model foundations. They observed that the load-settlement curves of piled raft foundations are similar to those of pile groups in the initial loading stage and have become similar to those of unpiled raft with increased loading. The interaction factors of the piled raft foundations all showed dependent variations with the settlement. So that the pile-raft, raft-pile interaction factors, and the pile group efficiency caused by the pile-pile interaction decreased with the initial range of settlement and increased with the increasing settlement. They found that the range of the pile-raft interaction factor is much larger than that of the raft-pile interaction factor. A schematic of different piled raft interactions is shown in Figure 1.16.

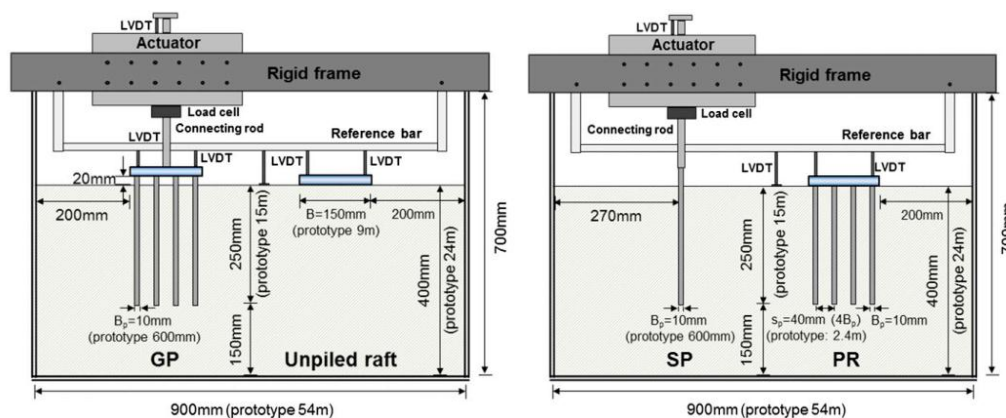


Figure 1.15 Schematic view of the centrifuge test and model foundations adapted from Park and Lee (2014)

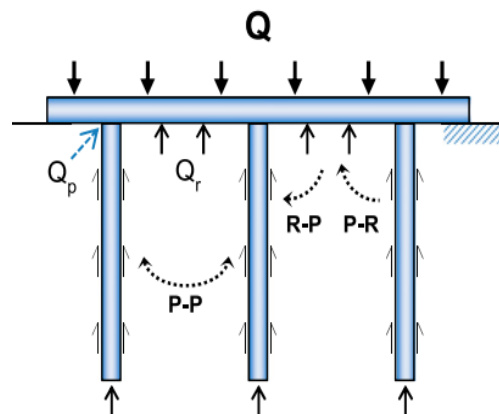


Figure 1.16 Schematic view of pile-pile, raft-pile, and pile-raft interactions for piled raft foundation (Park and Lee 2014)

Park and Lee (2015) performed centrifuge tests on different foundation models to assess the interaction effects of piled raft foundations in the case of soft and stiff clay conditions. They found that the pile group effect in clays is significant over the initial loading range and becomes less pronounced with the increasing settlement. According to the authors, the values of the interaction factors raft-pile, pile-raft varied initially, which converges to certain values around unity with the increasing settlement. The authors also reported that the decrease in the bearing capacity of the raft in piled raft foundation compared to that of the unpiled raft was due to the downward movement of the underlying soils near the surface, which resulted in a reduction of the contact pressure between the raft and the soil. The load distribution between piles in the piled raft is also studied in the experimental test. For the case of the stiff clay, the authors observed that the corner piles carried a higher portion of the load than the central piles. They explained that the lower load capacity of the central pile was due to the decrease in the shaft friction of the pile. However, the difference in the load responses of each pile in the group was not significant for the case of the soft clay.

In these two experimental tests of Park and Lee (2014, 2015), the effects of both pile-spacing and the number of piles on the interaction behavior of piled raft foundations are not studied. While these parameters should be the major factor in the piled raft foundation design.

Patil et al. (2015) conducted experimental laboratory tests to study the piled raft behavior under vertical loading in the case of sandy soil. Various models were considered including the unpiled raft and piled raft model with different pile configurations. Figure 1.17

shows the piled raft configurations considered in these experimental tests. The authors observed that the efficiency of the piled raft system in reducing settlement was minimal beyond a certain number of piles and that raft-soil stiffness has minimal effect on the load-settlement response for a given number of piles. However, the increase in the number of piles has a significant effect on the load-settlement response for a given raft-soil stiffness. Patil et al. (2015) concluded that the load carried by the raft in the piled raft decreases slightly with increasing the raft-soil stiffness for a given number of piles while, the increase in the number of piles decreases the contribution of the raft, for a given stiffness of the raft-soil.

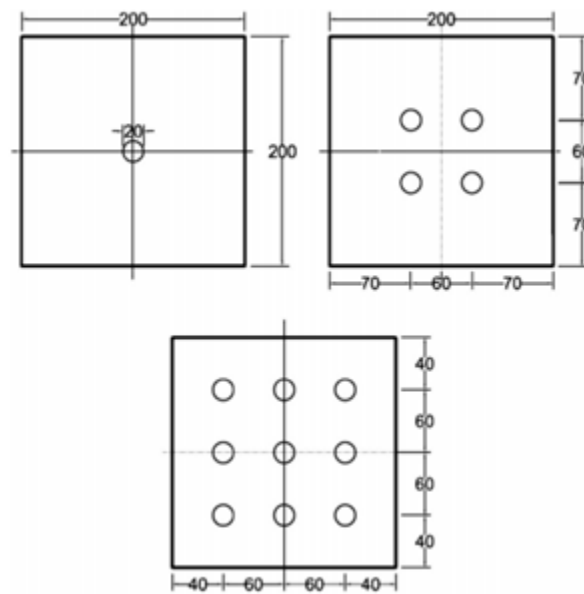


Figure 1.17 Piled raft configurations considered in these experimental tests (Patil et al. 2015)
(unit: mm)

1.4.2 Analytical and numerical studies

Hooper (1973) was the first who used the finite element method to understand the complex interaction of the piled raft foundations.

Zhuang and Lee (1994) used the finite element method to identify the load distribution between piles in the piled raft foundation. They noted that the load distribution between piles was affected by pile stiffness, raft stiffness, and pile length/width ratio. They also observed that as the pile length increases and the raft and piles stiffness decrease, the load distribution becomes more uniform.

Russo (1998) developed a numerical method for piled raft foundation, which considers the non-linearity of the unilateral contact at the interface between the raft and the soil, and the nonlinear load-settlement response. He reported that nonlinear analysis should be considered

for the piled raft foundation because piles serve as settlement reducers and their ultimate load capacity can be reached.

Poulos (2001) summarized the philosophy of using piles as settlement reducers and described the main requirements for piled raft foundation design methods. He made a comparison between the capacities and the limits of the current analysis methods of the piled raft behavior such as the simplified methods of analysis (the method of Poulos-Davis-Randolph (PDR) and the approach of Burland), approximate numerical methods (the Strip on Springs approach (GASP) and the Plate on Springs approach (GARP)) and the more rigorous numerical methods using the code FLAC 2D and 3D (Figure 1.18). He concluded that the simplified analytical methods can be used with some confidence for preliminary design purposes. However, the more complex analyses left for the detailed design phase, and that the two-dimensional analyses can lead to severe overestimates of settlement and pile loads due to the plane strain assumptions that are intrinsically present. Three-dimensional analyses are potentially the most accurate numerical methods available for the analysis of piled raft foundations. However, setting them up and running takes a long time. Moreover, Poulos noted that when the unpiled raft does not satisfy the design requirements, using a limited number of piles could improve the bearing capacity, the total and differential settlement behavior.

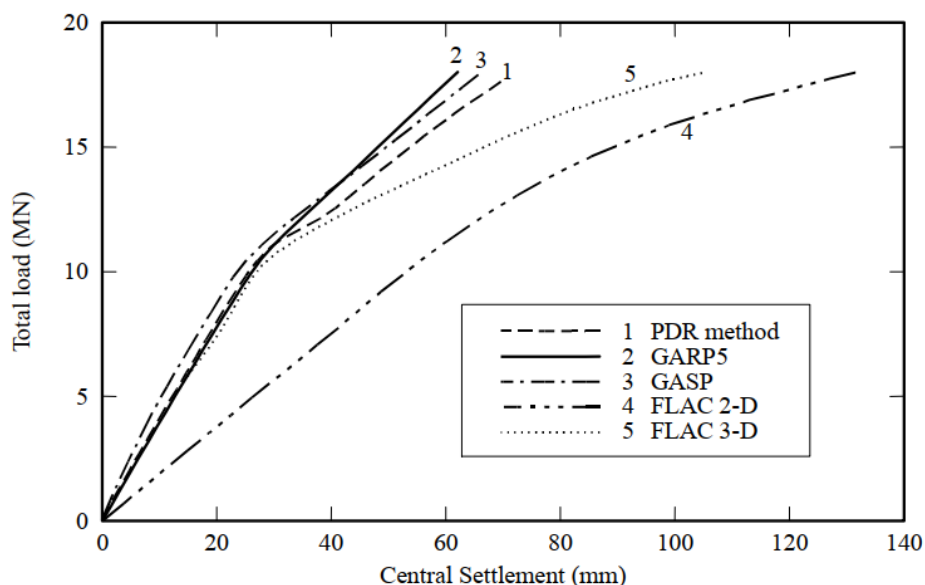


Figure 1.18 Comparison of different load-settlement analysis methods (Poulos 2001)

Reul and Randolph (2003) carried out an analysis of piled raft foundation embedded in an over-consolidated clay using the 3D finite element method. They observed that the raft-pile

interaction leads to an increase in the friction of the shaft of the piles with an increase in load or an increase in settlement.

de Sanctis and Mandolini (2006) performed a parametric study on various configurations of piled raft foundations using 3D finite element analysis. The authors focused on developing a simple conception to evaluate the bearing capacity of a piled raft foundation as a function of the unpiled raft and pile group bearing capacities, which can be simply evaluated by conventional bearing capacity theories. Figure 1.19 shows the piled raft configurations considered in this parametric study and also illustrates the mesh around the piles. Based on the numerical results, de Sanctis and Mandolini (2006) proposed a formula for the failure load coefficient η_r representing the effect of piles on the performance of the raft in the piled raft. They also suggested a value of unity for the failure load coefficient η_p representing the effect of the raft on the performance of the piles in the piled raft.

The suggestion of de Sanctis and Mandolini (2006), maybe limited for soft clays and under undrained conditions. However, for drained conditions, the interaction coefficient η_p may not be equal to 1 due to changes in the confinement stresses caused by the raft pressure on the soil surface, consequently an increase in the lateral friction resistance of piles.

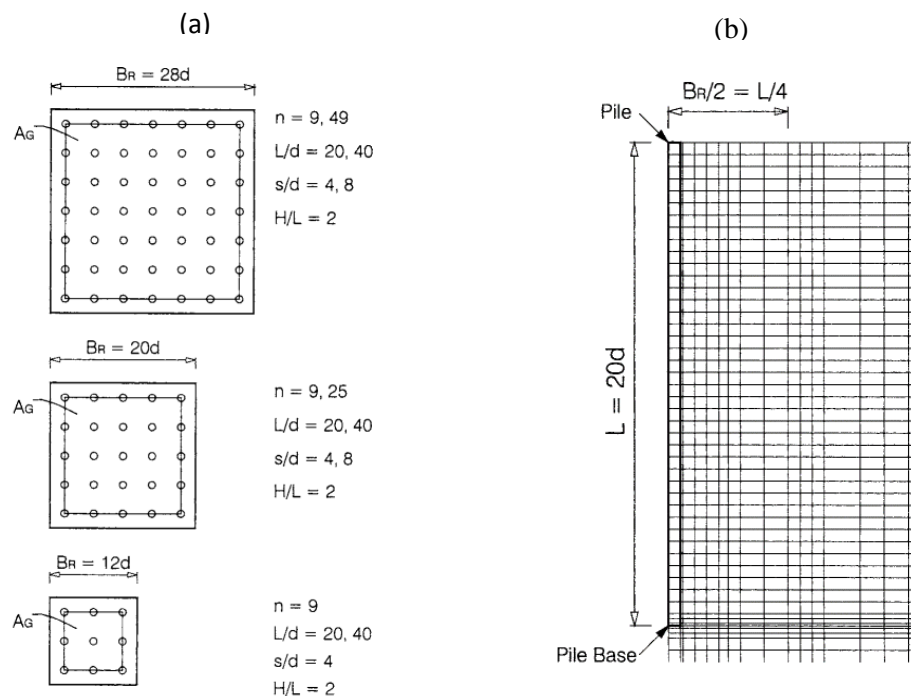


Figure 1.19 3D Parametric study of (a) piled raft configurations (b) finite element mesh around the pile (de Sanctis and Mandolini 2006)

Lee et al. (2010) carried out a series of 3D elastoplastic finite element analyses to study the behavior of the bearing capacity of a piled raft foundation subjected to vertical loading in soft and stiff clays by varying several parameters such as the pile configurations and length of the piles using different loading types. The 3D finite element mesh and the considered boundary conditions are shown in Figure 1.20. Lee et al. (2010) concluded that in clays, the use of a limited number of strategically-located piles could improve the bearing capacity and settlement performance of the foundation. The authors reported that the average settlement ratio decreases nonlinearly with the increase of the factor of safety and is influenced by the soil rigidity.

Nevertheless, because of the large amount of storage and the time needed in the 3D computations, the effects of soil conditions and pile configurations are not studied sufficiently, and the design formulas that can account for the settlement variation characteristics with the overall factor of safety of piled raft foundation under different soil conditions are not done.

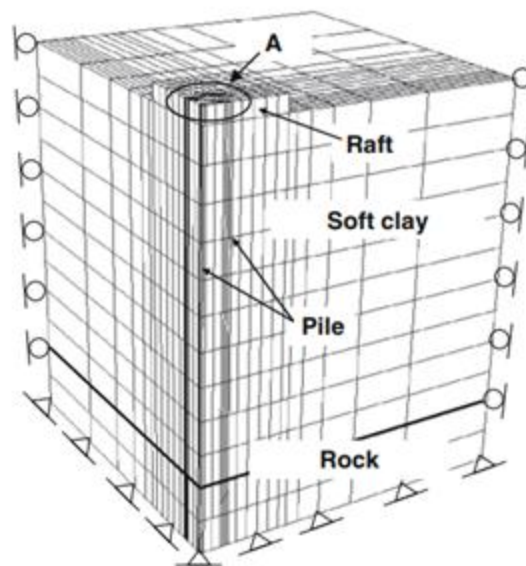


Figure 1.20 Typical mesh and boundary condition (Lee et al. 2010)

Cho et al. (2012) extended the research work of Lee et al. (2010) focusing on the load-settlement response of the piled raft foundation in clays using 3D finite element analyses. They found that the average settlement can be effectively reduced with wider pile spacing under the same number of piles. Moreover, the efficiency of piles in a piled raft foundation was maximized when the magnitude of the total applied load was similar to the ultimate load capacity of the pile groups. They also showed that the reduction ratio of soft clay (the ratio

between the average settlement of the piled raft foundation and the average settlement of the unpiled raft) was relatively smaller than that of stiff clay, although the real average settlement in the case of soft clay is larger than that in the case of stiff clay. The authors found that differential settlement was impressed not only by the number and length of piles but also by the load level.

Based on an analytical solution to investigate the load-settlement response and the bearing capacity behavior of the piled raft foundation by focusing on the nonlinear behavior of the load sharing between the raft and piles in piled raft foundations, Lee et al. (2014) proposed a load-sharing model using the nonlinear load–settlement response considering piled raft interaction effect by introducing a load capacity interaction factor (β). Based on the suggested load-sharing model, the load-sharing ratio α_p decreases considerably at an initial settlement level beyond which α_p decreases slightly as the settlement further increases.

The same authors also reported that the interaction effects of the piled raft foundations are not very significant for clay soils ($\beta = 1$), based on the results of the centrifuge test performed in their study. This may be limited in their case where the centrifuge test was performed for a given number and spacing of piles, although the interaction effects of piled raft foundations are influenced by various design parameters such as the number of piles and the pile spacing (Cooke 1986; Poulos 2001).

In 2015, the authors performed a series of 3D finite element analyses using the Plaxis software, to study the load-settlement response and the bearing capacity of the piled raft foundation embedded in sandy soils. They stated that the interaction effects of the piled raft foundation are significant in the case of sandy soils and that the unit value for the β factor may be limited for clay soils. Based on the numerical results, they proposed a design of the factor β as a function of settlement.

Using 3D finite element analysis, Park et al. (2016) studied the load-sharing behavior of the piled raft foundation installed with driven piles in sand. Various foundation types and pile configurations were considered in the analyses as shown in Figure 1.21. The authors aimed to identify the effect of the piles' installation method on the load sharing of the piled raft foundation. They observed that the values of the load sharing ratio in the case of driven piles were higher than those in the case of bored piles at the initial settlement level. However, after this level of settlement, the load sharing behavior becomes very similar in both cases of driven or bored piles. Therefore, they concluded that the load sharing model proposed by Lee et al. (2015) can be applied either in the case of driven or bored piles.

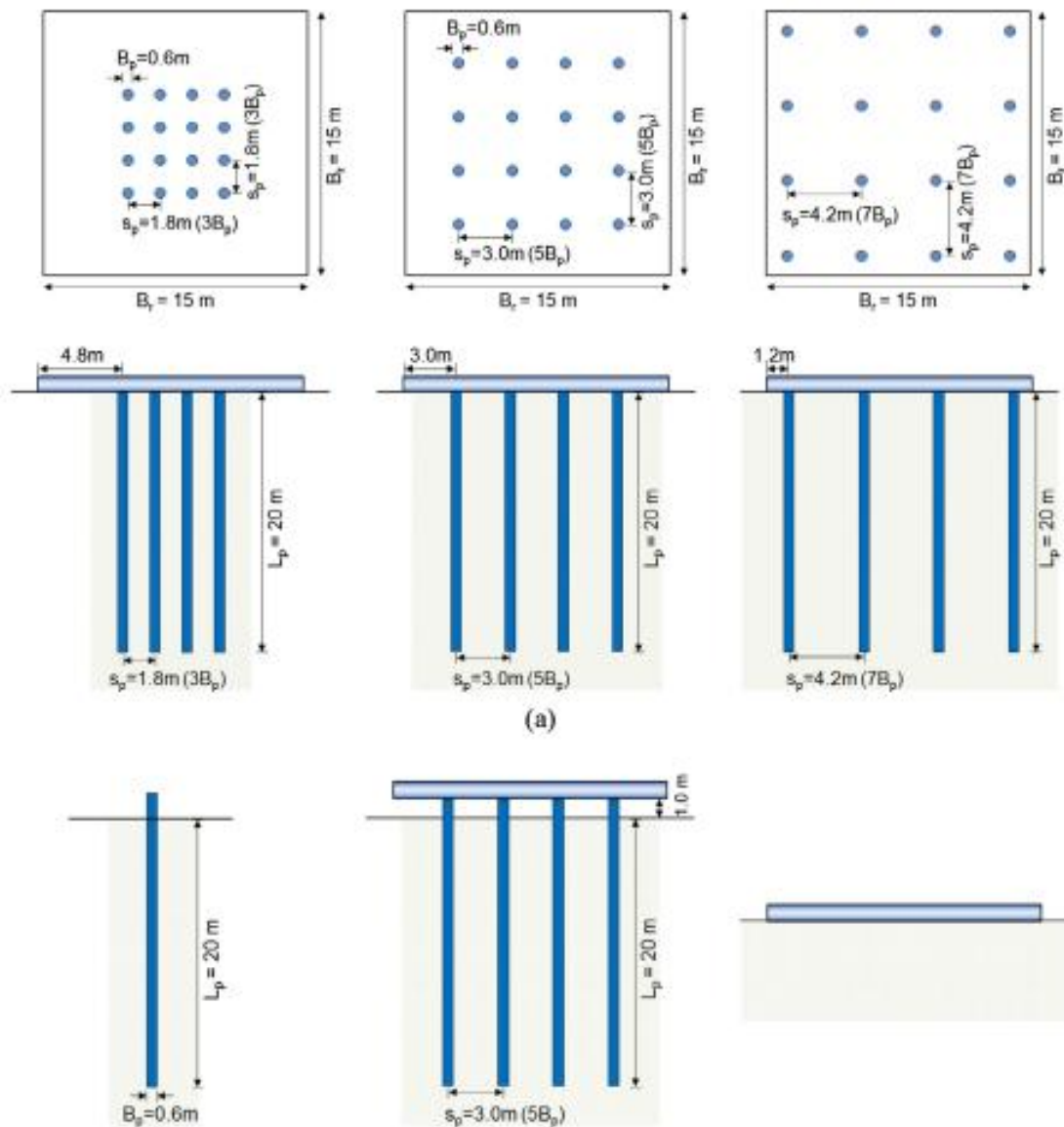


Figure 1.21 Pile configurations foundation types are considered in the numerical analysis carried out by Park et al. (2016).

Alshenawy et al. (2016) performed a series of 3D numerical analyses using the finite element method to study the load sharing ratio α_p of the piled raft foundation in the case of sandy soils. They concluded that the α_p ratio increases when the load-settlement curve is linear and decreases when the curve is nonlinear. They also found that the sand density is not the governing factor affecting the increase or decrease in the α_p ratio. Additionally, the influence of the incremental increase in pile length on the α_p ratio is more pronounced in short piles. The authors reported that the raft thickness has a negligible effect on the α_p , while the coefficient α_p decreases with the increase in the pile spacing.

The increase or the decrease of the load sharing ratio depends on the bearing capacity of piles. Wherein, the α_p ratio increases for a very low settlement range, which is not enough to mobilize the full capacity of the piles. However, for a settlement large enough to mobilize the full capacity of the piles, a considerable part of the applied load will be transferred to the raft (Phung 1993), consequently the α_p ratio increases. Moreover, Alshenawy et al. (2016) reported that the raft is assumed to be rigid for all considered thicknesses and therefore, no noticeable effect of the raft thickness on the α_p was noted.

Sinha and Hanna (2016) developed a 3D finite element model to examine the effect of governing parameters on the performance of piled raft foundations. Based on this developed model, they performed a parametric study using Abaqus software. From the results of this model, they concluded that a mesh of 30 times the pile diameter and twice its length is sufficient to examine the stated problem without boundary effects. However, the distance of the lateral borders should be proportional to the width of the raft not to the diameter of the pile, and also to the loading rate. They also found that the raft settlement increases with increasing pile spacing and decreases with increasing pile diameter (d) and length (L). The authors reported that for a pile spacing S_p greater than $6d$, the piled raft foundation tends to behave as an unpiled raft. It should be noted that despite the case of a very wide pile spacing ($S_p > 6d$), the increase in the number of piles can significantly affect the bearing capacity and the settlement performance of the raft.

Alnuaim et al. (2017) examined the performance of the piled raft foundation subjected to a vertical load and installed in sand, using a 3D finite element model to evaluate the effects of certain parameters on the load sharing mechanism such as raft thickness and width, pile diameter and spacing. The proposed modelling procedure was validated using experimental results from centrifuge tests. The authors found that the load carried by piles in the piled raft foundation was higher for the cases of the piled raft with a rigid raft compared to the case of a flexible raft. They explained that by the minimal interaction between the raft and the soil surface and that the load transmitted by the raft increased when the raft width increases. Also, they concluded that the portion of the load carried by the piles increased with the increase in the diameter of the pile.

Ghalesari and Choobbasti (2018) performed a parametric study using a 3D finite element method to study the settlement and bearing behavior of the piled raft foundation in clay. They found that the performance of the piled raft foundation is affected by the underlying soil conditions. Wherein, installing the foundation in a more rigid clay with higher

plasticity (CH) not only helps to improve the bearing capacity of the foundation but also decreases the average and differential settlements. The authors also reported that the pile arrangement and the geometry of the piled raft foundation have important effects on the bearing capacity and settlement performance. Although the performance of the piled raft foundation improved with the increase of the number and the length of the piles, and the raft thickness, there is an extent to which the increase in these parameters has little improvement effects. The authors also observed that for a given number of piles, increasing the pile spacing increases the bearing capacity of the foundation while the pile diameter has no significant effect on the bearing capacity. They concluded that the pile length is the most effective factor in determining the bearing capacity of a piled raft foundation.

Deb and Pal (2019) carried out a 3D parametric study using the finite element analysis for different types of foundations, piled raft, pile group, and unpiled raft, in clayey soil underlain by sandy soil taking various design parameters. In this parametric study, the authors developed prediction models to assess the load sharing ratio and interaction factors for piled raft foundations, subjected to vertical load, taking into account both safety and service conditions. However, because of the combined nature of the piled raft foundation, the failure interaction factors should be evaluated with caution, taking into account the different component sizes of the piled raft system which was not considered by the authors in this study.

Mali and Singh (2018) used a 3D numerical model to investigate the effect of various parameters such as spacing, length, and diameter of piles, and raft-soil stiffness ratio on the settlement, load-sharing, bending moments, and shear force behavior of large piled raft foundation. Different pile configurations were considered by the authors. Based on the obtained results, they reported that the average and differential settlement ratio decreased markedly with the increase of pile spacing up to $5d - 6d$ beyond which, it increased progressively. They observed that piled raft with the lower raft-soil stiffness ratio and larger pile group to raft width ratio was influential in decreasing the average settlement ratio. The authors also stated that the load sharing ratio decreased with the increase in pile spacing, and it is proportional to the pile length. While the bending moment ratio is proportional to pile spacing, and decreases with the increase in pile length up to pile group to raft width ratio of about 0.6 beyond which, it increased.

1.5 Summary

This chapter reviewed the literature on the analysis methods of the piled raft foundation where a classification of the analysis methods for the behavior of piled raft foundations is presented. The advantages and the limitations of each method are also outlined in this chapter. As concluded by several researchers such as Poulos, Randolph, or other recent researchers, only the 3D numerical analysis seem to be the most efficient tool to simulate the complex behavior of this system of foundations. Consequently, it is essential to perform a 3D modeling of the piled raft foundation with variation of the pile configurations, to correctly analyze the behavior of the piled raft interactions. Thus in the following chapters, we are interested in using 3D numerical modeling methods to provide further insight into the mechanical response of piled raft which helps the engineers to take a logical path in an iterative design process for a piled raft foundation.

According to all of these recent studies on the piled raft foundations reviewed in this chapter, a considerable number of research studies on the behavior of piled-raft foundations were carried out. Important contributions were made to study different aspects of piled-raft foundations, mainly for the resistant soils such as sands or stiff clays in comparison with those conducted for soft clay. However, most of these models are complicated due to the use of complex analytical and numerical approaches.

Despite the research effort carried out to date to assess the piled raft behavior and their encouraging results, limited research has been dedicated to the development of an optimal analytical design methodology based on numerical methods. The analytical design methodology was developed only to access the overall settlement of the piled raft foundation, but the forecasting of differential settlement is yet to be developed. Also, simple design models for the ultimate bearing capacity of piled raft are yet to be developed.

For design optimization purposes, further studies are required to provide further insights into the mechanical response and especially the interaction behavior of piled raft system. This also will help the engineers into taking a logical path in an iterative design process for a piled raft foundation. Nevertheless, to study the behavior of piled raft foundation system by using the numerical tools (FEM, FDM...), only 3D analysis can provide the optimal design methodology for the complex behavior of piled raft system.

CHAPTER 2

OVERVIEW OF THE NUMERICAL TOOL USED AND THE CONSTITUTIVE MODELS

2.1 Introduction

The constitutive models used in this thesis as well as the $FLAC^{3D}$ code (Itasca 2013), employed to develop the numerical simulations, will be presented in this chapter.

The numerical simulation of the behavior of a piled raft foundation, which is a combined nature of raft and piles that behave as a unit, a complex system is, which presents in particular, the extreme nonlinearities, and the multiple interactions between the raft-piles-soil and the three-dimensional geometry. These complex conditions require a well-adapted numerical tool. The present chapter presents the principles of the $FLAC^{3D}$ code which was used for our three-dimensional simulations.

$FLAC^{3D}$ is a three-dimensional explicit finite-difference program for engineering mechanics computation, especially for the soil mechanics problems. The code offers a wide range of capabilities to solve complex problems in mechanics, and especially in geomechanics. $FLAC^{3D}$ embodies special numerical representations for the mechanical response of geologic materials.

The writing of this chapter owes a lot to the $FLAC^{3D}$ manual, edited by Itasca (2013).

2.2 Constitutive models

This paragraph will be devoted to the presentation of the different rheological laws governing the behavior of soils. First, a brief description of the expressions for the case of isotropic and then orthotropic linear elasticity will be presented. After that, the basis for the formulation of an elastoplastic law will be laid. Finally, this chapter is interested in a perfectly plastic elastic model assuming as failure criterion that of Mohr-Coulomb.

2.2.1 Elastic model group

a. Elastic, isotropic model

In this elastic, isotropic model, strain increments generate stress increments according to the linear and reversible law of Hooke:

$$\Delta\sigma_{ij} = 2G\Delta\epsilon_{ij} + \alpha_2\Delta\epsilon_{kk}\delta_{ij} \quad (2.1)$$

where the Einstein summation convention applies, δ_{ij} is the Kronecker delta symbol, and α_2 is a material constant related to the bulk modulus, K , and shear modulus, G , as

$$\alpha_2 = K - \frac{2}{3}G \quad (2.2)$$

New stress values are then obtained from the relation

$$\sigma_{ij}^N = \sigma_{ij} + \Delta\sigma_{ij} \quad (2.3)$$

In the FLAC^{3D} code, as above, the writing of the behavior models uses the bulk modulus K and shear modulus G , rather than the Young Modulus E and the Poisson's ν ratio, the relations between these various parameters are expressed as follows:

$$K = \frac{E}{3(1-2\nu)} \quad (2.4)$$

$$G = \frac{E}{2(1+\nu)} \quad (2.5)$$

b. Elastic, Orthotropic Model

The orthotropic model accounts for three orthogonal planes of elastic symmetry. Principal coordinate axes of elasticity, labeled 1', 2', 3' are defined in the directions normal to those planes.

The incremental strain-stress relations in the local axes have the form

$$\begin{Bmatrix} \Delta\epsilon'_{11} \\ \Delta\epsilon'_{22} \\ \Delta\epsilon'_{33} \\ 2\Delta\epsilon'_{12} \\ 2\Delta\epsilon'_{13} \\ 2\Delta\epsilon'_{23} \end{Bmatrix} = \begin{bmatrix} \frac{1}{E_1} & -\frac{\nu_{12}}{E_2} & -\frac{\nu_{13}}{E_3} & & & \\ -\frac{\nu_{21}}{E_1} & \frac{1}{E_2} & -\frac{\nu_{23}}{E_3} & & & \\ -\frac{\nu_{31}}{E_1} & -\frac{\nu_{32}}{E_2} & \frac{1}{E_3} & & & \\ & & & \frac{1}{G_{12}} & & \\ & & & & \frac{1}{G_{13}} & \\ & & & & & \frac{1}{G_{23}} \end{bmatrix} \begin{Bmatrix} \Delta\sigma'_{11} \\ \Delta\sigma'_{22} \\ \Delta\sigma'_{33} \\ \Delta\sigma'_{12} \\ \Delta\sigma'_{13} \\ \Delta\sigma'_{23} \end{Bmatrix} \quad (2.6)$$

where the model involves nine independent elastic constants:

E_1, E_2, E_3 are Young's moduli in the directions of the local axes; G_{23}, G_{13}, G_{12} are Shear moduli in planes parallel to the local coordinate planes; and $\nu_{12}, \nu_{13}, \nu_{23}$ are Poisson's ratio where ν_{ij} characterizes lateral contraction in local direction i' caused by tensile stress in local direction j' .

By virtue of the symmetry of the strain-stress matrix, we have

$$\begin{aligned} \frac{\nu_{21}}{E_1} &= \frac{\nu_{12}}{E_2} \\ \frac{\nu_{31}}{E_1} &= \frac{\nu_{13}}{E_3} \\ \frac{\nu_{32}}{E_2} &= \frac{\nu_{23}}{E_3} \end{aligned} \quad (2.7)$$

In addition to those nine properties, the user prescribes the orientation of the local axes by giving the dip and dip direction of the (1', 2') plane and the rotation angle between the 1' axis and the dip direction vector (defined in positive sense from the dip direction vector). Default values for all properties are zero.

In the $FLAC^{3D}$ implementation of this model, the local stiffness matrix $[K']$ is found by inversion of the symmetric matrix in Eq. (2.6). Using $\Delta[\sigma']$ and $\Delta[\varepsilon']$ to represent the incremental stress and strain vectors present in the right and left members of Eq. (2.6), it may write as follows:

$$\Delta[\sigma'] = [K']\Delta[\varepsilon'] \quad (2.8)$$

In the global axes, the incremental stress-strain relations may be expressed as

$$\Delta[\sigma] = [K]\Delta[\varepsilon] \quad (2.9)$$

In $FLAC^{3D}$, the global stiffness matrix $[K]$ is calculated by applying a transformation of the form

$$[K] = [Q]^T[Q'][Q] \quad (2.10)$$

where $[Q]$ is a suitable 6×6 matrix involving direction cosines of local axes in global axes (Q is derived from the relations $\sigma'_{ij} = c_{ik} \times \sigma_{kl} \times c_{jl}$ where c_{ij} is direction cosine j of local axis i).

In particular, if the local axes are obtained from the global axes by positive rotation through an angle θ about the common $3 \equiv 3'$ axis, we have

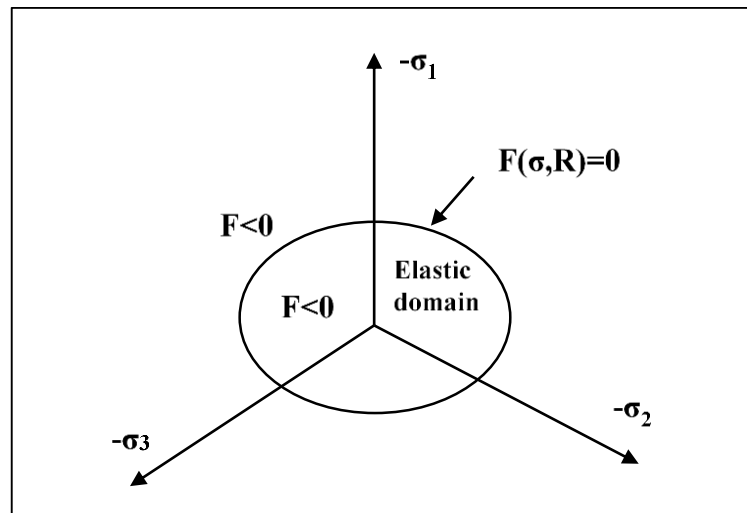


Figure 2.1 Load surface concept

Three cases of figure therefore arise:

- $F < 0$. Inside the surface, this domain is elastic;
- $F = 0$. The elastic strains can be, possibly, accompanied by plastic strains;
- $F > 0$. State of stresses physically impossible in elasto-plasticity.

When the point representative of the state of the stresses reaches the load surface $F = 0$, two cases of elastoplastic behaviors are possible (Figure 2.1):

- The load surface does not change and the expression of the load surface, therefore, does not contain a hardening parameter;
- The load surface changes during loading (elastoplastic model with hardening).

b. Hardening rule concept

The hardening of material results in the evolution of the surface of the threshold of plasticity. The uniaxial traction (or compression) test (Figure 2.2) will allow us to describe this notion of hardening.

- **Isotropic hardening**

The hardening is called to be isotropic, when the evolution of the load surface is governed by only one scalar parameter, e.g., the cumulated plastic strain (Figure 2.3).

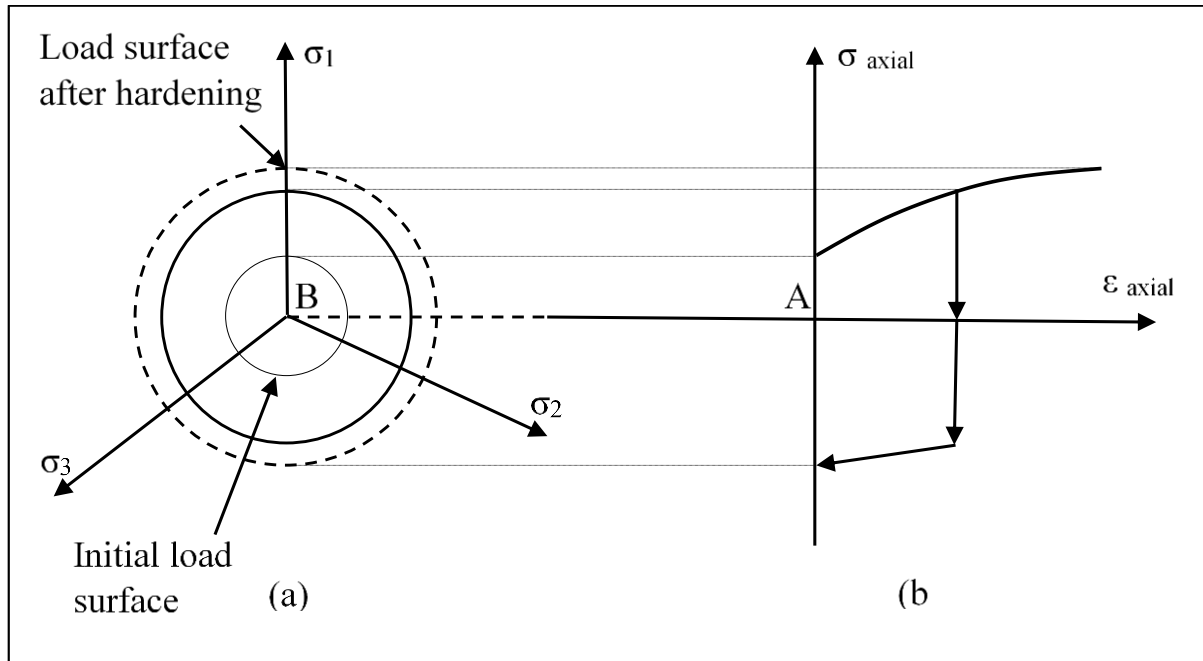


Figure 2.3 Description of isotropic hardening in projection: (a) in the deviatoric plane; (b) in the plane $\sigma_{axial} - \epsilon_{axial}$ in simple traction-compression.

Thus, in the plane $\sigma_{axial} - \epsilon_{axial}$ in simple traction and compression, the traction diagram succeeding that of compression is deduced from the latter by a homothety of the report (-1) and of the center, the point of null stress (point A of Figure 2.3). In the deflection plane, the load surface increases homothetically compared to point B.

- **Kinematic hardening**

The elasticity domain delimited by the load surface moves by translation in the space of the principal stresses (Figure 2.4) and without distortion of the initial load surface. the hardening, in this case, is characterized by a tensor variable defining the center of the load surface.

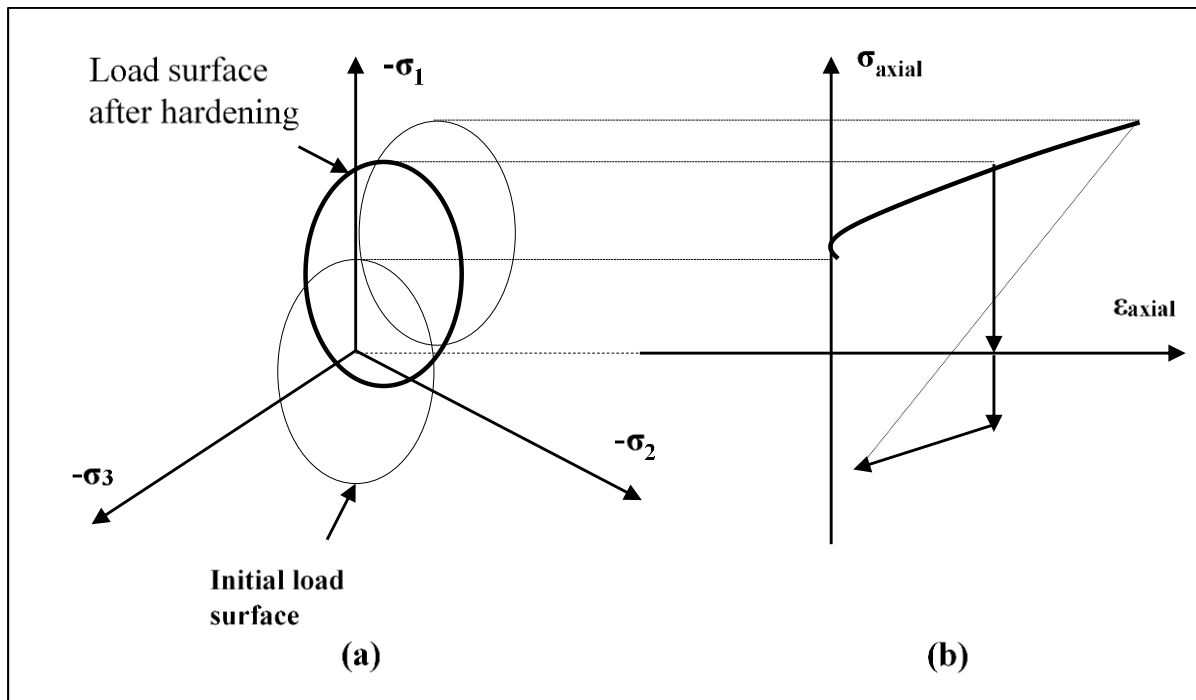


Figure 2.4 Description of kinematic hardening in projection: (a) in the deviatoric plane; (b) in the plane $\sigma_{axial} - \epsilon_{axial}$ in simple traction-compression.

- **Mixed hardening**

For anisotropic hardening, the load surface can sustain in addition to expansion/contraction and translation, rotation, and strain.

c. Flow rule concept

The plastic strain increment is characterized by its direction and its amplitude, the direction of the plastic strain increment is perpendicular to the surface defining the plastic potential $G(\sigma_{ij}) = 0$. The general shape of the plastic strain increment is given by Eq. 2.11 cited above. The flow rule is said to be either associated or non-associated.

- **Associated flow rules**

The flow rule is said to be associated with the load surface when the latter coincides with the surface representative of the plastic potential, which naturally amounts to considering $F = G$.

The direction of the plastic strain vector, in the space of the principal strains (confused with that of the principal stresses), is thus perpendicular to the load surface, $F = 0$, which means that to the gradient vector, normal to this surface. This leads to a flow rule of the form.

$$\varepsilon_{ij}^p = \lambda \frac{\partial F}{\partial \sigma_{ij}} \quad (2.14)$$

where

λ is the plastic multiplier (positive scalar)

For a stress state σ such as $F = 0$, two cases are possible:

1st case:

$$F(\sigma, R) = 0$$

$$\frac{\partial F(\sigma, R)}{\partial \sigma} d\sigma < 0$$

$$d\varepsilon = d\varepsilon^e \text{ and therefore } d\varepsilon^p = 0$$

This is a case of unloading and the stress increment is directed towards the interior of the current elastic domain.

2nd case:

$$F(\sigma, R) = 0$$

$$\frac{\partial F(\sigma, R)}{\partial \sigma} d\sigma > 0$$

$$d\varepsilon = d\varepsilon^e + d\varepsilon^p$$

This is a loading case and the stress increment is directed outside the current elastic domain.

The materials for which the flow rule is said to be associated, are declared to be standard. This is the case with metals or purely coherent soils.

- **Non-associated flow rules**

In the case of cohesionless soils, the flow rules are not associated. In this case, the direction of the plastic strain vector is perpendicular to the surface representative of the plastic potential, $G(\sigma_{ij}) = 0$ which is distinct from that representative of the function of plastic load $F(\sigma_{ij}) = 0$.

2.2.3 Mohr-Coulomb Model (linear elastic perfectly plastic model)

This is the model used in this thesis to represent the shear failure of the subgrade. This constitutive law is characterized by an isotropic linear elasticity of Hooke (E, ν), a load

surface $F(\sigma_{ij})$, and a plastic potential $G(\sigma_{ij})$. This is a 5-parameter model. Including 2 elastic parameters: E and ν , and 3 failure parameters (c , φ , and ψ) such as:

E : Young's modulus;

ν : Poisson coefficient;

c : Cohesion;

φ : Friction angle;

ψ : Dilation angle.

In Mohr's plane, the shape of the envelope curve of this criterion is a line called the equation coulomb line:

$$\tau = c + \sigma_n \tan(\varphi) \quad (2.15)$$

where

σ_n and τ correspond respectively to the normal stress and the shear stress on a given surface.

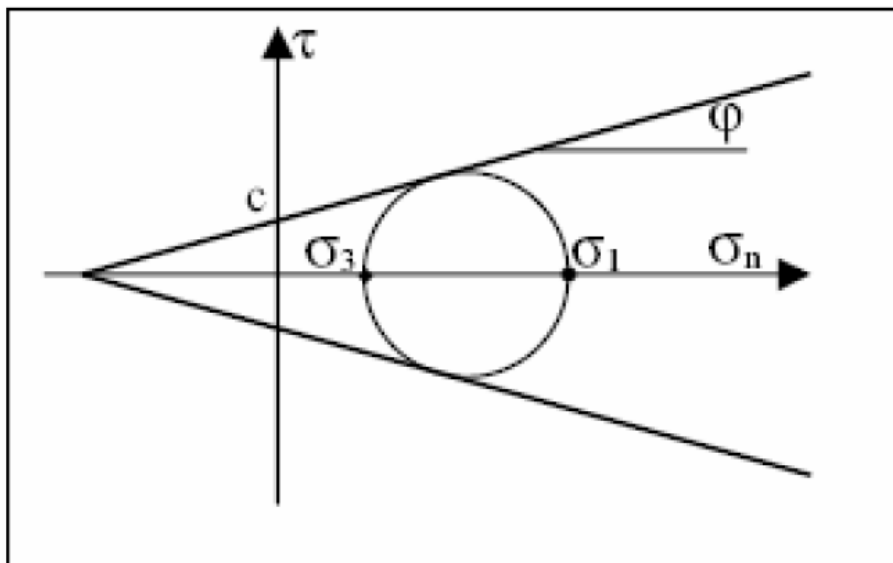


Figure 2.5 Representation of the Mohr-Coulomb criterion in the Mohr plane.

The representation of this criterion in the Mohr plane is given in Figure 2.5. The intermediate constraint σ_2 does not intervene in its formulation. In the case of a purely coherent material ($\varphi = 0$), it is said to be the Tresca criterion.

In the space of principal constraints, the area defined by the load function is a pyramid of which axis is the tri-sector, as shown in Figure 2.6. Its section in the deviatoric plane is an

irregular hexagon, comparable to that of the Tresca criterion (which is a particular case of Mohr-Coulomb when $\phi = 0$).

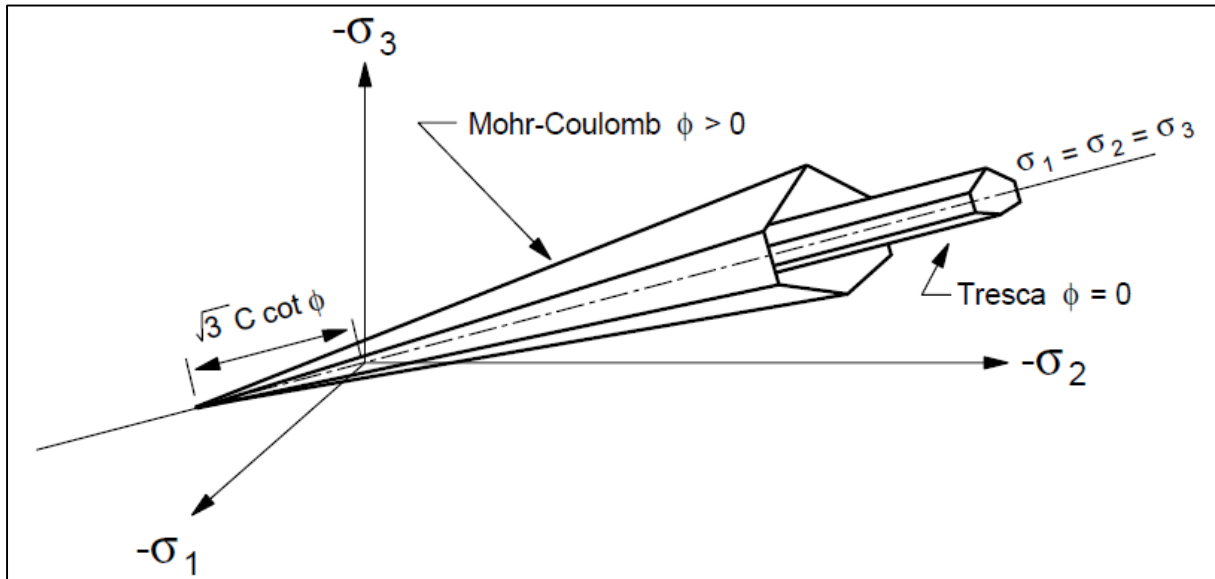


Figure 2.6 Mohr-Coulomb and Tresca yield surfaces in principal stresses space, (Itasca 2013)

The analytical expression of one of the planes of the pyramid, as a function of the principal stresses, is given by:

$$F(\sigma_1, \sigma_2, \sigma_3) = \sigma_1 - \frac{1+\sin \phi}{1-\sin \phi} \sigma_3 - \frac{2c \cos \phi}{1-\sin \phi} \quad (2.16)$$

where

σ_1 is the major principal stress; σ_3 is the minor principal stress.

Another parameter that can be taken into consideration, σ_t tensile strength, which corresponds to the introduction of an additional criterion (with its own flow rule) and thus modifies the initial model of Mohr-Coulomb which does not take into account this parameter.

The plastic shear potential corresponds to a non-associated flow law described by the equation:

$$G(\sigma_1, \sigma_2, \sigma_3) = \sigma_1 - \frac{1+\sin \psi}{1-\sin \psi} \sigma_3 \quad (2.17)$$

When the friction angle ϕ and the dilation angle ψ are equal, the flow rule is said to be associated.

The dilatancy is the change in volume that occurs with shear distortion of a material. Dilatancy is characterized by a dilation angle, ψ , which is related to the ratio of plastic volume change to plastic shear strain. This angle can be specified in the Mohr-Coulomb ubiquitous-

joint and strain-hardening/softening models in $FLAC^{3D}$. Dilation angle is typically determined from triaxial tests or shear-box tests. For example, the idealized relation for dilatancy, based upon the Mohr-Coulomb failure surface, is depicted for a triaxial test in Figure 2.7. The dilation angle is found from the plot of volumetric strain versus axial strain. Note that the initial slope for this plot corresponds to the elastic regime, while the slope used to measure the dilation angle corresponds to the plastic regime.

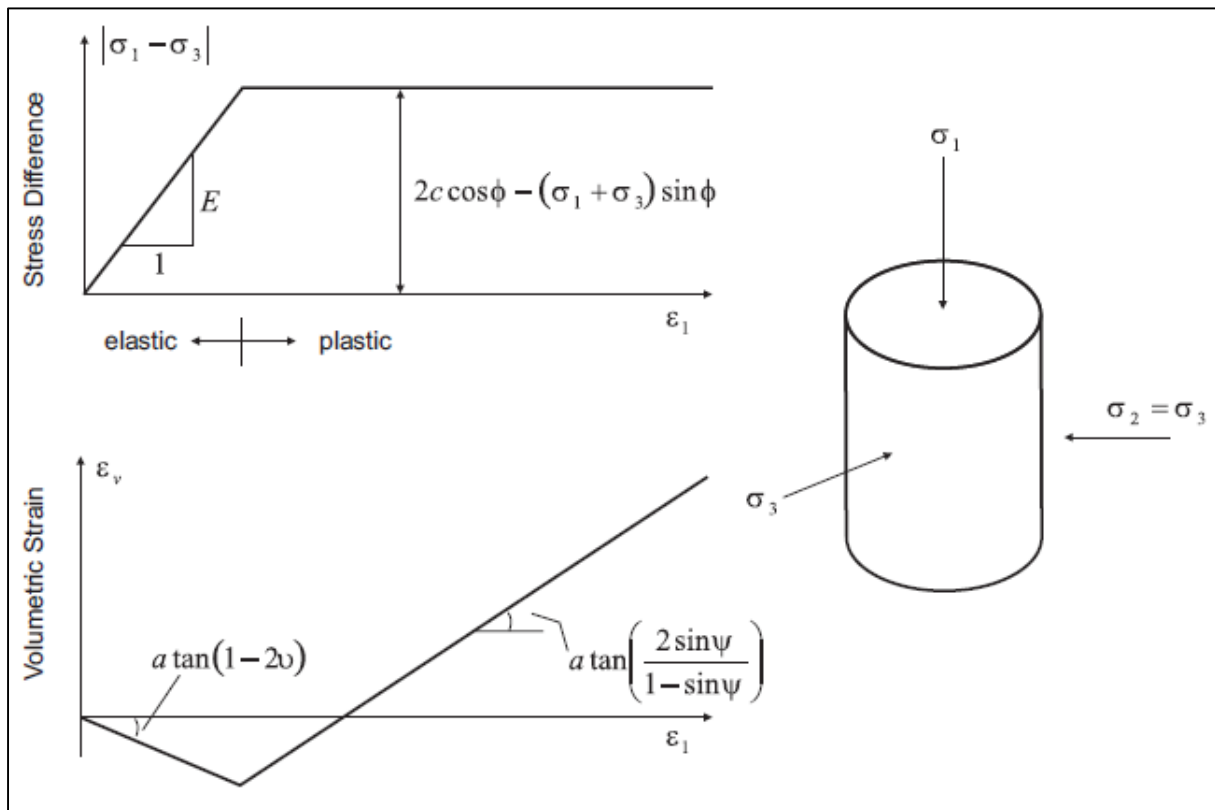


Figure 2.7 Modeling of dilation ψ from the triaxial test (Vermeer and de Borst, 1984)

For materials with internal friction of which plasticity criterion is of the Mohr-Coulomb type, an associated flow rule generally leads to overestimating the swelling which accompanies plasticization by shear. The bad agreement between the experiment and the calculations explains the introduction of the non-associated flow rules, of which plastic deformations derive from a plastic potential of the same mathematical form as the load function but the friction angle is replaced by the dilation angle ψ with $\psi < \phi$.

It should be noted that Vermeer and de Borst (1984) observed that the values of the angles of dilation are approximately between 0° and 20° for soils, rocks, and concrete. The default value for dilation angle is zero for all the constitutive models in $FLAC^{3D}$.

2.3 Description of the FLAC code

2.3.1 Overview

The FLAC user guide established by Itasca (2013) provides us with a detailed description of the FLAC (Fast Lagrangian Analysis of Continua) code which is designed and marketed by the Itasca company. It is available in two-dimensional version and three-dimensional. It is up to the user to work with the version that best satisfies their problem. Indeed, when the problem to be solved can be modeled in 2 dimensions, FLAC^{2D} makes it possible to refine as much as possible the meshes or the increments loading, with very reasonable times. However, some problems are, by their nature, three-dimensional, FLAC^{3D} then allows them to be simulated, but, given the increase in the number of zones, any refinement implies considerable computation times but, compared to other software, FLAC^{3D} remains competitive. However, the explicit, Lagrangian, calculation scheme and the mixed-discretization zoning technique used in FLAC^{3D} ensure that plastic collapse and flow are modeled very accurately. FLAC^{3D} offers an ideal analysis tool for solution of three-dimensional problems in geotechnical engineering.

This finite-difference code was developed to deal with the nonlinear problems of mechanics applied to geotechnics. Integrating an explicit method of solving the equations of mechanics, it is necessary to analyze the mechanical stability of the solutions obtained. The software integrates many constitutive models adaptable to a large number of materials, we can cite the elastic models, Mohr-Coulomb, Cam-Clay, Drucker-Prager, Double-Yield, etc.

2.3.2 Finite difference method

The finite difference method is one of the oldest methods of numerically solving a system of differential equations. For initial conditions and given boundary conditions, the solution is unique. Most of the methods using the finite differences adopt a discretization of the medium in rectangular meshes exclusively. The approach adopted by Itasca is based on the method of Wilkins (1964), which allows the formulation of finite difference equations for any element. We can give them any shape at the limits and vary the properties from one element to another. From this, it is therefore as efficient as the finite element method.

In the finite difference method, any derivative is directly replaced by an algebraic expression described in terms of variations at discrete places in space. These variables are undetermined everywhere else, unlike the finite elements for which shape functions describe the variations (stresses and displacements) throughout the massif.

The Flac code uses Lagrangian elements of which geometry is updated at each time step. This property makes it possible to deal with the problems in large displacements, without an additional algorithm.

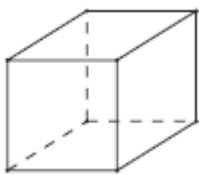
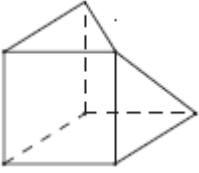
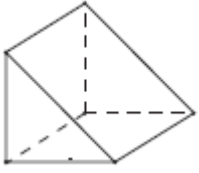
Moreover, the FLAC code is essentially distinguished by its explicit resolution scheme, which makes it possible not to combine the elementary matrices, thus allowing a substantial saving in memory space, namely in Random Access Memory (RAM). Indeed, only the variables at the end of each time step are stored and not the stiffness matrix, as that is the case for the finite element method.

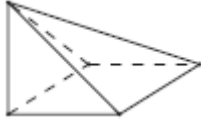
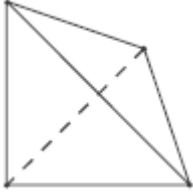
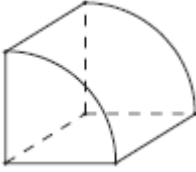
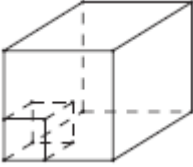
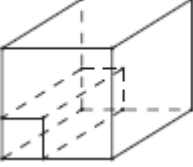
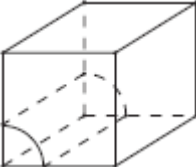
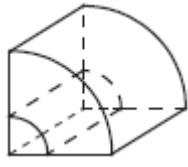
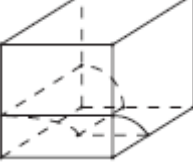
2.3.3 3D discretization

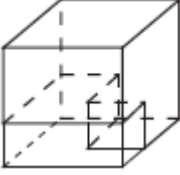
Grid generation in FLAC^{3D} involves patching together grid shapes of specific connectivity (referred to as primitives) to form a complete model with the desired geometry. Several types of primitives are available, and these can be connected and conformed to create complex three-dimensional geometries.

The FLAC^{3D} grid is generated with the generate zone command. This command actually accesses a library of primitive shapes; each shape has a specific type of grid connectivity. The primitive shapes available in FLAC^{3D}, listed in order of increasing complexity, are summarized, with their associated keyword, in Table 2.1. These primitive shapes can be applied individually or connected together to create the FLAC^{3D} grid.

Table 2.1 Summary of primitive mesh shapes, (Itasca, 2013)

Shape	Name	Keyword	Reference Points
	Brick	brick	8
	Degenerate Brick	dbrick	7
	Wedge	wedge	6

	Pyramid	pyramid	5
	Tetrahedron	tetrahedron	4
	Cylinder	cylinder	6
	Radial Brick	radbrick	15
	Radial Tunnel	radtunnel	14
	Radial Cylinder	radcylinder	12
	Cylindrical Shell	cshell	10
	Cylinder Intersection	cylint	14

	Tunnel Intersection	tunint	17
---	---------------------	--------	----

In FLAC^{3D}, the discretization process begins with the formation of zones according to the primitive shapes chosen by the user.

Among three-dimensional constant strain-rate elements, tetrahedral have the advantage of not generating hourglass deformations (i.e., deformation patterns created by combinations of nodal velocities producing no strain rate and, thus, no nodal force increments). However, when used in the framework of plasticity, these elements do not provide for enough modes of deformation. For more detail, the reader can refer to the work of Nagtegaal et al. (1974). In particular situations, for example, they cannot deform individually without change of volume as required by certain important constitutive laws. In those cases, the elements are known to exhibit an over-stiff response as compared to that expected from theory. To overcome this problem, a process of mixed discretization is applied in FLAC^{3D}, as described by Marti and Cundall (1982).

The principle of the mixed discretization technique is to give the element more volumetric flexibility by proper adjustment of the first invariant of the tetrahedral strain-rate tensor (This invariant gives a measure of the rate of dilation of the constant strain-rate tetrahedron). In the approach, a coarser discretization in *zones* is superposed to the tetrahedral discretization, and the first strain rate invariant of a particular tetrahedron in a zone is evaluated as the volumetric-average value over all tetrahedral in the zone. The method is illustrated in Figure 2.8. In the particular mode of deformation sketched there, individual constant strain-rate elements will experience a volume change incompatible with a theory of incompressible plastic flow. In this example, however, the volume of the assembly of tetrahedral (i.e., the zone) remains constant, and application of the mixed discretization process allows each individual tetrahedron to reflect this property of the zone, hence reconciling its behavior with that predicted by the theory.

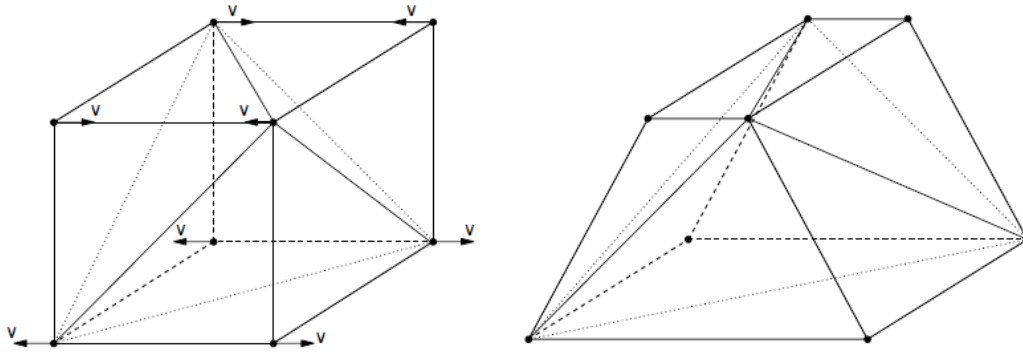


Figure 2.8 Deformation mode for which mixed discretization should be most efficient, (Itasca, 2013)

In FLAC^{3D}, a zone corresponds to an assembly of n_t tetrahedra, as illustrated in Figure 2.9 for the case $n_t = 5$. Consider a particular zone: the strain-rate tensor of a tetrahedron locally labeled l in that zone is first estimated, and then decomposed into deviatoric and volumetric parts - i.e.

$$\xi_{ij}^l = \eta_{ij}^l + \frac{\xi^l}{3} \delta_{ij} \quad (2.18)$$

where

η^l is the deviatoric strain-rate tensor, and ξ^l is the strain-rate first invariant.

$$\xi^l = \xi_{ii}^l \quad (2.19)$$

The first invariant for the zone is then calculated as the volumetric average value of the first invariant over all tetrahedra in the zone

$$\xi^z = \frac{\sum_{k=1}^{n_t} \xi^k V^k}{\sum_{k=1}^{n_t} V^k} \quad (2.20)$$

where

V^k is the volume of tetrahedron k .

Finally, the tetrahedron strain-rate tensor components are calculated from

$$\xi_{ij}^l = \eta_{ij}^l + \frac{\xi^z}{3} \delta_{ij} \quad (2.21)$$

Dilatant constitutive laws will produce changes in mean normal stress when yielding occurs. For a consistent technique, the first invariant of the stress tensor, derived after application of the strain-rate increment, must also be evaluated as a volumetric average for the

zone. In this process, the stress tensor of a particular tetrahedron l in a zone is first estimated and decomposed into deviatoric and volumetric parts:

$$\sigma_{ij}^l = s_{ij}^l + \sigma^l \delta_{ij} \quad (2.22)$$

where

$[s]^l$ is the deviatoric strain-rate tensor, and σ^l is the mean normal stress.

$$\sigma^l = \frac{1}{3} \sigma_{ii}^l \quad (2.23)$$

The first invariant for the zone is calculated as the volumetric average value over all tetrahedral in the zone:

$$\sigma^z = \frac{\sum_{k=1}^{n_t} \sigma^k V^k}{\sum_{k=1}^{n_t} V^k} \quad (2.24)$$

Finally, the tetrahedron stress-rate tensor components are calculated using:

$$\sigma_{ij}^l = s_{ij}^l + \sigma^z \delta_{ij} \quad (2.25)$$

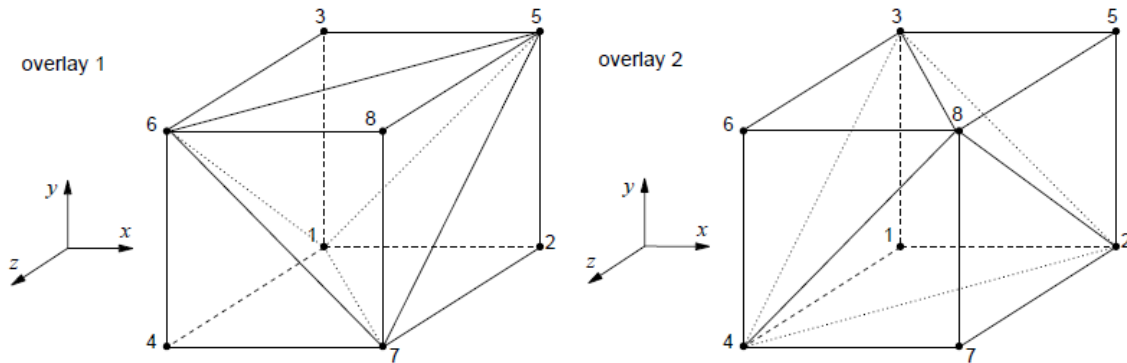


Figure 2.9 An 8-node zone with 2 overlays of 5 tetrahedral in each overlay, (Itasca, 2013)

In $FLAC^{3D}$, the discretization process starts with the coarser grid: zones are defined and then discretized (internally) into tetrahedral. An eight-noded zone, for instance, can be discretized into two (and only two) different configurations of five tetrahedral (corresponding to overlay 1 and 2 in Figure 1.9). The calculation of nodal forces (based on evaluation of strain rates and stresses) can be carried out using one overlay or a combination of two overlays. The advantage of the two overlay approach is to ensure symmetric zone response for symmetric loading. In this case, mixed discretization is carried out over the combination of two overlays, and nodal forces computations are evaluated by averaging over the two overlays.

2.3.4 Explicit solving scheme

The explicit solving scheme is based on the principle that part of the strain energy accumulated by the system is converted into kinetic energy which will propagate and dissipate in the surrounding material. This solving scheme integrates this phenomenon by taking into consideration the dynamic equations of motion. The unbalance induced in one area will spread throughout the mass. The objective of the method remains the solving of a static problem through dynamics. The general calculation sequence integrated into FLAC is shown in Figure 2.10.

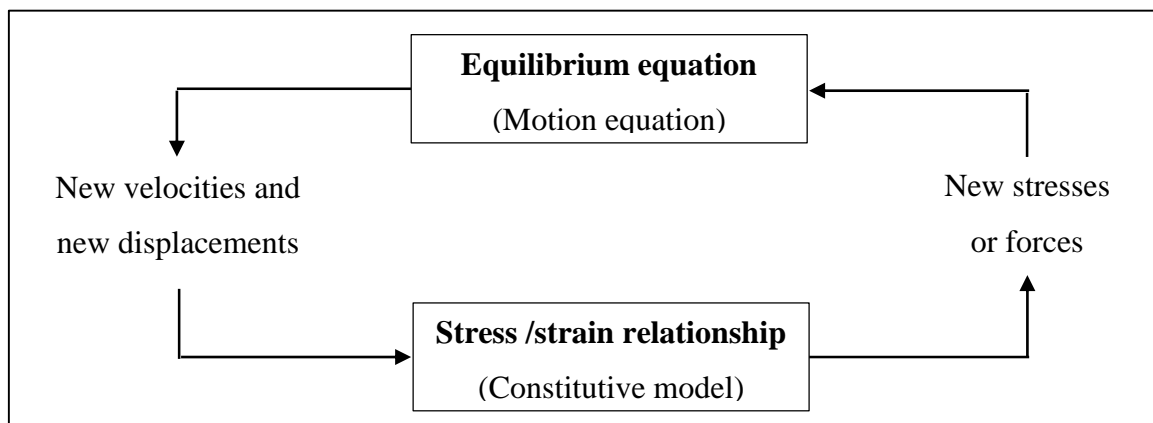


Figure 2.10 FLAC calculation sequence, (Itasca, 2013)

The procedure first uses the equations of motion to calculate the velocities and displacements from the acceleration, deduced from the resultant of forces and stresses. Recall that for a deformable solid in a lagrangian frame of reference, Newton's equation of motion is expressed by:

$$\rho \frac{\partial \dot{u}_i}{\partial t} = \frac{\partial \sigma_{ij}}{\partial x_j} + \rho g_i \tag{2.26}$$

where

ρ , t , u , x , g , are the density, time, velocity vector, position vector and acceleration due to volume forces, respectively.

Then the strains are deduced from the displacements (integrals of the velocities), and the new stresses are determined from the constitutive law.

In each calculation box of Figure 2.10, we update again all variables to be treated starting from known values which must, them, remained fixed during the calculations in this box. Thus the calculation of new stresses does not affect the velocities calculated in the

previous box. This assumption is justified if a small enough time step is chosen so that the information cannot pass from one element to another during this time interval. Adjacent elements will therefore not be able to affect each other during a calculation stage. All this is based on the idea that the velocity of the "computational wave" is always higher than that of physical waves, which makes it possible to freeze the known and used values for the duration of the calculations using them.

To constitute an operational algorithm, the motions must be damped to arrive at a stationary state (equilibrium or permanent flow). The damping used consists in imposing on each node a damping force of which modulus is proportional to the modulus of the unbalanced net force and of which direction is such that it always produces negative work.

The stability criterion for controlling the equilibrium state of the entire system is based on the maximum unbalanced force. The user defines the force below which the residual unbalance is assumed to be satisfactory.

Unlike the explicit method, in an implicit method, each element communicates with every other element during a calculation step, so it is necessary to iterate before satisfying both the equilibrium and compatibility equations. The major disadvantage of the explicit method is the condition on the time step, when the latter is very small, it may be necessary to perform a large number of steps before arriving at the static solution. Therefore, the explicit method proves to be inefficient for all linear problems and in particular in small displacements. The preferred domain of the method would be more the study of non-linear systems and large displacements.

2.3.5 Modeling methodology

To install a model to perform a simulation with FLAC, the following logical steps must be followed:

- Grid generation;
- Choice of constitutive model and material properties;
- Boundary and initial conditions;
- Loading and sequential modeling;
- Ways to improve modeling efficiency; and
- Interpretation of results.

2.3.6 Interfaces

There are several instances in geomechanics in which it is desirable to represent planes on which sliding or separation can occur, e.g. joint, fault, or bedding planes in a geologic medium; an interface between a foundation and the soil; a contact plane between a bin or chute and the material that it contains; a contact between two colliding objects; and a planar “barrier” in space, which represents a fixed, non-deformable boundary at an arbitrary position and orientation.

FLAC^{3D} provides interfaces that are characterized by Coulomb sliding and/or tensile and shear bonding. Interfaces have the properties of friction, cohesion, dilation, normal and shear stiffnesses, tensile and shear bond strength.

An interface is represented as a normal stiffness and a shear stiffness between two planes in contact.

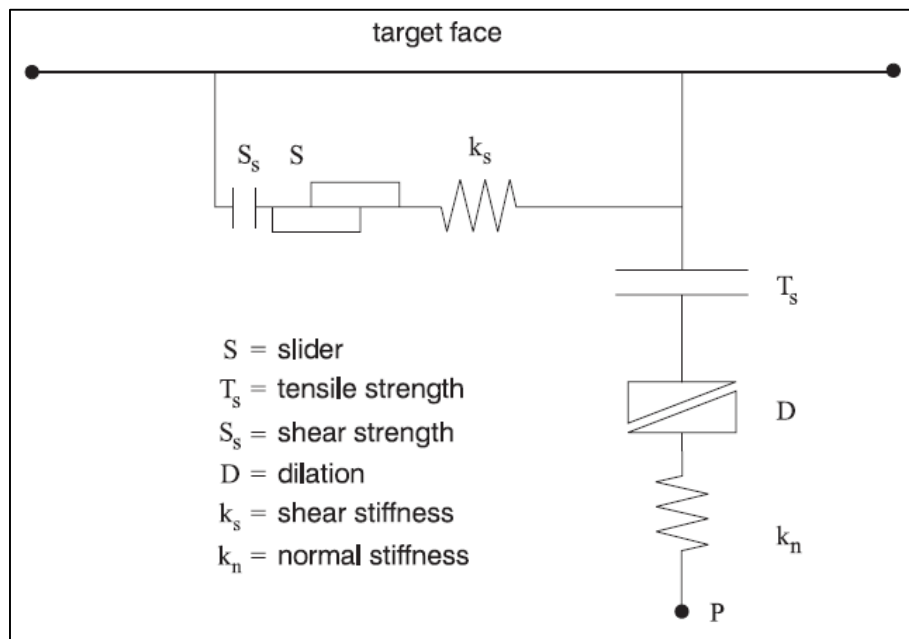


Figure 2.11 Components of the bonded interface constitutive model, (Itasca, 2013)

For the choice of the characteristics of the interface: cohesion, dilatancy, limit traction, and friction are generally taken equal to those of the least resistant material.

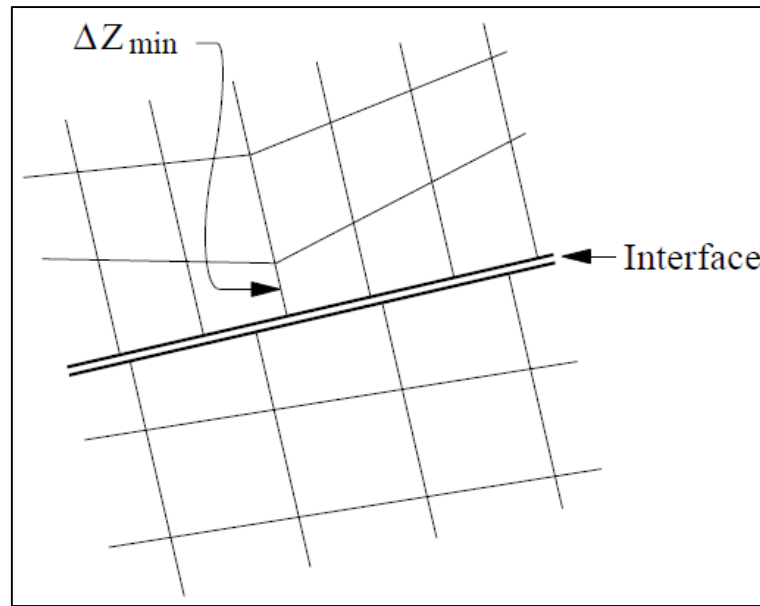


Figure 2.12 Zone dimension used in stiffness calculation, (Itasca, 2013)

The stiffnesses k_n and k_s are more difficult to estimate. FLAC recommended that k_n and k_s can be set to ten times the equivalent stiffness of the stiffest neighboring zone, as is a good rule-of-thumb. The apparent stiffness (expressed in stress-per-distance units) of a zone in the normal direction is:

$$\max \left[\frac{\left(K + \frac{4}{3}G \right)}{\Delta z_{in}} \right] \quad (2.27)$$

where

K and G are the bulk modulus and the shear modulus respectively, and z_{min} is the smallest dimension in the normal direction (see Figure 2.12)

This recommendation makes it possible not to penalize calculation times when considering an interface.

The Coulomb shear-strength criterion limits the shear force by the following relation:

$$F_{s \max} = cA + \tan \varphi (F_n - pA) \quad (2.28)$$

where

A is the representative area associated with the interface node; p is pore pressure (interpolated from the target face); φ is the friction angle of the interface surfaces; and c is the cohesion along the interface.

If the criterion is satisfied (i.e., if $|F_s| \geq F_{s \max}$), then sliding is assumed to occur, and $|F_s| = F_{s \max}$, with the direction of shear force preserved.

The normal and shear forces that describe the elastic interface response are determined at calculation time $(t + \Delta t)$ using the following relations.

$$F_n^{(t+\Delta t)} = k_n u_n A + \sigma_N A \quad (2.29)$$

$$F_{si}^{(t+\Delta t)} = k_{si}^{(t)} + k_s \Delta u_{si}^{(t+(1/2)\Delta t)} A + \sigma_{si} A \quad (2.30)$$

where

$F^{(t+\Delta t)}_n$ is the normal force at time $(t + \Delta t)$; $F^{(t+\Delta t)}_{si}$ is the shear force vector at time $(t + \Delta t)$; u_n is the absolute normal penetration of the interface node into the target face; Δu_{si} is the incremental relative shear displacement vector; σ_n is the additional normal stress added due to interface stress initialization; σ_{si} is the additional shear stress vector due to interface stress initialization ; and A is the representative area associated with the interface node.

2.4 Summary

The complex conditions relating to the load-bearing capacity problem require a well-adapted numerical tool. In this present thesis, we have used the FLAC^{3D} code which, thanks to its explicit mode of resolution in Lagrangian elements, makes it possible to simulate nonlinear problems with good numerical stability. Regarding the constitutive laws, we have retained the perfectly plastic linear elastic model of Mohr-Coulomb for the foundation soil.

CHAPTER 3

NUMERICAL INVESTIGATION ON PILE GROUP EFFICIENCY EMBEDDED IN SOFT CLAY

3.1 Introduction

Deep foundations are widely used in tall buildings, bridges, towers, offshore and other special structures. This type of foundation is designed to transmit the applied forces to the surrounding soil at a significant depth which usually exceeds ten diameters. The deep foundations are often group of piles where, in practice, piles are always driven or bored by group.

Due to the effect of the interaction between piles, the behavior of a group of piles may be different from that of individual pile and the limit vertical load of a group of n piles (Q_{GP}) may be less than n times the limit load of an individual pile (Q_{SP}) working under the same conditions. The group effect is evaluated using the efficiency coefficient of the bearing capacity of pile group (C_g) which is defined as the ratio of Q_{GP} to n times Q_{SP} .

Despite the research efforts carried out to date to assess the pile group efficiency and their encouraging results, discrepancies are still observed during comparison between the results of the formulas already developed and field or laboratory test measurements (Helmy 2002; Park and lee 2015).

Numerical methods such as finite difference, finite element and boundary element method, have been widely developed in the last two decades because they are less costly and may be used to consider more complex cases compared to field and model tests. However, the literature review reveals that few investigations have been carried out to evaluate adequately the efficiency of the pile group and to date; no simple method of design using a 3D numerical model has been developed.

In this context, the present study focuses on the evaluation of pile group efficiency based on the load-settlement response, considering several pile configurations. The aim of the present study is to perform a full 3D numerical analysis, using the FLAC^{3D} code (Itasca 2013), of the overall load response of pile group and to determine the effects of piles number and pile spacing on the freestanding pile group performance embedded in soft clay conditions. The numerical obtained results are validated by comparing them to those of similar subgrade-structure and in comparable geological conditions provided within the literature.

3.2 Numerical analysis

3.2.1 Mesh and constitutive modeling

The behavior of the group of piles (GP) embedded in soft clay condition is investigated by performing numerical computations using the explicit finite difference code FLAC^{3D} (Itasca 2013). The FLAC^{3D} code leads to rigorous treatment which is an effective tool in the analysis of the bearing capacity problems of different foundation schemes. Since the problem geometry is doubly symmetrical only a quarter of the whole mesh was modeled to reduce the size of the model and the time needed for numerical computation. The numerical model consists of a deep foundation modeled with solid elements embedded in the ground volume. Based on the results obtained from the preliminary simulations, the horizontal distance of the mesh boundary was set to 40 m, and a depth of 20 m was assumed in this study. A roller boundary is used to fix all nodes in the horizontal direction along the lateral boundaries. However, all nodes on the bottom surface are restrained in both horizontal and vertical directions. These boundaries are supposed to be impervious. Figure 3.1 shows a typical mesh used in this 3D numerical study.

The contact between piles and the surrounding soil was simulated using an interface element defined by Coulomb's shear strength criterion. The interface element was assumed as able to slip (Jeong et al. 2004; Lee et al. 2010; Ghalesari et al. 2015). In order to install the soil-pile interfaces, the grid representing the soil is created first and interfaces are attached to the zone faces with the pile. The cylinder pile grid is created separately and then it is moved downward into contact with the interface elements (Itasca 2013). Detachment was made impossible by adjusting the separation failure criterion to a significant value (tensile strength = 10^8 Pa). It is expected that stress concentrations will occur around the piles, and so a relatively fine mesh was proposed here, while a coarser mesh was used further from the piles

in order to reduce computation time. Such a refinement study resulted in using the mesh presented in Figure 3.1.

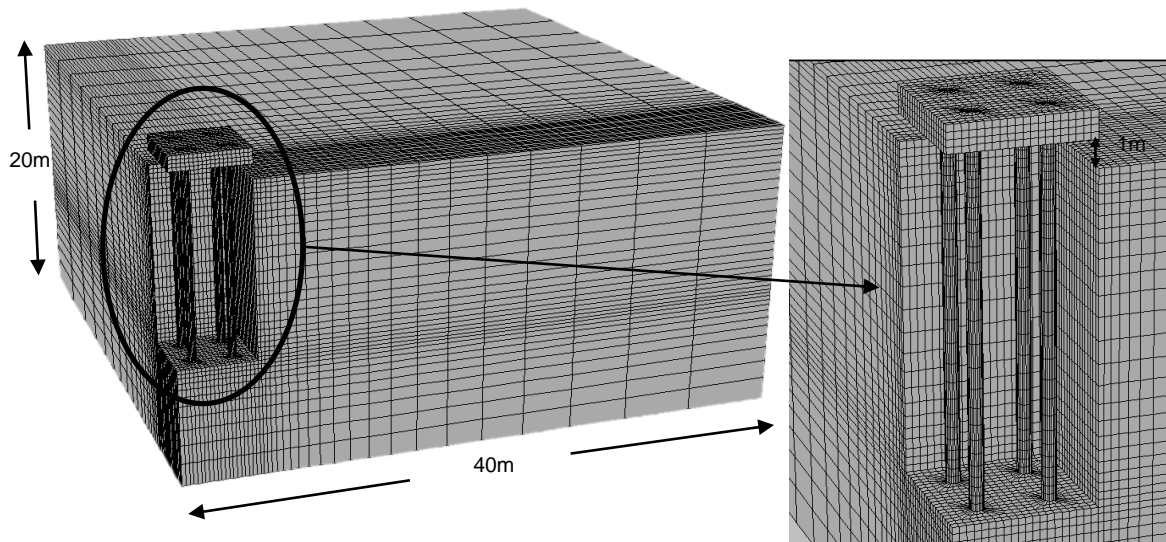


Figure 3.1 Grid used in FLAC^{3D} simulations

The piles were modeled as linear elastic material with an Elastic modulus of 30 GPa and Poisson's ratio of 0.2. The linear elastic perfectly plastic constitutive law using the Mohr–Coulomb failure criterion was used to describe the mechanical behavior of soil in this 3D parametric study. The Mohr–Coulomb model is widely used in the modeling of geotechnical problems and has the advantage of requiring few soil parameters. Note that all these parameters can be obtained from the standard soil tests. The use of a more complex constitutive model that takes into account the nonlinear behavior will probably requires the estimation of specific soil parameters from special tests such as triaxial tests equipped with local strain gauges, K_0 oedometer tests, the resonant column tests, hollow cylinder torsion tests. As a result, the number of soil parameters to be evaluated would be greater, and their interdependence is not evident (Houhou et al. 2019).

To prescribe the water conditions, a general water table is defined at the free surface, under which the water pressure distribution is hydrostatic. This pore pressure is imposed at any point of the mesh and the analysis was then performed by a mechanical computation not coupled to the flow (by setting flow off and set the water bulk modulus to zero for this mechanical-only calculation). In this way the pore pressure field will not be changed by the volumetric strain. This is the long-term behavior and the analysis type is effective analysis.

The analysis of group of piles involved three stages, namely initial stage, installation stage and the loading stage. In the initial stage, the model is first brought to an equilibrium

stress-state under gravitational loading (involved only the soil volume). In the second stage the piles installation is simulated only by substituting the properties of the piles zones from the properties representing the soft clay material to those representing the concrete piles material. The pile installation is not explicitly represented in this study. The analyses assumed that the piles were “wished-in-place” and hence, did not consider local changes in stresses or soil properties associated with drilling and concreting. In the loading stage, a uniformly distributed vertical load is gradually applied on the foundation surface.

The loading was performed by displacement control method which was simulated by imposing a vertical velocity (Itasca 2013). Then, the load taken by the piles was obtained by summing the vertical reaction of the displaced nodes belonging to the piles head. As the level of errors in such calculation scheme depends on the applied velocity, preliminary simulations have been carried out, by testing the magnitude of the applied velocity. The downward velocity of 10^{-8} m/s was chosen.

3.2.2 Validation

A popular example presented by Poulos (2001) is used to validate the modeling procedure carried out in this study. In order to assess the efficiency of different analytical methods of piled raft performance analysis, Poulos (2001) used a group of 9 identical piles capped by a rectangular raft (a pile group in which the raft directly touches the ground surface). Each pile has a length of 10 m and diameter of 0.5 m. The raft is 10 m by 6 m with a thickness of 0.5 m. The piles, raft and soil are modeled with elastic properties. Table 3.1 summarized the comparison between the results of the central settlement and corner pile settlement obtained from the present study and the four methods of analyses presented by Poulos (2001) such as Poulos-Davis-Randolph method (PDR), Geotechnical Analysis of Raft with Piles (GARP5), Geotechnical Analysis of Strip on Piles (GASP), and Simplified Burland method. To enhance the comparison, the numerical results reported by Ata et al. (2015) are also presented in the Table 3.1. It can be seen that the results of the present study are in good agreement with those of the different above mentioned methods.

Table 3.1 Comparison of results

Approach	Central settlement (mm)	Corner pile settlement (mm)
Simplified PDR	36.8	-
Raft with piles (GARP5)	34.2	26
Strip on piles (GASP)	33.8	22
Simplified Burland	33.8	29.7
Numerical results reported by Ata et al. (2015)	31	23.5
Present study	32.4	24.1

The validity of the modeling procedure done in this study is also proved by comparing the obtained numerical results with the results of the vertical loading case carried out by Horikoshi et al. (2003) employing geotechnical centrifuge testing in order to simulate piled raft under different types of loading. The model consisted of a square raft (4 m wide and 2 m thick) rigidly connected to four piles. The raft and piles models were made of aluminum and Toyoura sand was used as the model ground (Horikoshi et al. 2003). Each pile has a length of 8.5 m and a diameter of 0.5 m. The pile spacing was set to 2 m. Note that the prototype scale is considered in this analysis. According to Horikoshi et al. (2003) and Matsumoto et al. (2004), the internal friction angle for Toyoura sand used in centrifuge tests is about 45° and the interface structures friction angle is 22.9°. The soil and interface properties, used in this numerical analysis are the same used by Horikoshi et al. (2003) and Alnuaim et al. (2013) for validation purpose. These parameters are summarised in Table 3.2.

Table 3.2 Input parameters of soil and interface properties (Alnuaim et al. 2013)

Parameters	Soil
Unit weight, γ (kN/m ³)	14.6
Young's modulus, E_{ref} (kPa)	4500
Incremental modulus of elasticity (kPa/m)	6500
Poisson's ration, ν	0.175
Friction angle, ϕ'	45°
Interface friction	22.9°

Figure 3.2 shows a comparison between the load-settlement curves resulting from the current numerical analysis and the centrifuge test conducted by Horikoshi et al. (2003). It can be noted that the results obtained from the present numerical study agree well with those of the experimental test.

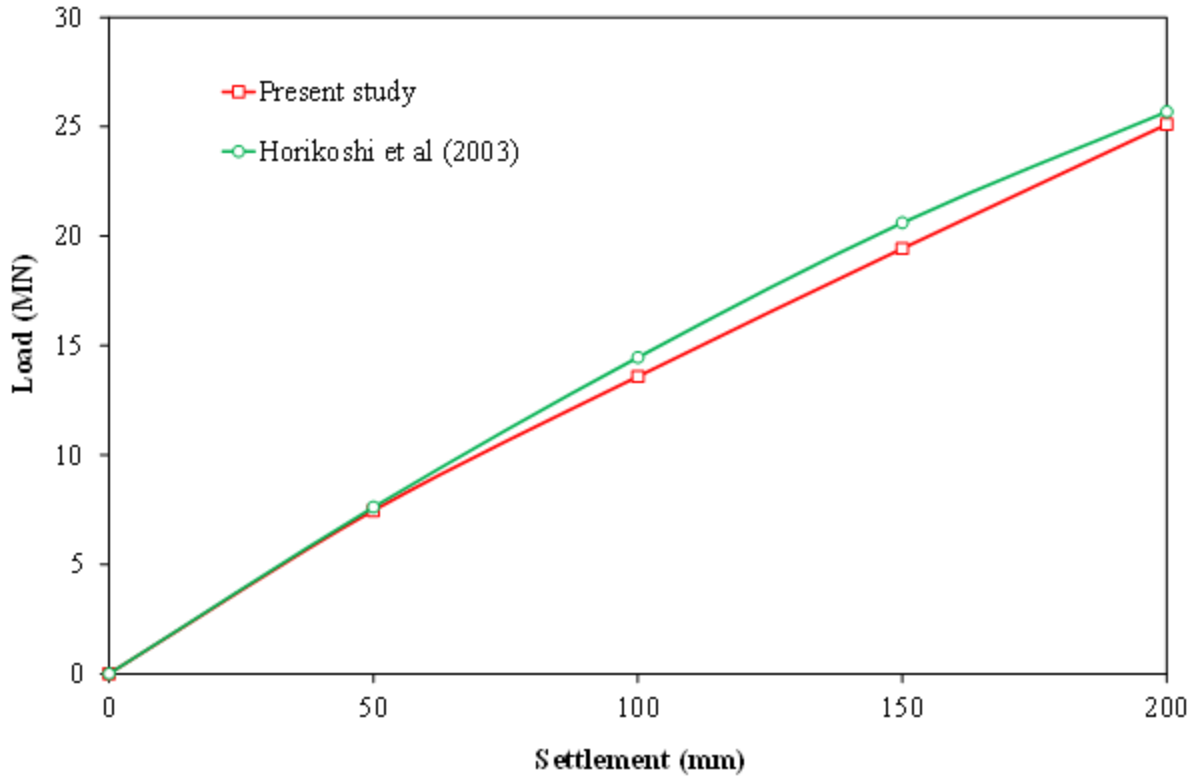


Figure 3.2 Comparison between results of present study and those of the centrifuge test conducted by Horikoshi et al. (2003)

3.2.3 Parametric study

A 3D parametric study was carried out to analyze the behavior of group of piles subjected to vertical loading embedded in a soft clay profile using variable number of piles n and pile spacing S_p , considering the full interactions between the piles.

Three pile configurations were considered, including 2×2 , 3×3 and 4×4 piles, for each pile configuration four pile spacing were examined, $S_p = 3d$, $4d$, $5d$, and $6d$. The length L and diameter d of all piles were 12 and 0.5 m, respectively.

The properties of the homogeneous soft clay and the elastic properties of foundations used by Nguyen (2008) are retained for this parametric study and summarized in Table 3.3.

To define the bearing capacity in foundation design, a settlement equal to 10% of the pile foundation diameter is often adopted (Cooke 1986; Conte et al. 2003; Rose et al. 2013).

However, in the present parametric study, the comparison between the different configurations considered was made for a settlement range which extends beyond 10% d in order to provide further insight for the mechanical response of group of piles. The settlement (s) achieved in this analysis is $s = 20\% d$.

Table 3.3 Material parameters used in the analyses (Nguyen 2008)

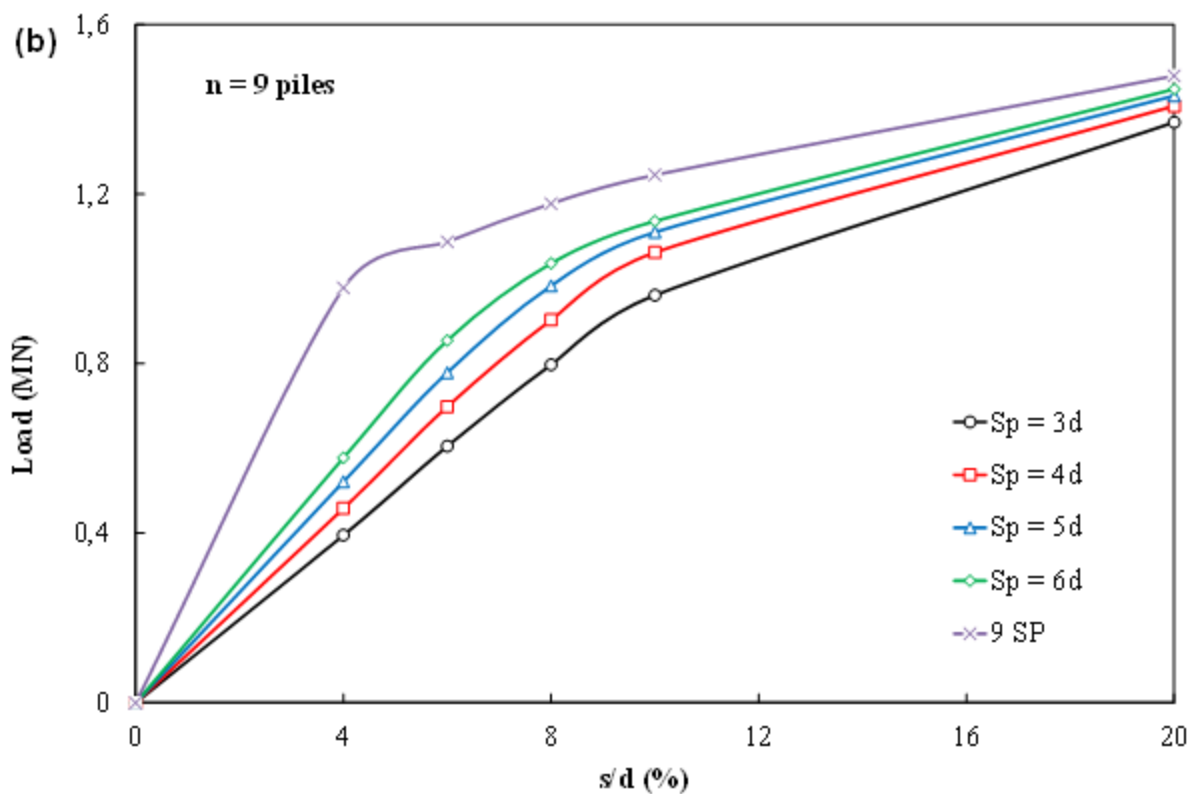
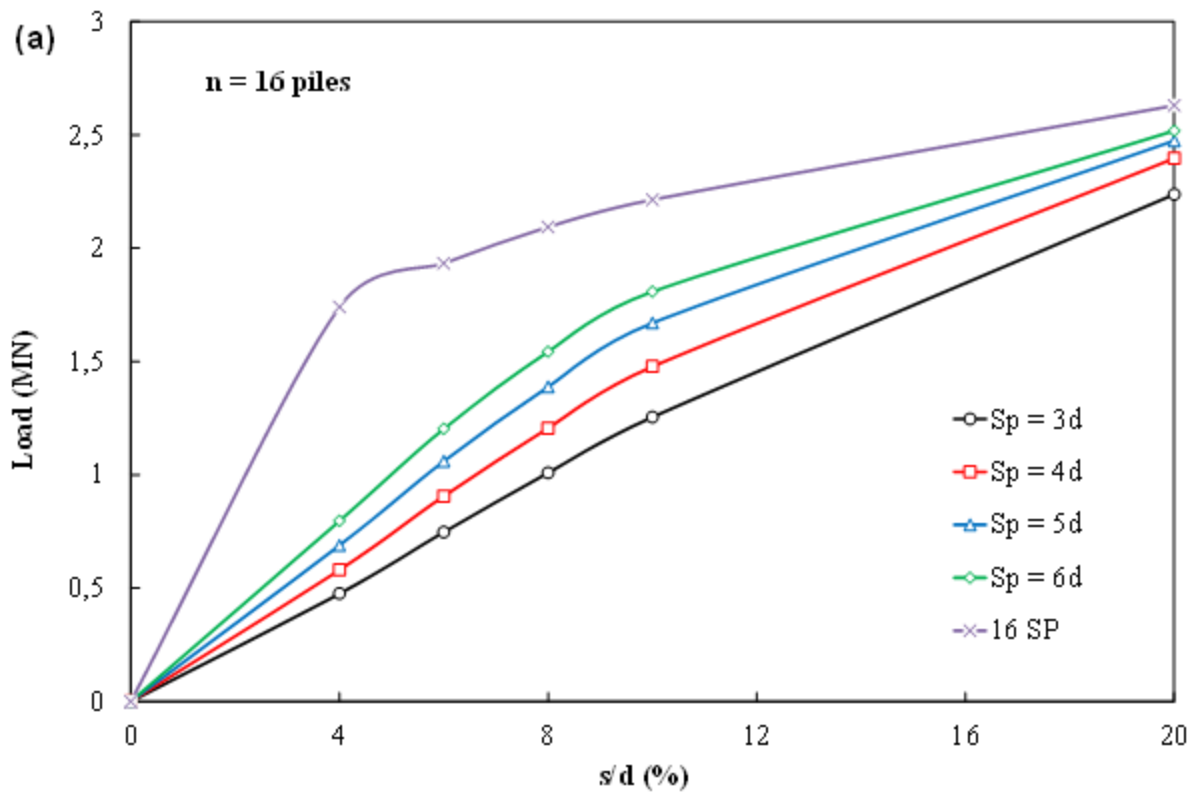
Materials	Model	E (MPa)	c' (kPa)	ϕ' ($^\circ$)	ν	γ (kN/m ³)
Foundation	Elastic	30 000	-	-	0.2	25
Soft clay	Mohr-Coulomb	4.8	15	31	0.3	14

3.3 Results and discussion

The load-settlement curves of group of 16, 9, and 4 piles for different pile spacing and using the corresponding n -times individual pile (SP) load response are shown in Figure 3.3. From Figure 3.3 (a), where the load-normalized settlement curves of group of 16 piles and using 16 times individual pile load response are considered. It can be seen that the load carrying capacity of group of 16 piles was lower than that of 16 times individual pile for the entire settlement range and for all pile spacing considered in this study. This is due to the effect of the interaction between piles in the group which is known as pile-to-pile interaction effect. Generally, it is the added settlement happened in a pile in the pile group due to the effect of the adjacent pile. However, it should be mentioned that increasing of S_p has a positive effect on pile group efficiency. It should be noted that as the pile spacing decreases the shape of the load response curve becomes linear.

From Figure 3.3b, it can be noted that, up to a settlement range of 10% d , the load carrying capacity of 9 piles group for all pile spacing was lower than that of 9 times individual pile. However, beyond this settlement range, all the load response curves converge towards that of 9-times individual pile.

Regarding to the case of $n = 4$, as shown in Figure 3.3c, the load carrying capacities of group of 4 piles and 4 times individual pile load response are almost identical, with a slight difference in the initial settlement range ($s/d \leq 6\%$) depending on S_p values.



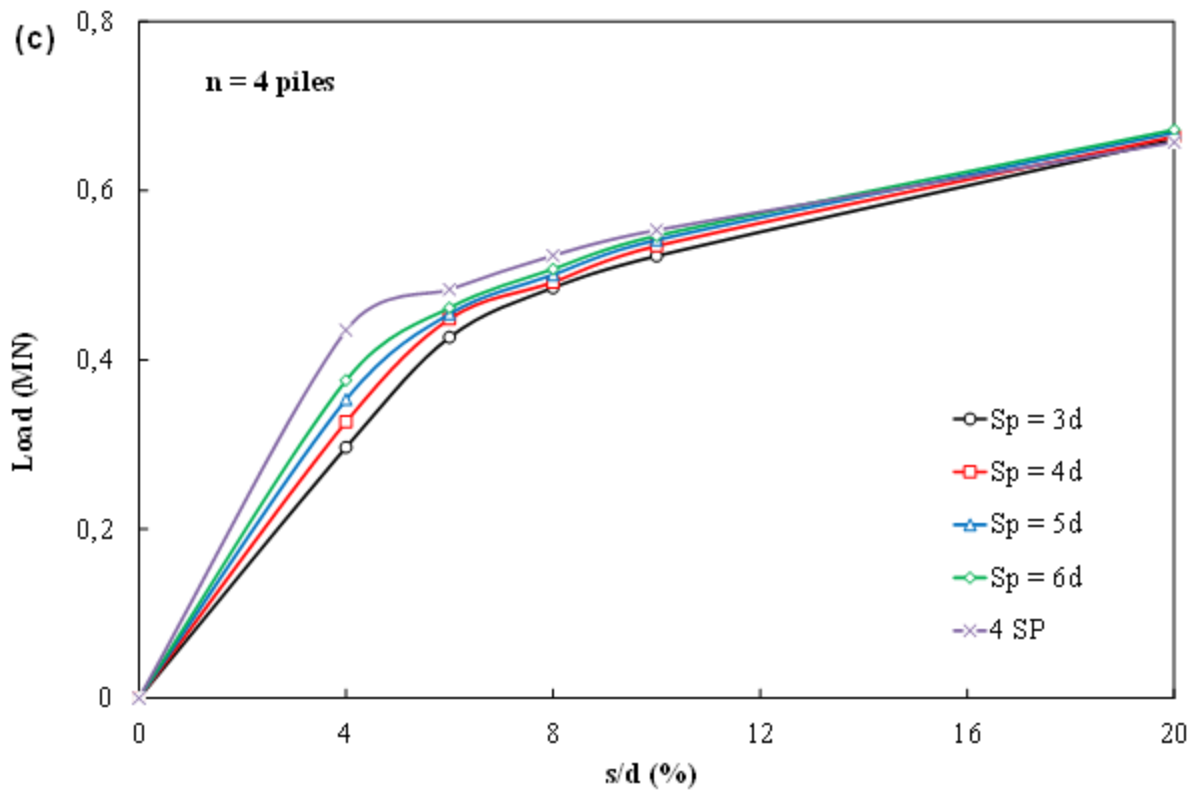


Figure 3.3 Load-settlement curves of piles group for different n and S_p

From all above, it can be noted that the pile-to-pile interaction effect was significant for large number of piles.

The installation of piles by a group with close spacing develops a superposition of stress field beneath piles due to the action of all piles. This superposition of stress field leads to change the settlement behavior of the individual pile depending on the pile spacing. For illustration, Figure 3.4 visualizes the influence zones of soil beneath the piles presented by contours of the maximum shear strain increment for the case of 16 piles with different pile spacing. It can be seen that the bearing pressure of pile group with close pile spacing ($S_p = 3d$) is mobilized at the base of the block of piles due the full superposition of stress field but with increasing of pile spacing, the shear strain gets developed at the base of each pile individually.

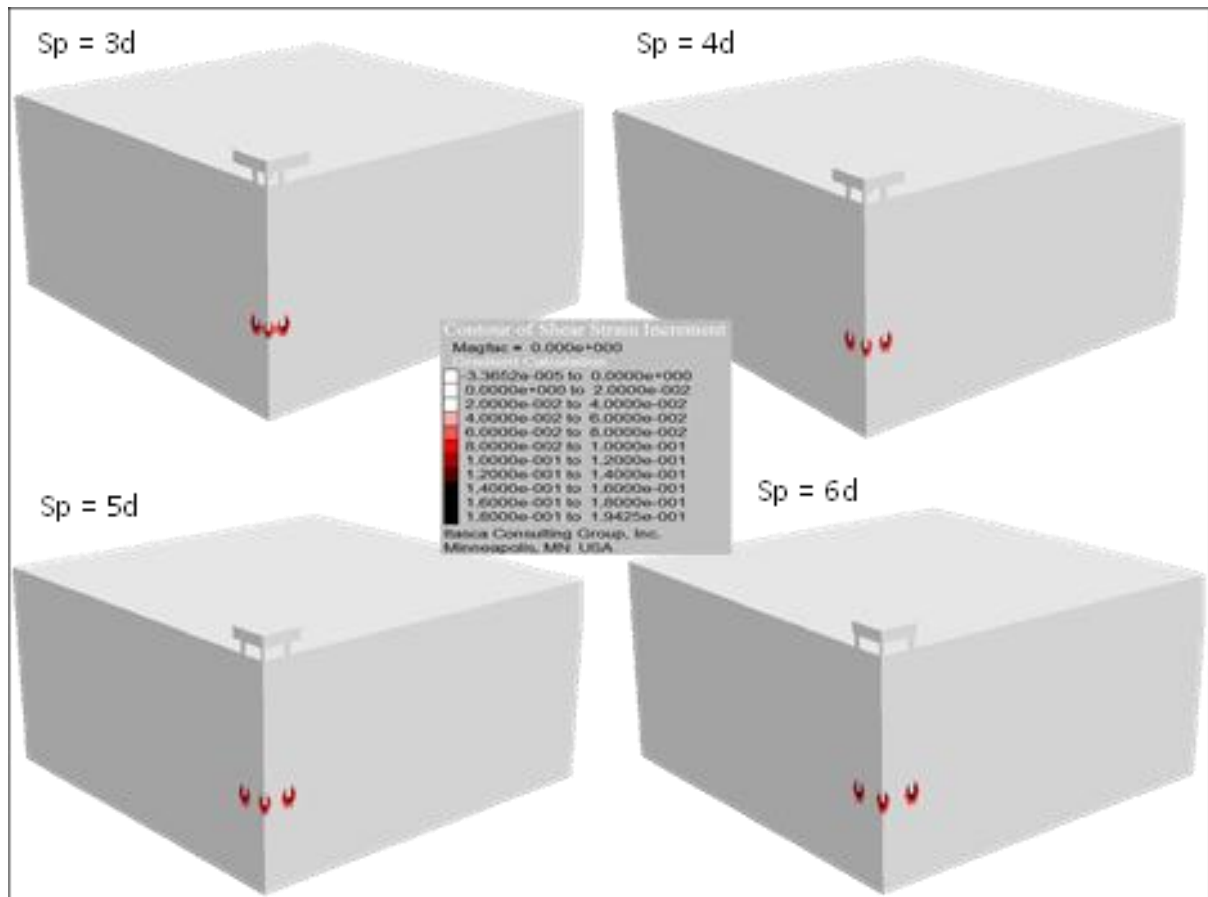


Figure 3.4 Maximum shear strain development for group of 16 piles with different pile spacing

From the results obtained from all the cases considered, it can be noted that the effect of pile spacing becomes more significant when the number of piles increases depending on settlement level.

Moreover, the efficiency coefficient of the pile group obtained from this parametric study is lower than unity for all considered configurations.

It can be concluded that using a value of C_g of unity for pile group in clay (value used by several researchers e.g. de Sanctis and Mandolini 2006; Lee et al. 2014; Park and Lee 2015) leads to overestimate the bearing capacity of group of piles essentially for the cases of large piles number.

The efficiency of the pile group embedded in soft clay is very important either in the case of a small piles number or in the case of large pile spacing.

The load carrying capacity of pile group increases with increasing of piles number. For example, the load carrying capacity of group of 16 piles at $S_p = 6d$ and $s = 0.1d$ is about 60%

and 220% higher than that of group of 9 piles and 4 piles, respectively. However, the pile group bearing capacity can be improved simply by increasing the pile spacing without increasing the number of piles. As an example, the bearing capacity of group of 9 piles at $S_p = 6d$ is very comparable to that of 16 piles at $S_p = 3d$.

The influence zones is also presented by the magnitude of soil displacement for groups of 16 and 9 piles of different piles spacing as shown in Figure 3.5. It can be seen that the soil displacement develops and gets changed depending on pile spacing and number of piles. Wherein, for the close piles spacing, the soil displacement occurs as a block in a conical shape, while as pile spacing increases, a punching of piles occurs individually.

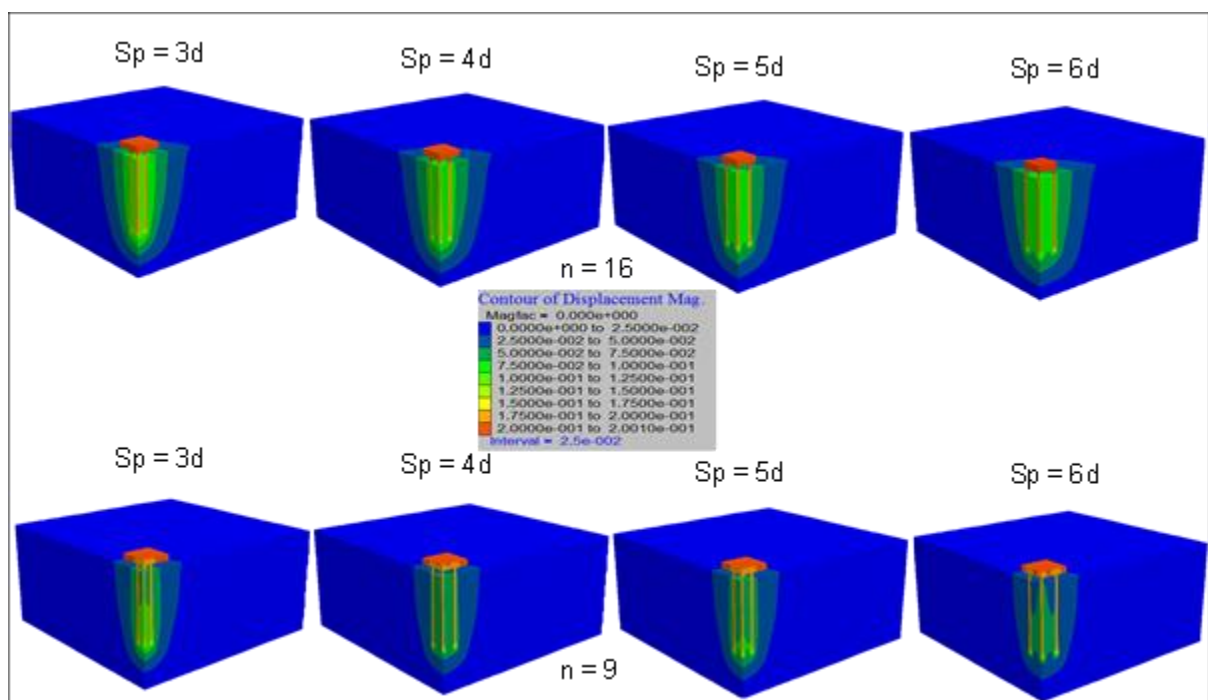
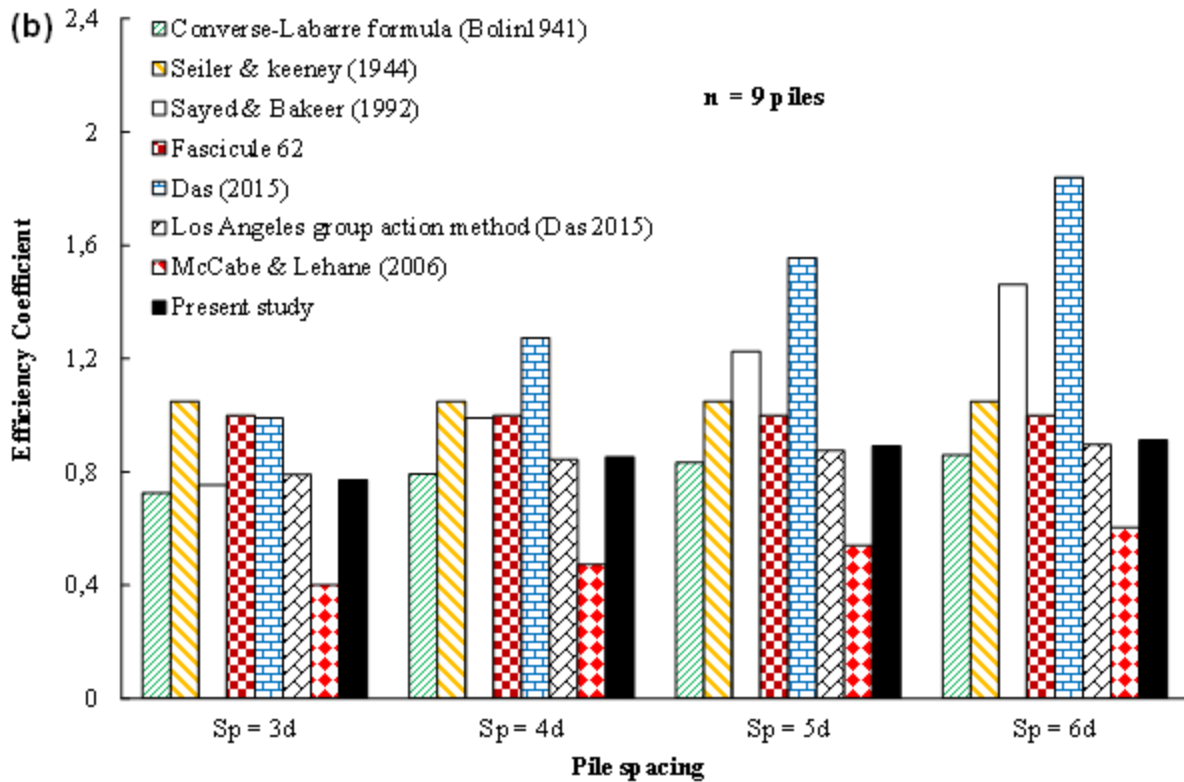
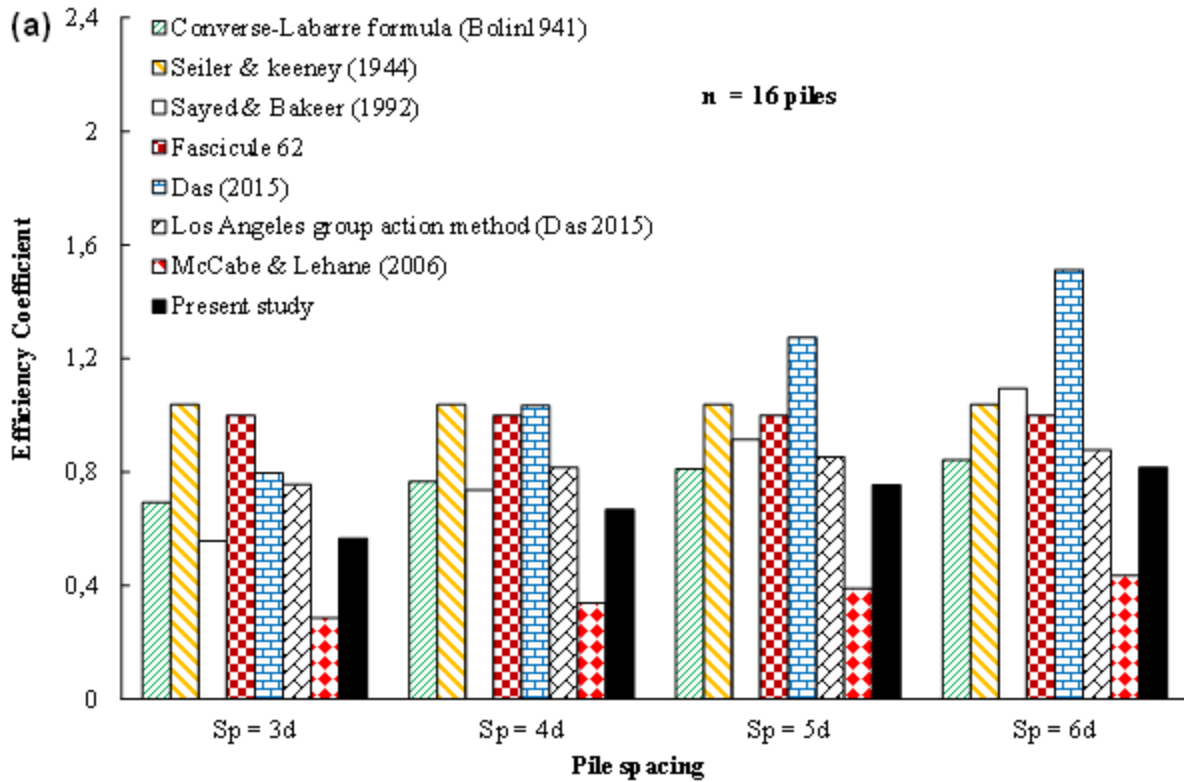


Figure 3.5 Soil displacement for groups of 16 and 9 piles with different pile spacing

The values of the efficiency coefficient C_g of the pile group are calculated from the results obtained and are presented in Figure 3.6. In order to compare these obtained values with those calculated from the most popular formula available in the literature (see section 1.3.1 in Chap. 1).



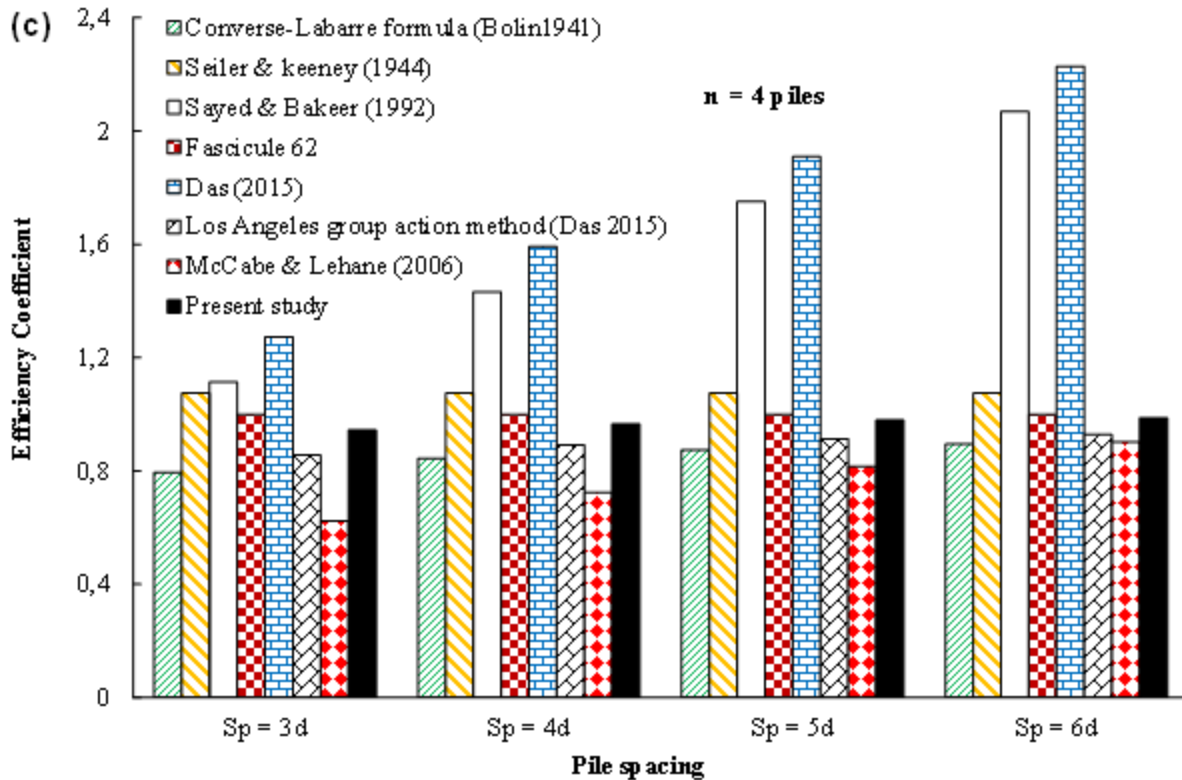


Figure 3.6 Comparison of C_g values calculated from the present study and different formulas available in the literature for different n and S_p

For the case of group of 16 piles (Figure 3.6a), the present study results were very close to those calculated using the Converse-Labarre formula (Eq. 1.18) and Los Angeles group action method (Eq. 1.23) for $S_p = 6d$. However, for the case of $S_p = 3d$, the Converse-Labarre and Los Angeles group action methods overestimate the present study results of about 18% and 25%, respectively. This is explained by the fact that at failure the pile group with close pile spacing behaves as a block due to the increased interaction between piles as shown in Figure 3.7. Referring to the experimental work of Cooke (1986), the pile group fails as a block when the ratio S_p/d is smaller than 4.

The pile group collapse by failure of the individual piles or the overall piled block and this is depending on the vicinity between piles of the group. As an example, Figure 3.7 shows some cases of the collapse mechanism obtained from the present analyses presented by the plastic zone for group of 16 piles with different pile spacing. From the case of the close pile spacing, $S_p = 3d$, it can be seen that the collapse occurs on the vertical surfaces at the perimeter of the block and on the horizontal surface at the base of the block. While, for the cases of the wide pile spacing, $S_p = 4d$, $5d$ and $6d$, the collapse appears individually at the base of each pile.

Nevertheless, the numerical results agree well to those calculated using Los Angeles group action method and Converse-Labarre formula for the case of 9 and 4 piles, for the different pile spacing considered.

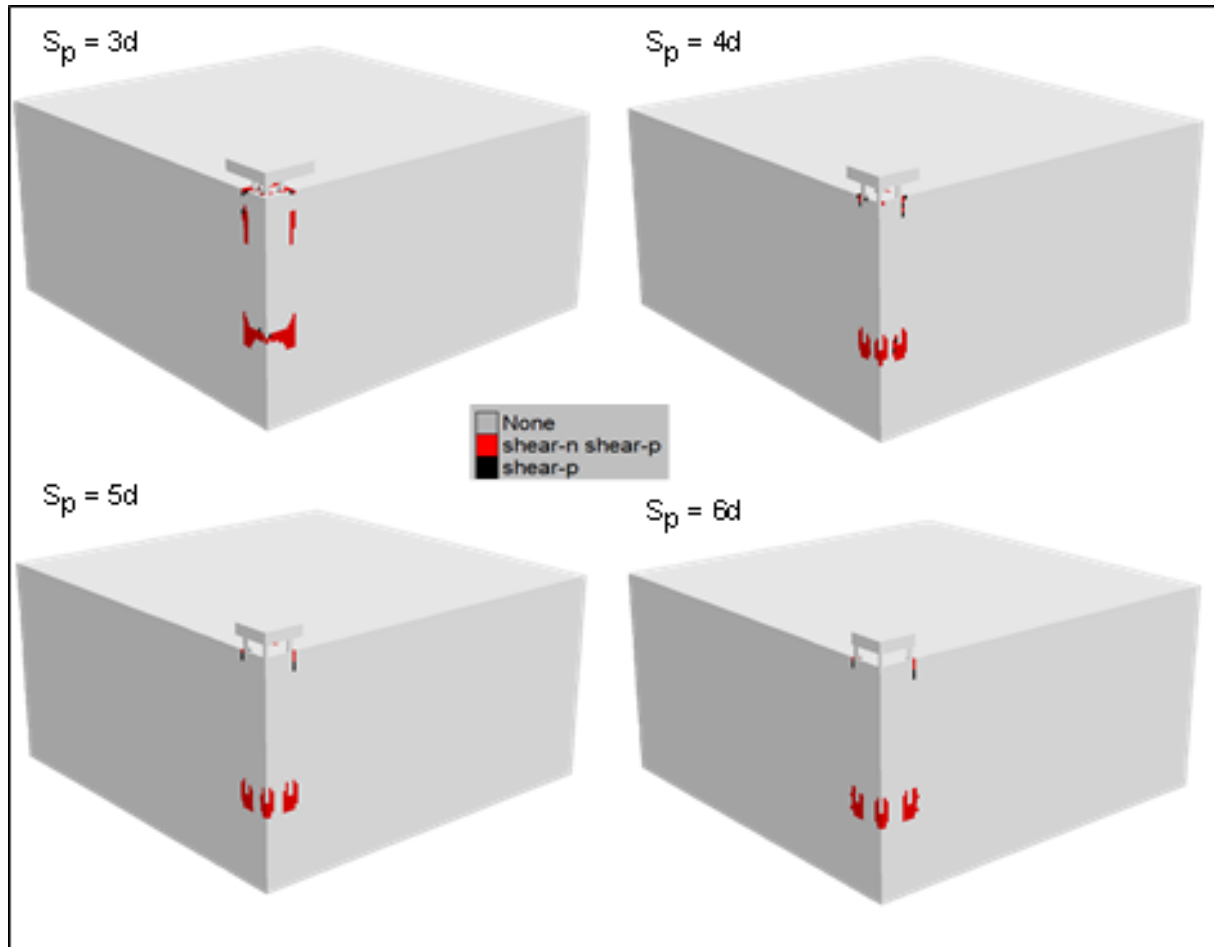


Figure 3.7 Plastic zone for group of 16 piles with different pile spacing

Regarding to Figure 3.6, the values of C_g calculated using the formula proposed by Das (2015) (see Eq. 1.22) greatly exceed the value of unity and therefore are significantly higher than those of the present study, which leads to severe overestimation of bearing capacity of group of piles. However, in clay, the pile group efficiency C_g is often lower than unity (Cooke 1986; de Sanctis and Mandolini 2006).

The method suggested by Sayed and Bakeer (1992) (see Eq. 1.20) overestimates the bearing capacity of pile group either in cases of small piles number or wide pile spacing as shown in Figure 3.6.

The C_g values obtained using the formula proposed by Seiler and Keeney (1944) (see Eq. 1.19) are slightly higher than unity and trend to be constant irrespective of piles number and pile spacing. It can be concluded that this method limits the effect of both, the piles

number and pile spacing. While these last two parameters were very decisive in estimating the efficiency of the pile group.

For clays, Fascicle 62 neglected the group effect if the pile spacing S_p is greater than $3d$. However, the 3D numerical analyses presented in this study prove that a C_g value of unity for pile groups in clay can considerably overestimate the bearing capacity, mainly for cases of large piles number as shown in Figure 3.6a.

It can be seen that a considerable difference was observed with C_g values calculated using the formula proposed by McCabe and Lehane (2006) (see Eq. 1.24), which presents the lowest values, notably for a large number of piles. As an example at $S_p = 6d$, the C_g values obtained using this formula underestimate the present study results of about 10%, 52%, and 87% for 4, 9, and 16 piles, respectively.

In order to develop an appropriate mathematical formula of C_g , using a nonlinear least-squares method, the expression of C_g was defined, as depicted in Eq. (3.1). The analysis was carried out by minimizing the mean square error between the proposed model and the present numerical results.

$$C_g = -12.68 \left(\frac{S_p}{d \times n} \right)^{0.2} + 26 \left(\frac{S_p}{d \times n} \right)^{0.1} - 12.35 \quad (3.1)$$

This proposed formula is shown in Figure 3.8. It can be noted that the suggested formula of C_g is efficient for calculating the ultimate bearing capacity of pile group foundations embedded in soft clay subjected to vertical loads.

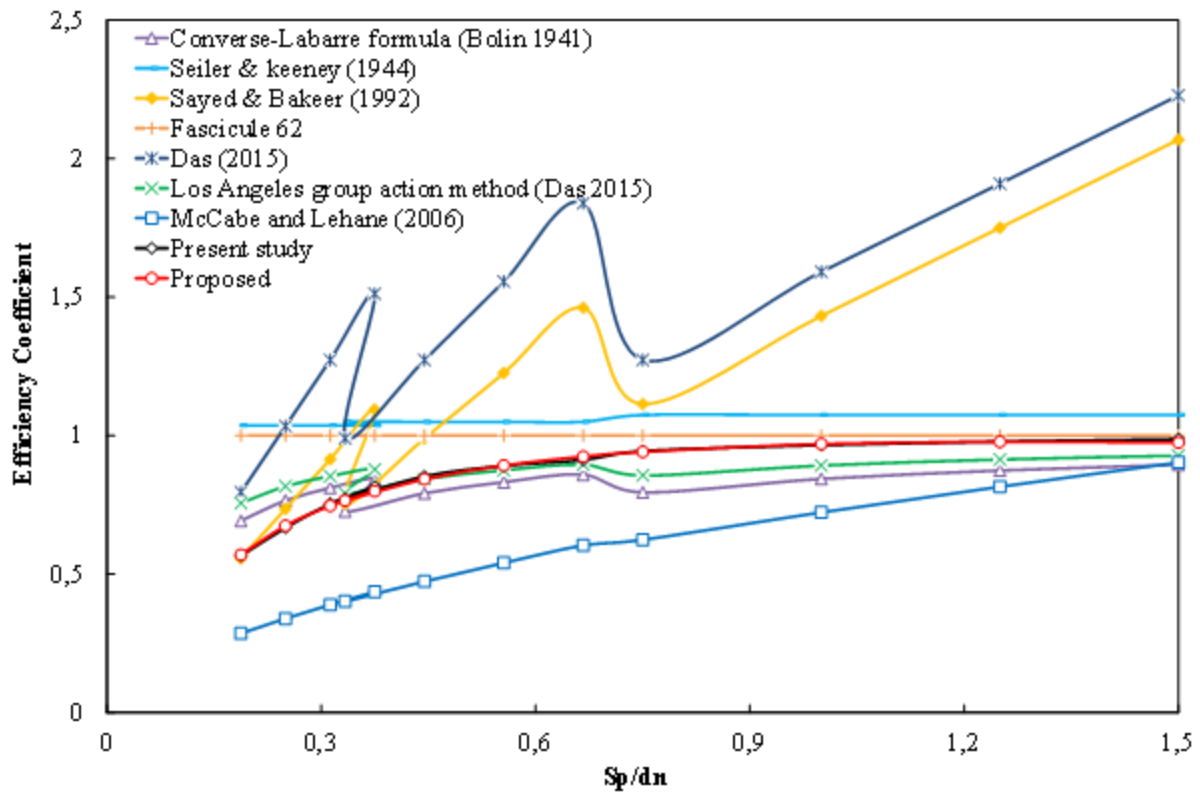


Figure 3.8 Comparison of C_g values calculated from: the proposed formula, the obtained results of FLAC^{3D}, and the popular formulas available in the literature

3.4 Summary

The interaction effects and load-carrying behavior of group of piles embedded in soft clays were studied using explicit finite difference code FLAC^{3D}. For this purpose, several types of pile configurations were considered. Based on the numerical analyses results obtained and within the range of the parameters tested and soil conditions, the following conclusions can be drawn:

- The efficiency coefficient of the pile group was often lower than unity for different pile spacing and piles number due to interaction effects between piles. So a value of efficiency coefficient of unity for pile groups in clay could considerably overestimate the bearing capacity of group of piles essentially for cases of large piles number.
- Although the bearing capacity of the pile group increases with increasing number of piles, the efficiency of the pile group embedded in soft clay is very important in the case of a small number of piles. Whereas, the pile group bearing capacity can be improved simply by increasing the pile spacing without increasing the number of piles.

- Among all popular formulas considered in this study, the Los Angeles group action and Converse-Labarre methods lead to comparable C_g values to those obtained from present 3D numerical results. While, the method suggested by McCabe and Lehane would have required a higher number of piles to ensure the stability of the structure which requires more resources e.g. concrete, energy...
- Based on the present finite difference analysis results, a new efficiency coefficient formula was proposed as a function of pile spacing and the number of piles.

CHAPTER 4

3D NUMERICAL STUDY OF THE BEHAVIOR OF PILED RAFT FOUNDATIONS IN THE SOFT CLAY

4.1 Introduction

Tall buildings and offshore structures are often built on piled raft foundations where the piles are used for enhancing the performance of the raft to satisfy the design requirements.

The design requirements may be related to the increasing of the overall bearing capacity and/or reduction of the average/differential settlements. In the piled rafts design, the sharing load between the raft and piles is considered, and the piles are used up to a load level that can be of the same order of magnitude as the bearing capacity of a comparable single pile or even greater (Reul and Randolph 2003). The overall load response of piled raft is linked to a complicate soil-structure interaction system, including the pile-soil, pile-pile, raft-soil, and pile-raft interactions (de Sanctis and Russo 2008; Park and Lee 2015; Lee et al. 2015; Mali and Singh 2018).

Despite the research efforts carried out and their encouraging results, there is a still confusion on piled raft interaction effects for drained soft clay conditions. Thus, further numerical investigations and experimental studies are required to provide more insight into the mechanical response of piled raft system.

In this context, this research focuses on studying the piled raft behavior embedded in soft clay condition. The aim of the present study is to perform a full 3D numerical analysis, using the FLAC^{3D} code (Itasca 2013), of the overall load response, load sharing behavior, pile load distribution, and effects of the interactions of piled raft foundation subjected to vertical static loading in soft clays. For this purpose, several types of foundations were considered including piled raft, group of piles, unpiled raft, and single pile. The study results are

validated by comparing them to those of similar subgrade-structure and in comparable geological conditions provided within the literature.

For design optimization purposes, the interactions behavior and the performance of the piled raft foundation is also investigated by varying some parameters as piles number and pile configuration. The change in these settings produces a wide variety of cases to be studied. The concluded observations from the parametric study provide further insight into the mechanical response of piled raft and aim at helping the engineers in taking a logical path in an iterative design process for a piled raft foundation.

4.2 3D numerical modeling

4.2.1 Modeling procedure and post analysis

The behavior of the piled raft foundation scheme embedded in soft clays was investigated by performing 3D numerical analyses using the finite difference formulation with the numerical code FLAC^{3D} (Itasca 2013).

To reduce the size of the mesh and the huge time required for running such a complicate 3D problem, only a quarter of the piled raft is modeled, since the problem geometry is doubly symmetrical.

To minimize the boundary effects on the behavior of the ground close to the foundation, the horizontal distance of the mesh boundary from the raft edges was set to 40 m (a distance greater than 2.5 times the size of the raft) and the mesh extends vertically at depth equal to two times the pile length. This extension of boundaries is kept fixed in all the numerical analyzes whatever the spacing and the number of piles.

A roller boundary was used to fix all nodes in the horizontal direction along the lateral boundaries. However, on the bottom of the model all nodes were restrained in both horizontal and vertical directions. The boundary condition and FLAC^{3D} mesh used for piled raft in the numerical analyses is shown in Figure 4.1. The raft is modeled using 12-noded radial cylinder solid elements and brick elements with 8 nodes, and piles are modeled by 6-noded cylindrical solid elements available in FLAC^{3D}. Despite solid elements do not explicitly predict internal efforts (unlike structural elements: Shell, Beam, Pile ...), they have the advantage of representing these structural elements (raft and piles) in a more realistic way.

Sensitivity study of the mesh density exhibits that it is required to have a refined mesh in the zones of high stress gradient. Thus, a relatively fine mesh was chosen close to the pile-

soil and raft-soil interface while a coarser mesh was used further from the piles and raft in order to reduce computation time. Such a refinement study resulted in using the mesh presented in Figure 4.1. The numerical models of the several foundation types considered in this investigation are shown in Figure 4.2.

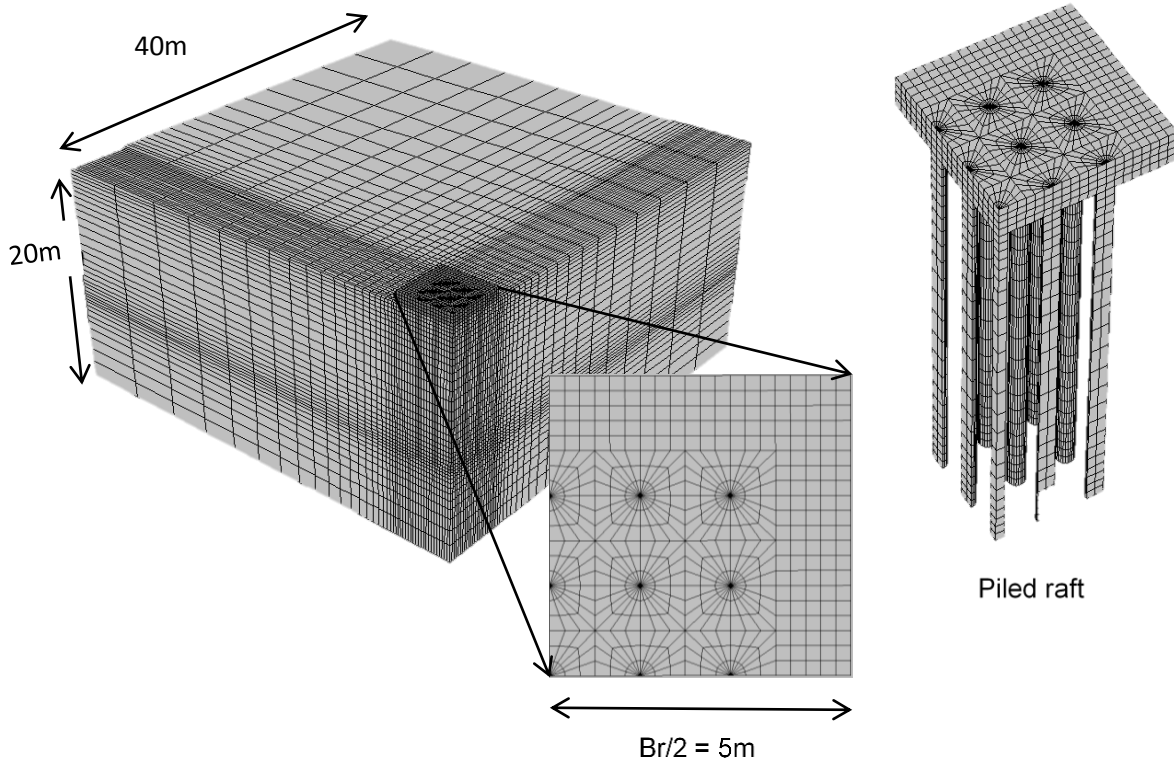


Figure 4.1 Detail of FLAC^{3D} grid used in numerical analyses

The raft was assumed to be rigid and the pile head was rigidly connected with the raft to ensure continuities in the displacement and stress distribution across the attached grids. Therefore, the grid volume of the raft is placed directly on those of piles head without setting up an element interface. In this way the differential settlement of the raft is limited. The verification of the supposition of rigid raft can be conducted by using the raft–soil stiffness ratio (K_{rs}) formula proposed by Horikoshi and Randolph (1997) in Eq. 4.1:

$$K_{rs} = 5.57 \frac{E_r}{E_s} \frac{1-v_s^2}{1-v_r^2} \left(\frac{B_r}{L_r} \right)^{0.5} \left(\frac{t_r}{L_r} \right)^3 \quad (4.1)$$

where

E_r and E_s are the Young's modulus of the raft and soil respectively, v_r is the Poisson's ratio of the raft and v_s is the Poisson's ratio of the soil, B_r , L_r and t_r are the width, length, and

thickness of the raft, respectively. In this study the calculated value of K_{rs} using Eq. 4.1 is about 33. According to Luo et al. (2018), values of $K_{rs} > 5$, the raft can be assumed as rigid.

In order to allow for soil-pile relative displacements, the contact between the soil and pile was described as able to slip. From the literature, the pile-soil interface has two types of modeling techniques, one using a slip interface element as it is used by Jeong et al. (2004), Achmus et al. (2009), Lee et al. (2010) or Alshenawy et al. (2016), and another is without using an interface element, the lateral contact pile-soil was assumed by a thin layer as it is used by Reul and Randolph (2003) or de Sanctis and Mandolini (2006), the thickness of this layer should be defined with caution after several attempts. For that reason, in the current study, slippery elasto-plastic interface elements have been used. The Mohr-Coulomb failure criterion was used to the interface element to simulate the occurrence of the slippage at the pile shaft when the shear stress reaches the soil yield strength. FLAC^{3D} provides interfaces that are characterized by normal and shear stiffnesses, and sliding properties (friction angle and cohesion). In order to install the interfaces, the grid representing the ground is created first and interfaces are attached to the zone faces with the piles. The cylinder pile grid is created separately and then is moved into contact with the interface elements (Itasca 2013). For more details about the slip interface elements, the reader should refer to FLAC^{3D} manual and the work of research done by Jeong et al. (2004) or Lee et al. (2010).

Both the raft and the piles are made from reinforced concrete which is modeled as a linear elastic material with a Young's modulus of 30 GPa and Poisson's ratio of 0.2. The material behavior of soil in this study is simulated with a linear elastic-perfectly plastic constitutive law using the Mohr-Coulomb failure criterion. The Mohr-Coulomb model, widely used in the modeling of geotechnical works, has the advantage of needing few input parameters and that all these parameters can be obtained from the standard soil tests. The use of a more complex constitutive model that takes into account the nonlinear behavior will probably requires the estimation of specific input parameters from unusual tests. As a result, the number of input parameters to be evaluated would be greater, and their interdependence is not evident (Houhou et al. 2019).

In this study, the analysis type of the numerical simulation was effective drained analysis to get the long term behavior for the piled raft system in soft clay. A general water table is defined at the free surface, under which the water pressure distribution is hydrostatic. Since the present study focuses on the long-term behavior, the simulation is conducted by a mechanical mode and the pore-pressure field can be uncoupled from the mechanical field (by

setting flow off and set the water bulk modulus to zero for this mechanical-only calculation). In this way, the pore pressure field will not be changed by the volumetric strain.

Since the bored pile causes a limited stress change in the soil during pile installation, the stress change in the soil was therefore neglected in these analyses. The numerical simulation has been performed according to three subsequent stages: (1) Gravity loading for generation of the initial stress field; (2) Raft and piles installation, by assigning the properties of concrete to the foundation components zone; (3) Vertical raft loading, i.e. step by step application of a uniformly distributed vertical velocity on the raft surface.

The obtained preliminary results allow choosing a relevant magnitude of loading that ensures high accuracy of results. Thus, the foundation loading was simulated by imposing a vertical downward velocity of 10^{-8} m/s on the upper face of the raft. Then, the loads taken by the raft and by the piles were obtained by integrating vertical stresses along the raft surface and the pile heads respectively. As a result, the axial pile load (P_p) was calculated from the vertical stresses in the pile head elements using the following equation:

$$P_p = \sum \sigma_i \times S_i \quad (5.2)$$

where

σ_i is the vertical stress along the pile head at cylindrical solid element i ; and S_i is the segment cross section area of element i .

The piled raft system can be characterized as a consequence of the load sharing between their components using the load-sharing ratio (α_p), which is the ratio of the sum of all pile loads ($\sum P_p$) to the total vertical load of the foundation (P_{total}), proposed by Mandolini (2003) as follows:

$$\alpha_p = \frac{\sum P_p}{P_{total}} \quad (5.3)$$

So, the load-sharing ratio describes the portion of the load carried by the piles. $\alpha_p = 0$ corresponds to an unpiled raft, while the value of unit represents freestanding pile group (foundation supported by piles only). Thus, $0 < \alpha_p < 1$ describes a piled raft foundation.

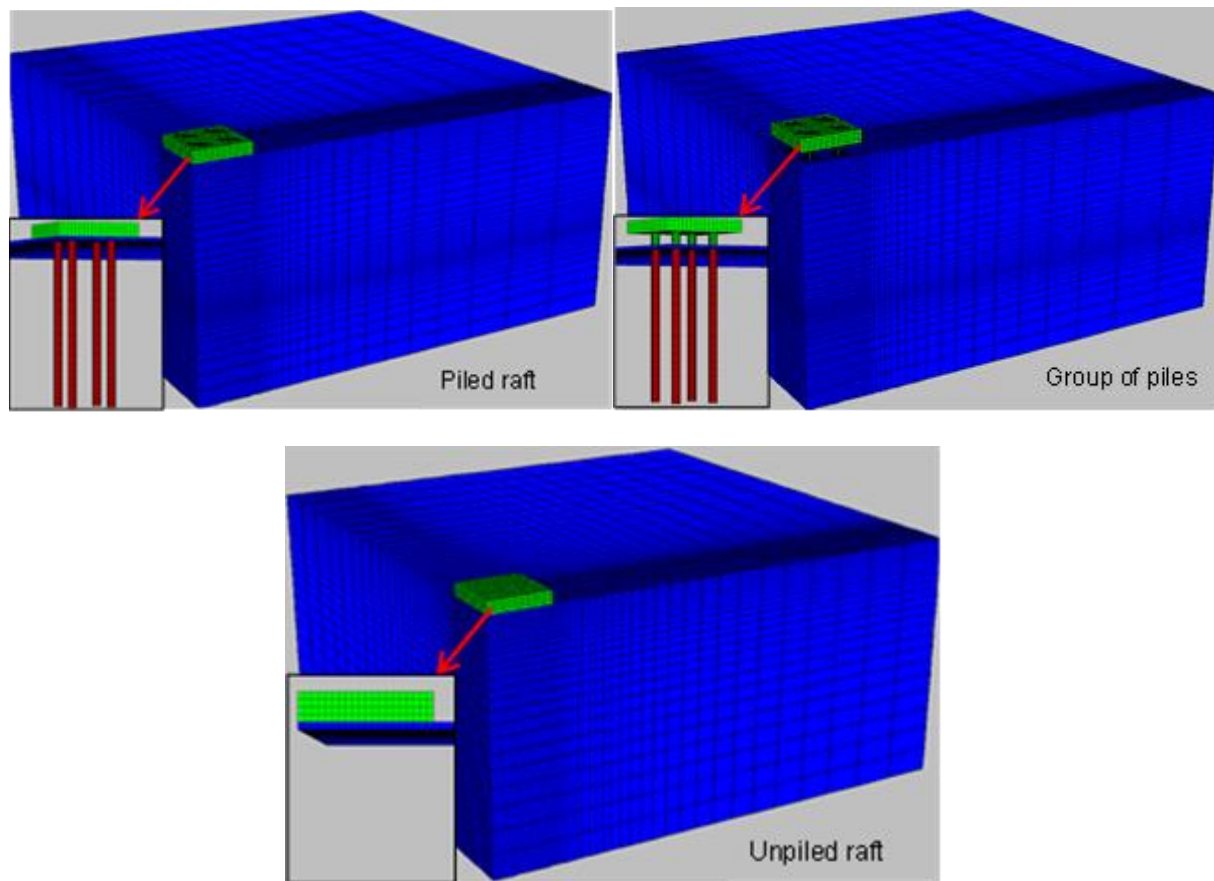


Figure 4.2 FLAC^{3D} meshes used for several foundation types considered in numerical analyses

4.2.3 Validation of numerical model

Numerical models based on the modeling procedure presented above are developed, and their accuracy is validated by comparing with the results of other existing numerical methods and experimental measurements of similar subgrade-structure and in comparable geological conditions provided within the current literature.

- **Case 1**

To prove the validity of the modeling procedure done in this study, the obtained numerical results were compared with those available in the literature, especially the studies carried out by Sinha and Hanna (2016), and Mali and Singh (2018). It is a case of piled raft system which consists of square raft in plan with dimensions of 24×24 meters and thickness equals 2 m. The square raft rests on 16 circular piles with diameter of 1.0 m and length of 15 m entirely embedded in soft clay. The piles used are uniformly placed under the raft with pile spacing (S_p) equal to 6 times the piles' diameter (d). The loading was simulated by applying a uniformly distributed vertical load on the foundation surface. The soil and foundation

parameters used in the numerical model are summarized in Table 4.1. Figure 4.3 shows a comparison between the load-settlements behavior of piled raft resulting from the current finite difference analyses and the finite element analyses of Sinha and Hanna (2016), and Mali and Singh (2018). It can be seen that the results obtained from the present numerical study agree well with the previous numerical works.

Table 4.1 Material parameters used in the analyses (Sinha and Hanna 2016)

Parameter	Clay	Pile	Raft
Young's modulus, E (MPa)	54	25,000	34,000
Poisson's ration, ν	0.15	0.2	0.2
Unit weight, γ (kN/m ³)	19	25	25
Friction angle, ϕ' (°)	20	-	-
Cohesion, c' (kPa)	20	-	-

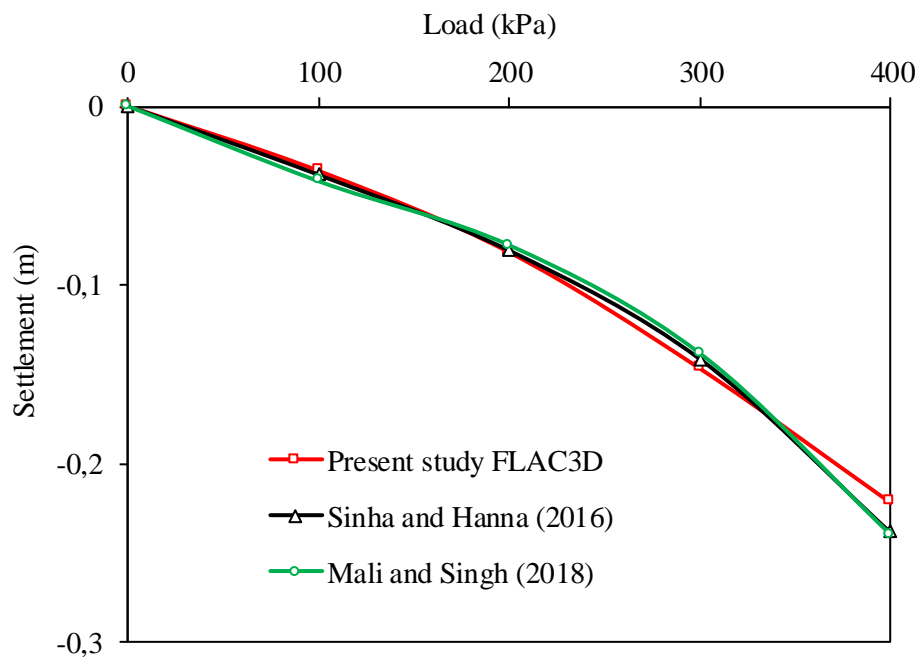


Figure 4.3 Comparison between results of present study and previous numerical works of load-settlements behavior of piled raft

- **Case 2**

The obtained computational results were also compared with those of the centrifuge test reported by Horikoshi and Randolph (1996) to prove the validity of the modeling procedure

presented in this study. The centrifuge test was conducted for a circular PR model embedded in a clay layer having nine piles with pile spacing of 2.5 m, a length of 15 m, and a diameter of 0.32 m. The circular raft is 14 m in diameter and 0.05 m in thickness. The prototype scale is considered in this analysis. Since the interface friction coefficient was not provided by the authors, an average interface friction coefficient of 0.3 was used to simulate the contact pile-soil, as recommended by Lee et al. (2010). The material parameters of the soil and PR were adopted from reference values reported by Horikoshi and Randolph (1996), as detailed in Table 4.2. Constant values of Young's modulus and shear strength parameters were assumed to simplify the analysis. The axially applied load was 12 MN.

Table 4.2 Material properties, adopted from Horikoshi and Randolph (1996)

Parameters	Soil	Pile	Raft
Young's modulus: E , MPa	16.8	40 000	40 000
Poisson's ratio: ν	0.4	0.16	0.16
Density: γ , kN/m ³	17.5	20	20
Undrained shear strength: C_u , kPa	41.4	-	-

The results of the present numerical analysis and the centrifuge model test are presented in Table 4.3. It can be noted that the measurements and the numerical results are in good agreement, both in terms of average settlement and load carried by piles. A similar trend was found by Lee et al. (2010) and Ghalesari and Choobbasti (2018).

Table 4.3 Comparison of the results

Results	Average settlement (mm)	Load carried by piles (%)
Measured	22	19
Present study (FLAC ^{3D})	22.6	21.7

4.3 3D numerical analysis of piled raft interaction in drained soft clay conditions

In this study, 3D finite difference analyses are performed to investigate the behavior of piled raft foundation system in drained conditions of soft clays. The overall objective of the present parametric study focuses on the effects of multiple interactions between raft-pile-soil on the piled raft behavior in the case of soft clay.

4.3.1 Parametric study

A broad parametric study was carried out to analyze the behavior of piled raft (PR) foundation system subjected to vertical loading embedded in a soft clay profile using variable number of piles and pile spacing under a square raft, considering the 3D interactions between the soil, piles and raft. To check the piled raft interaction effects for soft clay conditions, various types of foundations were considered, including PR, unpiled raft (UR) and group of piles (GP). To reduce the huge amount of storage and time needed for numerical computation, small dimensions for foundations were considered in this parametric study as well as general dimensions assumed by most researchers.

The piled raft simulated in this analysis is composed of a square raft of 10 m in width and 1 m in thickness, and piles of 12 m in length in different configurations. This foundation was selected to allow for utilizing four commonly used pile spacing values (i.e. $3d$, $4d$, $5d$ and $6d$), with a pile diameter d of 0.5 m without changing the raft size. Three cases of uniformly pile arrangements, 2×2 ; 3×3 and 4×4 were examined, corresponding to $n = 4$, 9 and 16 piles, respectively. All the aforementioned pile spacing was investigated for each pile arrangement. So there are 12 pile configurations in total. Figure 4.4 shows the pile configurations considered in the present parametric study for different number of piles and pile spacing.

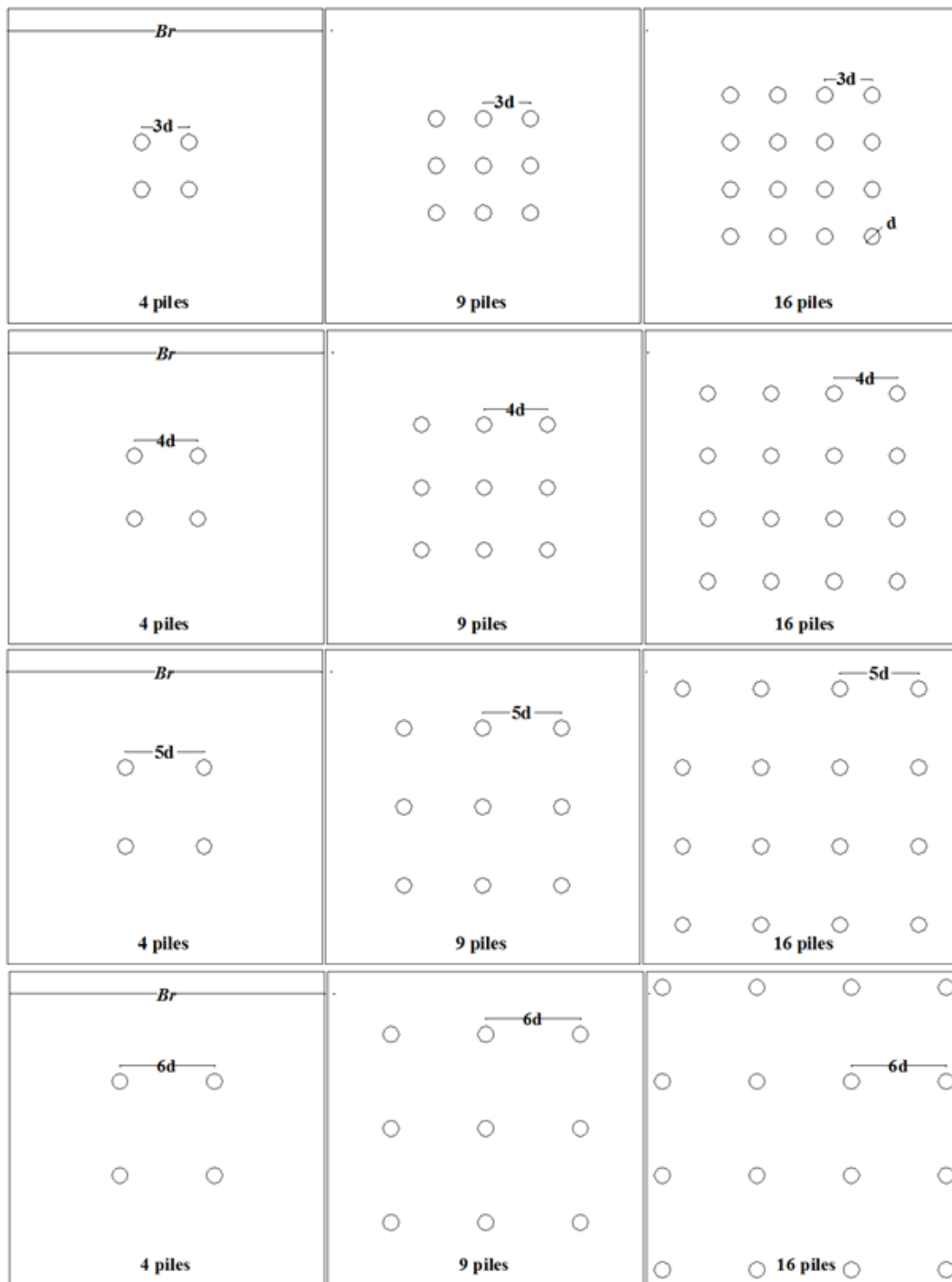


Figure 4.4 Pile configurations considered for parametric analysis

The drained characteristics of the soft clay were adopted from reference values reported by Nguyen (2008). To simplify the numerical computation, average values of drained Young's modulus and shear strength parameters c' and ϕ' were assumed for the soil profile. Table 4.4 summarizes the foundation and soft clay parameters used in the parametric analysis.

Table 4.4 Material parameters used in the parametric study

	Model	E (MPa)	c'(kPa)	ϕ' (°)	ν	K_0	γ (kN/m ³)
Foundation	Elastic	30 000	-	-	0.2	-	25
Soft clay	Mohr–Coulomb	4.8	15	31	0.3	0.5	14

4.3.2 Computed results

- **Load-settlement response**

The load-normalized settlement behavior obtained from analyses of UR, GP and PR in the case of $n = 16$ and $S_p = 4d$ are plotted in Figure 4.5. As expected the load-carrying capacity of PR is higher than those of UR and GP. So, adding a number of piles to the raft helps to avoid excessive settlements and to enhance the bearing capacity of the foundation. Furthermore, the load-carrying capacity obtained from GP was found to be higher than those obtained from UR until a settlement level (s) of $1.5\% B_r$, a difference of about 25% is noted at $s = 1\% B_r$, as shown in Figure 4.5. However, after this settlement range, the trend is reversed, so that the load carrying capacity obtained from UR becomes higher than that obtained from GP, at ultimate state ($s = 10\% B_r$) the UR bearing capacity has been almost doubled compared to that of GP. It should be noted that the load carrying capacity of piles is mobilized earlier than that of the raft due to the smaller piles size in respect of the raft. These results are in good agreement with those found by Lee et al. (2014).

The load-normalized settlement behavior of the piled raft components, namely the raft (Rpr) and the piles (Ppr), obtained from the present analyses in the case of $n = 16$ and $S_p = 4d$ are given in Figure 4.6. For purpose of comparison, the PR load response is plotted in the same figure. Until a certain settlement level of $6\% B_r$, it can be seen that the load carrying capacity of the component P_{pr} (Q_p) is greater than that developed by the component R_{pr} (Q_r). At settlement level of $s = 1\%$ the Q_p is larger than Q_r by about 100%. Nevertheless, after the settlement level of $6\% B_r$, the load-carrying capacity obtained from R_{pr} becomes higher than that obtained from P_{pr}, a difference of only 7% was found at ultimate state.

From Figs. 5.5 and 5.6, it can be seen that the unpiled raft and the group of piles behave in a significantly different way than the raft and piles components of PR foundation scheme due to the piles and raft interaction effects.

Moreover, for the initial settlement range up to $s = 0.5\% B_r$ (corresponds to ultimate state of piles $s = 10\% d$), the load carrying capacity of the Ppr is very close to that of the PR.

After this settlement level, the Ppr shows smaller values than those of PR. This can be explained by that at initial loading stage, the almost of applied loads are carried by the piles, in the following loading stage the portion of load carried by the raft increases and becomes more important.

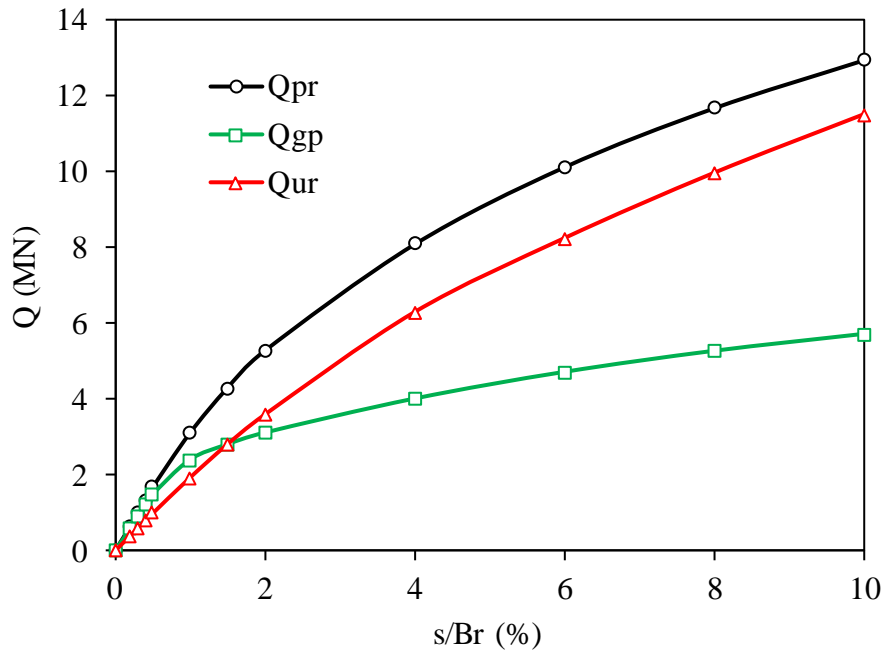


Figure 4.5 Load-normalized settlement curves of PR, UR and GP for $n = 16$ and $S_p = 4d$

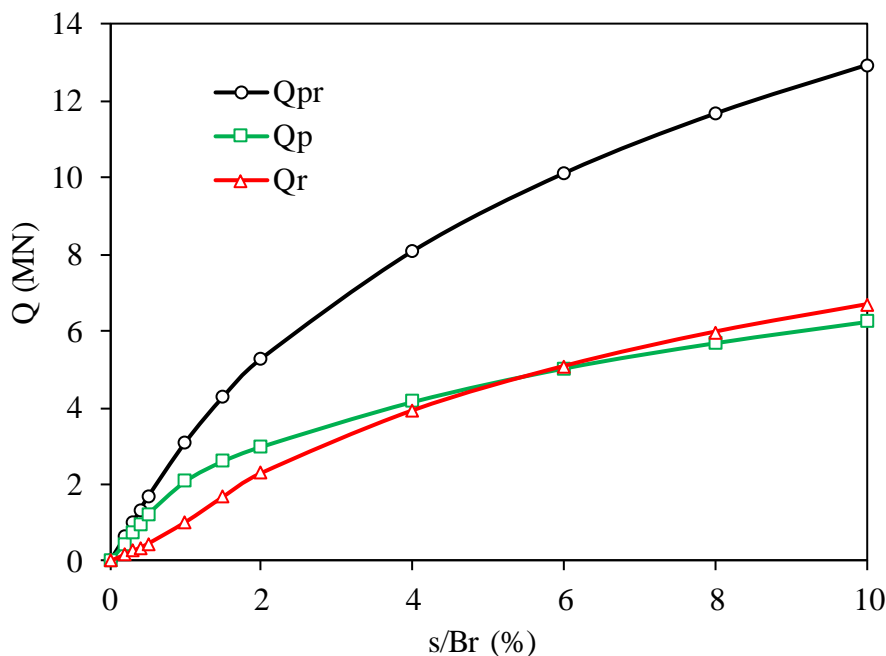


Figure 4.6 Load-normalized settlement curves of PR, Ppr and Rpr for $n = 16$ and $S_p = 4d$

The load evolution of PR, UR and GP in the case of $n = 9$ and $S_p = 4d$ is shown in Figure 4.7. It can be seen that the load-carrying capacities obtained from GP and UR are very comparable until a certain settlement level of $0.4\% B_r$. However, after this settlement level, the UR load-carrying capacity becomes higher than that obtained from GP, at ultimate loading state, the UR bearing capacity was about 260% greater than that of the GP.

Figure 4.8 shows the load-normalized settlement behavior of the piled raft and their components in the case of $n = 9$ and $S_p = 4d$. It can be noted that the load carrying capacity of Ppr, unlike the case of 16 piles; is at most 25% more important than that of Rpr until a certain settlement level of $1\% B_r$. But after this settlement level, the load capacity carried by Rpr becomes higher than that of Ppr, at ultimate state of loading, unlike the case of 16 piles; Q_r is about 140% more important than Q_p .

From Figs. 5.7 and 5.8, it should be noted that interaction effects between piled raft components are not as obvious as those observed in the case of $n = 16$. As a result, the importance of PR interaction effects depends on the number of piles, so that as piles number increases as PR interaction effects become more significant.

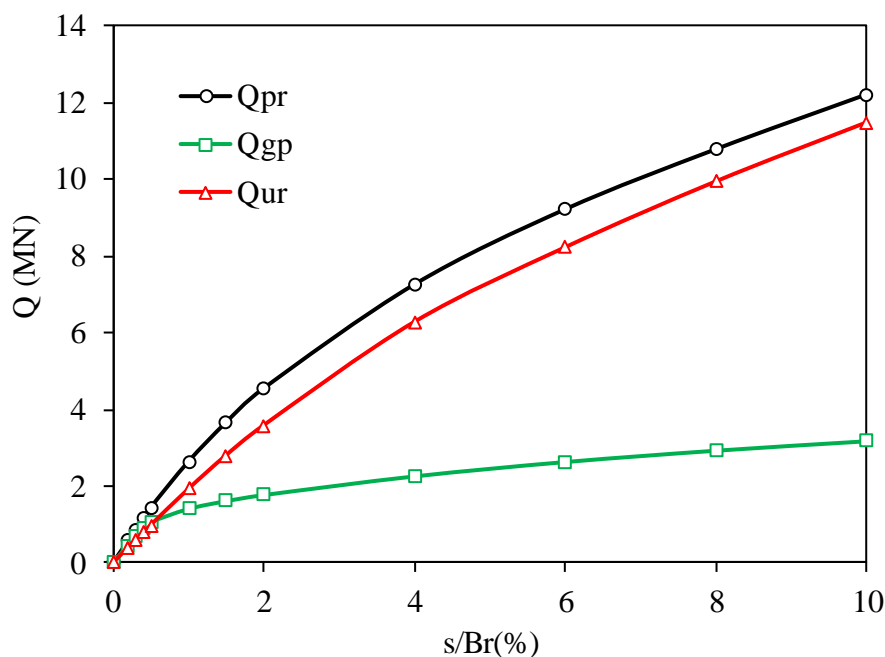


Figure 4.7 Load-normalized settlement curves for $n = 9$ and $S_p = 4d$, PR, UR and GP

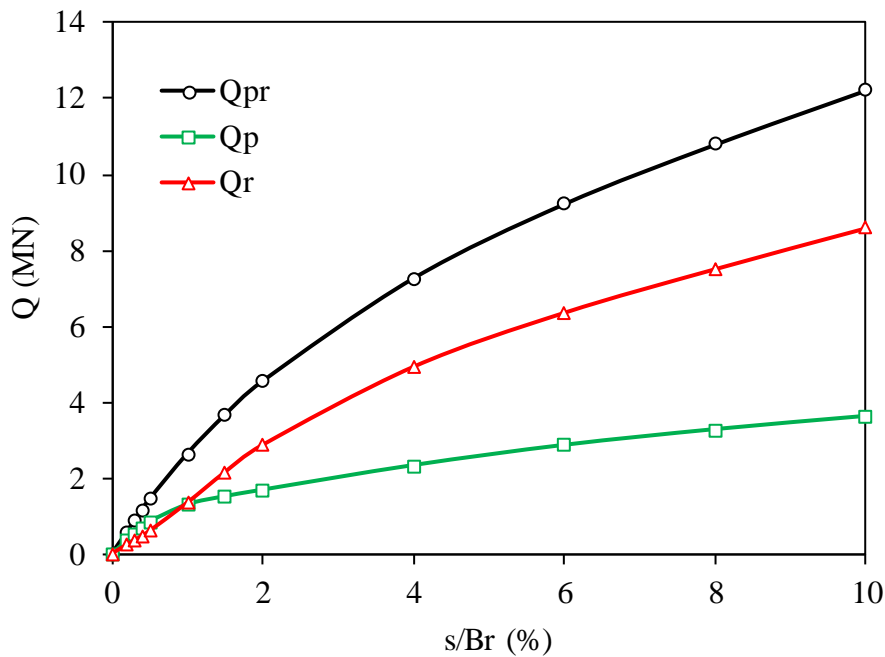


Figure 4.8 Load–normalized settlement curves for $n = 9$ and $S_p = 4d$, PR, Ppr and Rpr

Since Lee et al. (2014) and among others reported that the PR interaction effects are not very influential in the drained clay conditions, the ultimate bearing capacity of PR foundation should be the sum of those of UR and GP, so it can be expressed as follows:

$$Q_{pr} = Q_{ur} + Q_{gp} \quad (5.4)$$

where

Q_{pr} , Q_{ur} and Q_{gp} are the ultimate bearing capacities of PR, UR and GP, respectively.

For comparison purpose, the load carrying capacity curve of PR is plotted in the same figure with the curve resulted from the sum of the two load carrying capacities of UR and GP as shown in Figure 4.9 for the case of $n = 16$, $S_p = 3d$ and $6d$.

It can be seen from this figure that the sum of Q_{ur} and Q_{gp} is significantly greater than Q_{pr} for the entire settlement range; a difference up to 35% can be noticed at ultimate state. This confirms that in drained soft clay conditions, there are a noticeable interaction effects between raft and piles of piled raft. Similar trends and results were found for all cases of n and S_p considered in this parametric study. Consequently, the neglect of the piled raft interaction effects, as in the aforementioned works of research, could considerably overestimate the ultimate bearing capacity of the piled raft system.

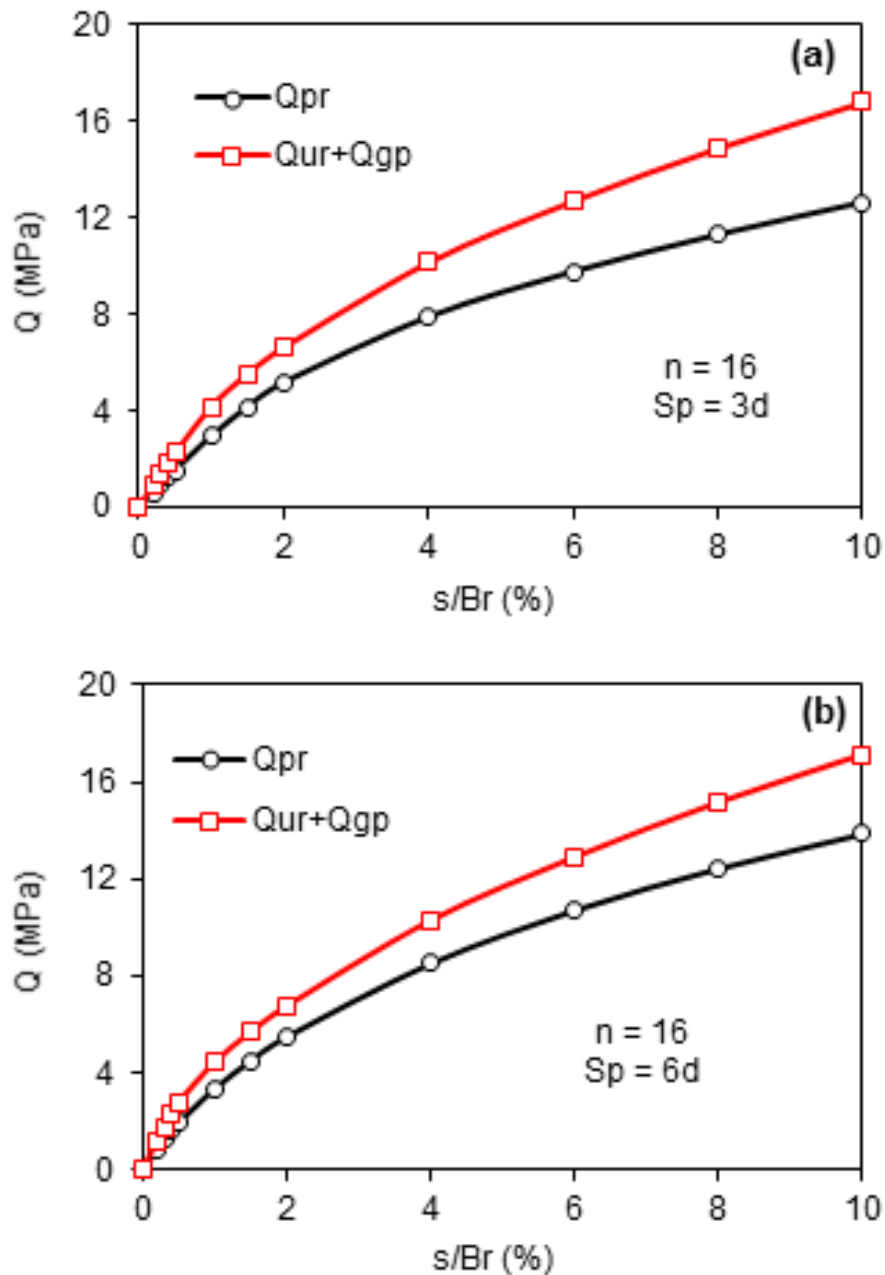


Figure 4.9 Evolution of load capacities of PR and the sum of UR and GP in the case of 16 piles with $S_p = 3d$ and $6d$

To study the effect of number of piles and their spacing on the PR performance, various pile configurations with different values of n and S_p were tested as shown in Figs. 5.10 and 5.11. For comparison purpose, the load capacity evolution of UR is added in the Figure 4.10. From this figure, as expected, the load carrying capacity of PR increases with the number of piles for all considered values of S_p . The effect of n depends substantially on the pile spacing so that as the pile spacing increases as the effect of n on the PR performance becomes significant.

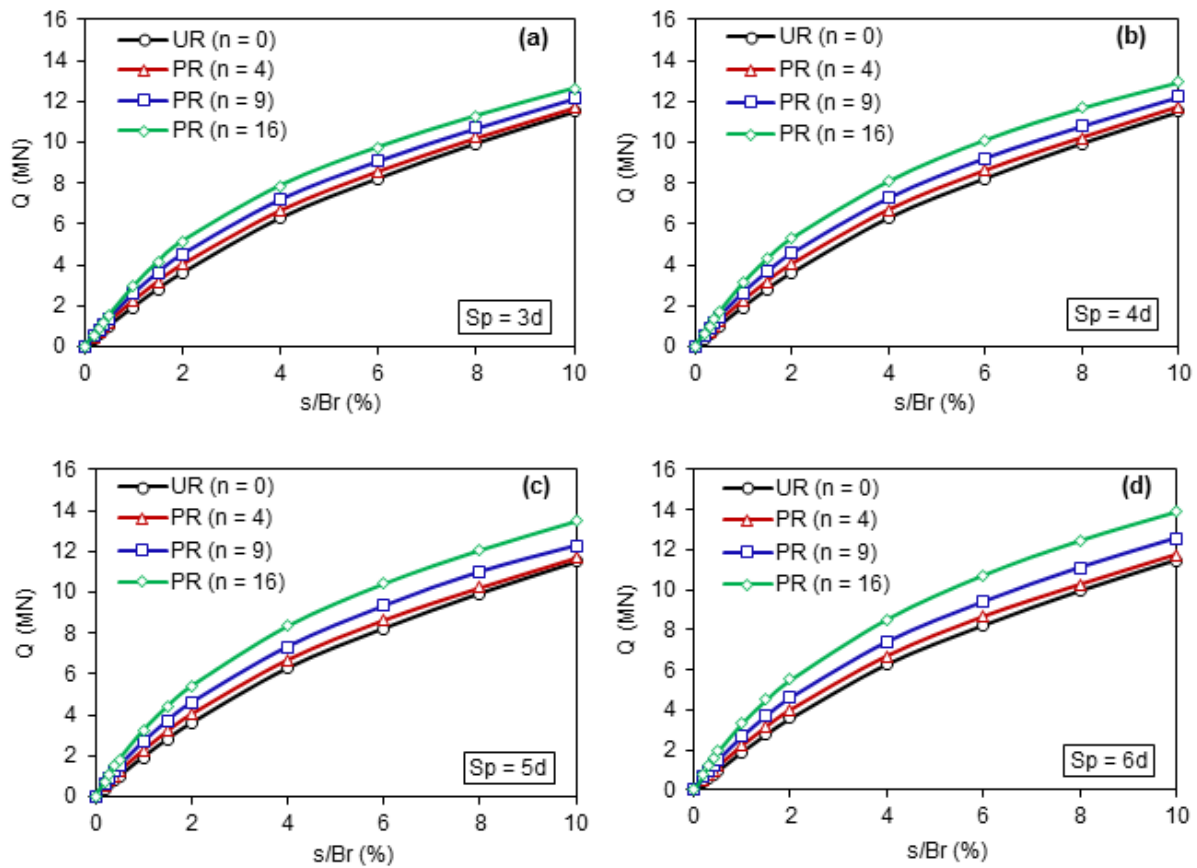
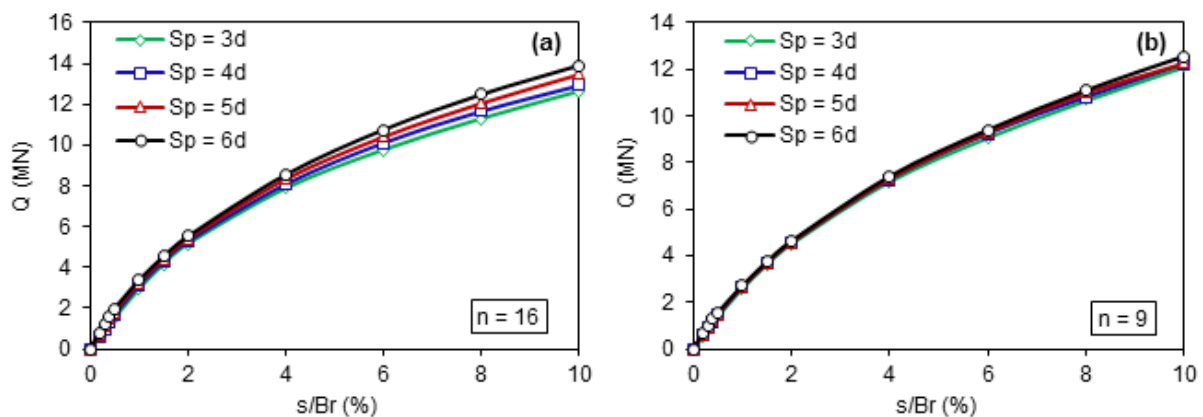


Figure 4.10 Load–normalized settlement curves of UR and PR for different values of n and S_p

From Figure 4.11(a), case of $n = 16$, increasing of S_p has a negligible effect on load-settlement response of PR until a settlement level of about $s = 4\% B_r$ beyond which the S_p effect becomes noticeable at least for the cases analyzed in this parametric study. As n decreases (Figs. 11b and 11c) as the effect of S_p becomes less pronounced regardless of the settlement level. So, it can be concluded that the S_p effect depends on both piles number and settlement level.

From Figs 5.10 and 5.11, it can be noted that the piles number has a significant effect on bearing capacity and load-settlement response of PR comparing to the pile spacing effect.



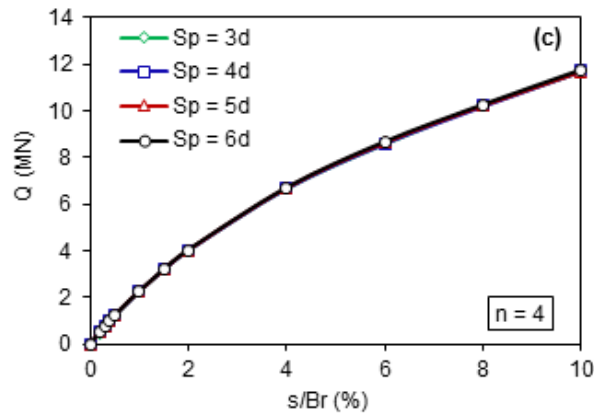


Figure 4.11 Load–normalized settlement curves of PR for different values of S_p for given values of n

- **Load sharing between piles and raft**

In piled rafts system, the raft component is in contact with the ground surface between the piles and which consequently contributes to the distribution of loads, a proportion of load is directly transferred to the subsoil by the direct contact pressure of the raft and the rest of the load is carried by piles. For this reason, the load sharing between PR components must be studied. The proportion of the load carried by the piles to the total applied load for piled raft foundation can be expressed by the load sharing ratio as described in Eq. (5.3). Figure 4.12 shows the evolution of the coefficient α_p based on normalized settlement level for different pile configurations. At low settlement levels ($s < 1\% B_r$), the evolution curves of the coefficient α_p of all pile configurations differ from each other and then became close to each other by increasing the settlement level. This finding is in good agreement with experimental observations noted by Lee et al. (2014). This behavior can be explained by the fact that the piles at low settlement levels carry most of the applied load, and then the raft contribution gradually increases with increasing the settlement level. From Figure 4.12a, corresponding to the case of 16 piles, it can be seen that the pile spacing has a positive relationship with the load sharing ratio at low settlement levels ($s < 1\% B_r$). In other words, increasing S_p leads to a significant increase of α_p . Nevertheless, after this settlement level, the pile spacing has become of little effect. The same trend was observed in Figs. 12b and 12c corresponding to the cases of 9 and 4 piles respectively. However, it should be mentioned that the effect of pile spacing on the load sharing ratio at initial settlement level becomes less important as the number of piles decreases.

From the obtained results, it can be concluded that the coefficient α_p is inversely proportional to the settlement level and it is even higher when the number of piles is

increased, and this is valid regardless of the pile spacing. Moreover, the range of initial settlement, wherein α_p is proportional with S_p , enlarges with increasing number of piles. This positive relationship takes place because the PR interaction effect is influenced by the increased friction of piles skin caused by the increased in confining stress in the soil due to the raft pressure (Katzenbach et al. 2000). The higher raft pressure corresponds to the largest value of S_p . On the other hand, as the settlement further increases, the PR interaction effect represents less mobilization of pile skin friction due to reduced relative displacement between piles and surrounding soils, as soils beneath the raft are forced to move downward upon loading (Han and Ye 2006).

It can also be seen from Figure 4.12 that the decrease of the coefficient α_p in the case of 4 piles is represented by a steeper slope curve than that of the case of $n = 9$, then of $n = 16$, which means that the raft contribution is significant for a small piles number. This is because increasing the number of piles reduces the contact area between the raft and the soil; therefore, the raft contribution becomes less important.

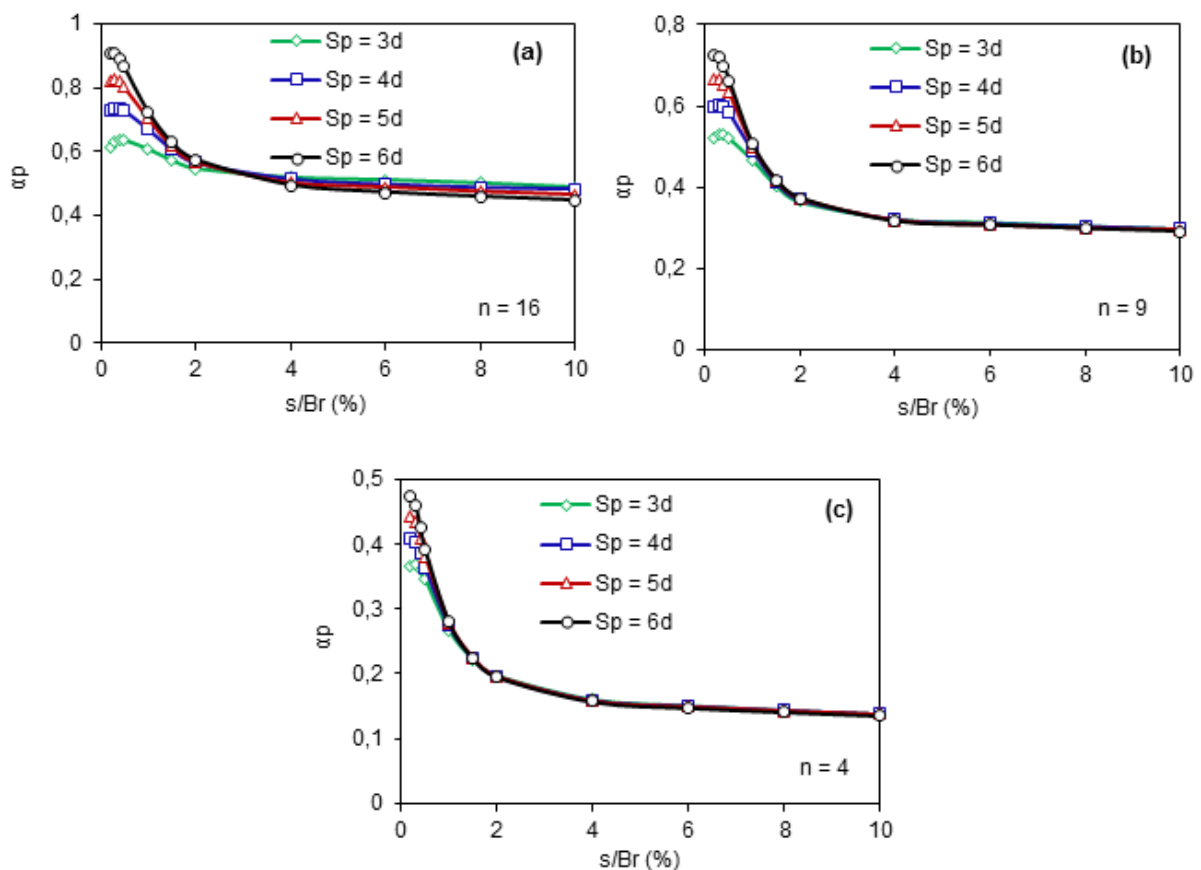


Figure 4.12 Evolution of the load sharing ratio according to the settlement level for different values of pile spacing and piles number

- **Pile load distribution**

For design optimization purposes it is required to know how the applied load is transferred to the subsoil by the PR components and to define with caution the different factors affecting this aspect. In cases where piles are essential to ensure the stability it is important not only to predict the load sharing between PR components but also to know the load distribution between piles of PR.

The pile load distribution of the PR foundations has been the topic of continuous research effort. One can refer to the work of Reul and Randolph (2003), Lee et al. (2010), Hussien et al. (2016) or Luo et al. (2018). The analysis is generally based on ultimate state of settlements. Nevertheless, little attention has been paid to the load distribution of piles occurring at small settlement level (initial settlement case or the case of low loading at service state). Thus, the pile load distribution of the PR foundations is also investigated in this numerical study. The effect of S_p was first studied for a given value of settlement and secondly the effect of settlement by fixing the value of S_p on the pile loads distribution. All the considered variants were tested for two different values of piles number namely $n = 16$ and $n = 9$.

Figs. 5.13 and 5.14 show the load distributions between piles of PR for different values of S_p and settlement in cases of 16 and 9 piles, respectively. At initial settlement level ($s = 0.2\% B_r$), it can be seen from these figures that the center pile (P1) carried lower load than the lateral pile (P2) and then the corner pile (P3), thus P3 carries the highest load portion. However, the load distribution behavior is reversed at ultimate state ($s = 10\% B_r$), where the highest load portion was supported by the pile P1. It should be noted that this behavior is independent of S_p and n either at initial or ultimate settlement levels. From Figs. 5.13 and 5.14, it can also be seen that at initial settlement level, the increase of S_p increases linearly and noticeably the load portion carried by each pile wherever its position. Whereas at ultimate state, the pile spacing affect the portion of the load carried by pile depending on its position. Increasing S_p increases linearly the load portion carried by the corner pile (P3) and reduces that carried by the center pile (P1). Thus, at ultimate state, the difference between the portion of the load carried by P1 and that supported by P3 is very pronounced in the case of small spacing ($S_p = 3d$) than that in the case of large spacing ($S_p = 6d$). For $S_p = 3d$ (Figure 4.13), the portion of the load supported by P3 is less than that of P1 by about 28%. However, in the case of $S_p = 6d$ the portion of the load carried by P3 is smaller than that of P1 by only 13%. According to the results obtained from this parametric analysis, it can be noted that the pile

load distribution is affected by the pile position, pile spacing and settlement level; however, it is irrespective of pile number.

The above-mentioned results show that the piles near to the center of the raft are more affected by the PR interaction effects which represent increasing pile skin friction caused by increases in confining stress within the soil by raft pressure than the lateral piles and then the corner piles. This is depending on settlement level or total load imposed on the raft surface. It can be also noted that at initial settlement level, the portion of the load carried by pile increases depending on its distance from the center of the group. But at ultimate state, the portion of the load taken by pile increases depending on its nearness of the center of the group.

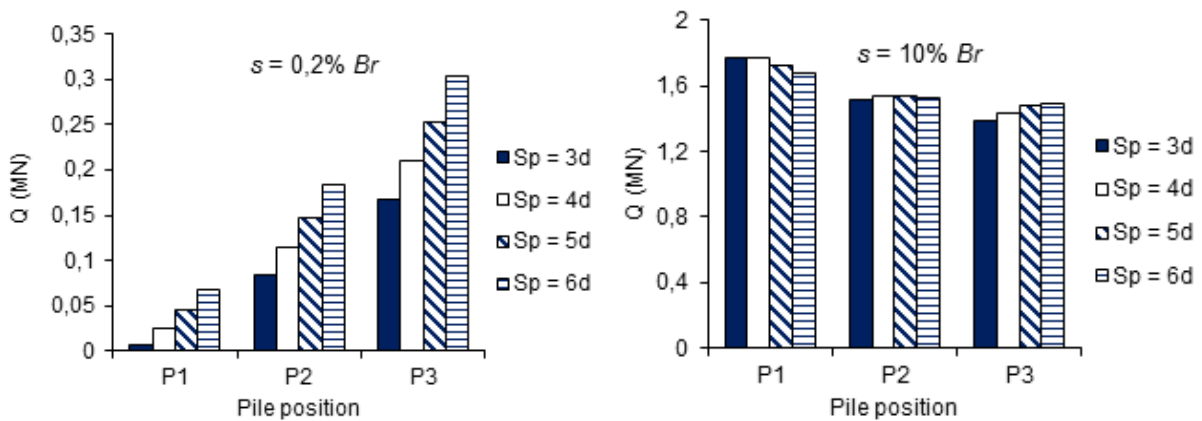


Figure 4.13 Load distributions between piles of PR for different values of pile spacing S_p and settlement level s in the case of 16 piles

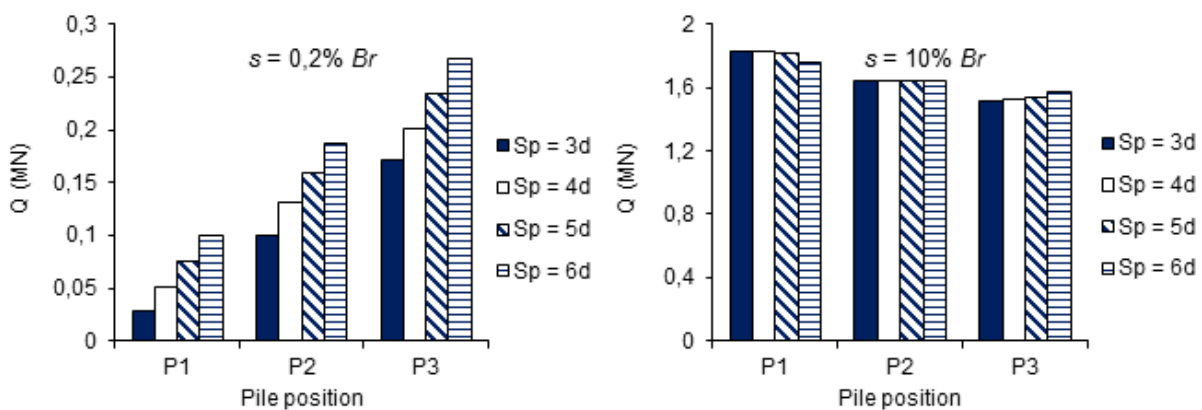


Figure 4.14 Load distributions between piles of PR for different values of pile spacing S_p and settlement level s in the case of 9 piles

4.4 3D numerical investigation of piled raft interaction factors in soft clay conditions

In this study, using the code FLAC^{3D}, a broad parametric study has been carried out to investigate the behavior of piled raft foundations subjected to vertical static loading in soft clays considering the full 3D interactions between the soil, piles, and raft.

The purpose of this study is to assess the multiple interactions between the components of piled raft foundation system subjected to vertical loading in the case of soft clays. For this purpose, several types of foundations were considered including piled raft, group of piles, unpiled raft, and single pile. For design optimization purposes, the interaction behavior in the piled raft foundation system is also investigated by changing some parameters as piles number and pile configurations. The change in these settings produces a wide variety of cases to be studied.

The present numerical study focuses in particular on the evaluation of the raft-pile failure interaction factor. The latter should be the ratio of the load-carrying capacity of piles component, obtained at a settlement level of 10% of the raft width, to the ultimate load of the group of piles, obtained at a settlement equal to 10% of the piles' diameter. It should be noted that most researchers (Mali and Singh 2018; Park and Lee 2014; de Sanctis and Mandolini 2006) go wrong when they estimate the failure interaction factor because they do not take into account the different component sizes of the piled raft. To evaluate the failure load factor η_p , most researchers use $Q_{gp,ult}$, and Q_p at the same settlement level (10% Br), therefore the value of η_p is often underestimated because the bearing capacity of a pile group $Q_{gp,ult}$ is estimated at a level of settlement equal to 10% d , which represents a low value compared to that obtained at 10% Br . As for the value of η_r , this problem does not arise because $Q_{ur,ult}$, and Q_r are both estimated at 10% Br .

Because of the large amount of storage and time required for numerical calculation, several numerical studies were not conducted until a settlement of 10% Br . Hyperbolic extrapolation is often used to estimate the ultimate load of the piled raft (de Sanctis and Mandolini 2006; Lee et al. 2010). In this study, the ultimate load capacities of each foundation type are obtained at a settlement level of 10% Br .

4.4.1 Parametric Study

An extensive parametric study was carried out to analyze the behavior of piled raft system subjected to vertical loading embedded in a soft clay profile using a variable number of piles and pile spacing, considering the full interactions between the soil, piles, and raft.

Various types of foundations were modeled, including piled raft (PR), unpiled raft (UR), group of piles (GP), and single pile (SP) in order to investigate the piled raft interactions behavior. Figure 4.15 shows the various types of foundations used in this parametric study.

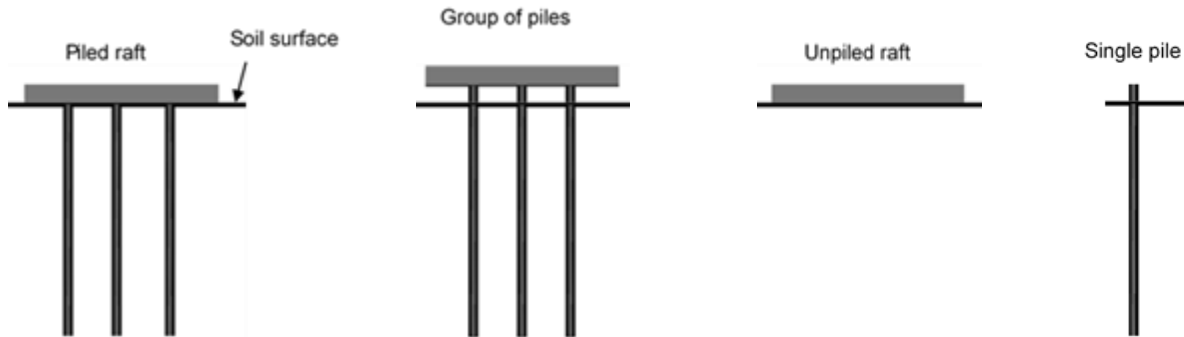


Figure 4.15 Various types of foundations used for 3D numerical parametric study.

The PR foundations modeled using $FLAC^{3D}$ were composed of a square raft with width $B_r = 10$ m, thickness $t = 1$ m, and piles of 12 m in length (L) in different configurations. Four cases of uniformly pile arrangements of 2×2 , 3×3 , 4×4 , and 5×5 were considered, corresponding to piles number of $n = 4$, 9, 16, and 25 piles respectively. The foundation size was selected to allow for employing four commonly used pile spacing values (i.e. $3d$, $4d$, $5d$, and $6d$) for $n = 4$, 9, and 16 piles and two pile spacing values ($3d$ and $4d$) for $n = 25$ piles, with a pile diameter of 0.5 m, without changing the raft size. 14 pile configurations in total were considered in this 3D numerical parametric study as shown in Figure 4.16.

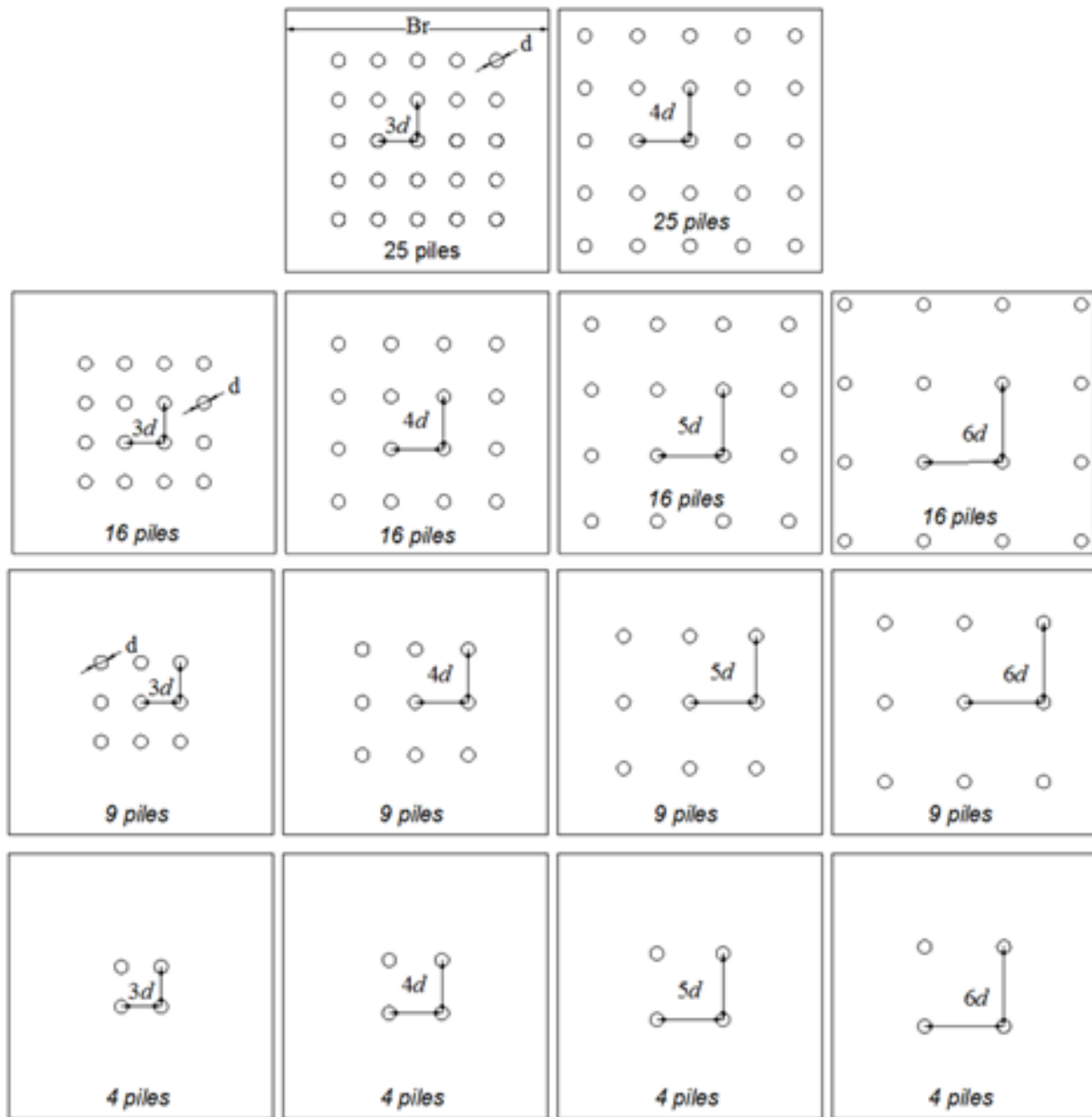


Figure 4.16 Various configurations of piled raft considered for parametric analysis

In this numerical study, attention was concentrated on the long-term response of a piled raft embedded in soft clay, so the soft clay was simulated using the drained shear strength parameters, ϕ' and c' . The concrete material of the structural components and the properties of the soft clay used in this study are summarized in Table 4.5.

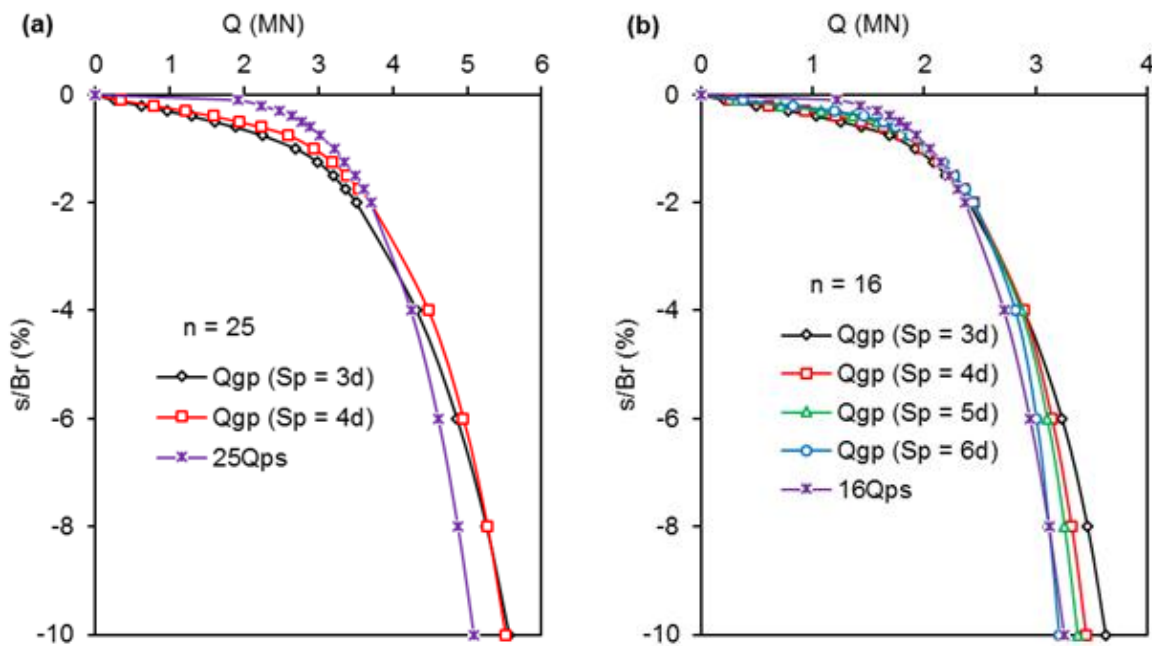
Table 4.5 Material parameters used in the analyses, adopted from Jeong et al. (2004)

	Model	E (MPa)	c' (kPa)	ϕ' ($^\circ$)	ν	γ (kN/m ³)
Foundation	Elastic	30 000	-	-	0.2	25
Soft clay	Mohr-Coulomb	5	3	20	0.3	18

4.4.1 Assessment of piled raft interaction effects from the computed results

• Pile group effect

Figure 4.17 presents the load-normalized settlement curves obtained from FLAC^{3D} for GP with different piles number and pile spacing and using n times SP load responses. Using the load-normalized settlement curves of GP of 25 piles and 25SP in Figure 4.17a, it can be seen that 25SP exhibit a higher load-carrying capacity than that of the GP up to a certain settlement level of $s = 2\% Br$ for $S_p = 3d$ and $s = 3.5\% Br$ for $S_p = 4d$ (a difference of about 73% and 44% can reach for $S_p = 3d$ and $4d$, respectively at $s = 0.5\% Br$, which corresponds to the ultimate state of the piles, $s = 10\% d$). However, after the settlement levels of $s = 2\% Br$ and $s = 3.5\% Br$, the load-carrying capacity of GP overestimates that of 25SP for both $S_p = 3d$ and $4d$. A difference of about 8.5% is observed at $s = 10\% Br$. It can also be noted that the load-carrying capacity obtained from GP for $S_p = 4d$ was higher than that obtained from GP for $S_p = 3d$ until a settlement level of $s = 6\% Br$ (a difference of about 68% was noticed at $s = 0.5\% Br$). However, after this settlement level, the load-carrying capacities obtained from GP for the case of $S_p = 3d$ and $4d$ became very comparable.



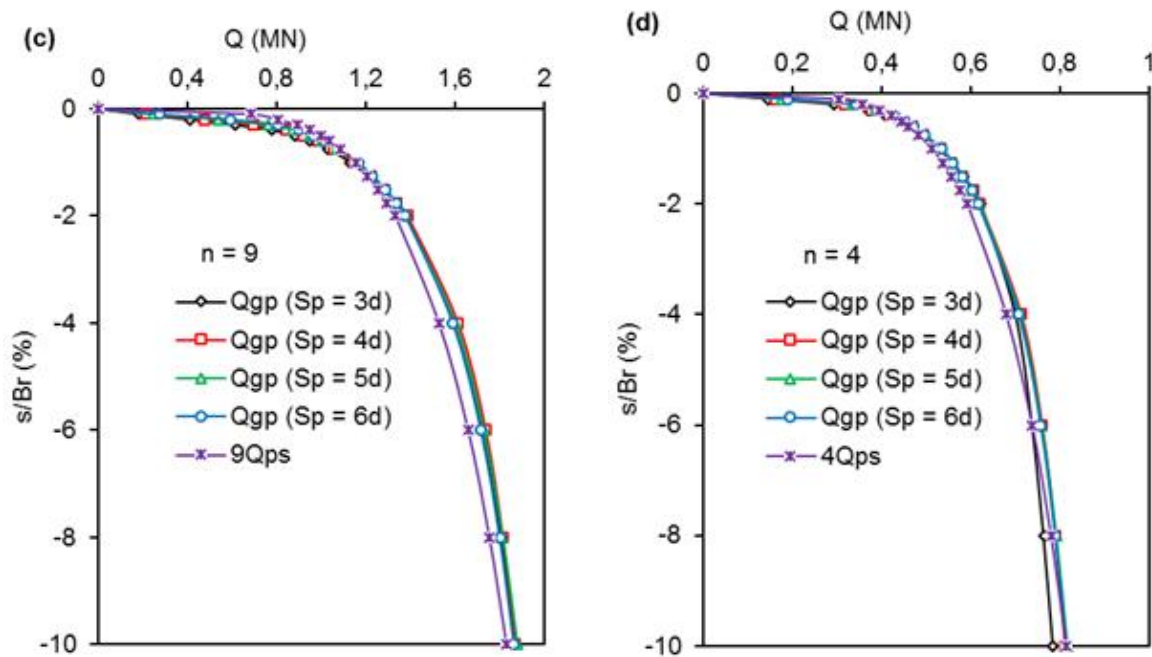


Figure 4.17 Load-normalized settlement curves of GP for different n and S_p and using n times SP load responses.

The load-normalized settlement curves of GP of 16 piles with different S_p , and 16SP are plotted in Figure 4.17b. It can be observed that 16SP exhibits a higher load-carrying capacity ($16Q_{ps}$) than that of the GP (Q_{gp}) up to a certain settlement level of $s = 1.25\% Br$, beyond which $16Q_{ps}$ becomes lower than Q_{gp} as much as the pile spacing decreases.

From Figures 5.17c and 5.17d, it can be noted that both the load-carrying capacity and pile group effect in the case of a small group of piles is not significantly affected by pile spacing.

For all the above, it can be indicated that the pile group interaction effect is significant initially and then becomes negligible with the increasing settlement. Similar results and trends were observed from the centrifuge test realized by Park and Lee (2015). However, it should be noted that this is substantially depending on piles number.

Moreover, and for all the above, it can be revealed that at the initial settlement range, the load-carrying capacity of the GP of n piles approaching that of n times SP as pile spacing increases. This can be explained by the effect of vicinity between piles, as the pile spacing increases as the pile in the group behaves like a single pile. The mobilized zone of the ground beneath the piles is represented by contours of the maximum shear strain increment obtained by FLAC^{3D} for the case of 16 piles and different pile spacing as shown in Figure 4.18. It can

be seen that the group of piles with $S_p = 3d$ fails as a block but with increasing pile spacing, the collapse mechanism becomes to be similar to that of the isolated pile.

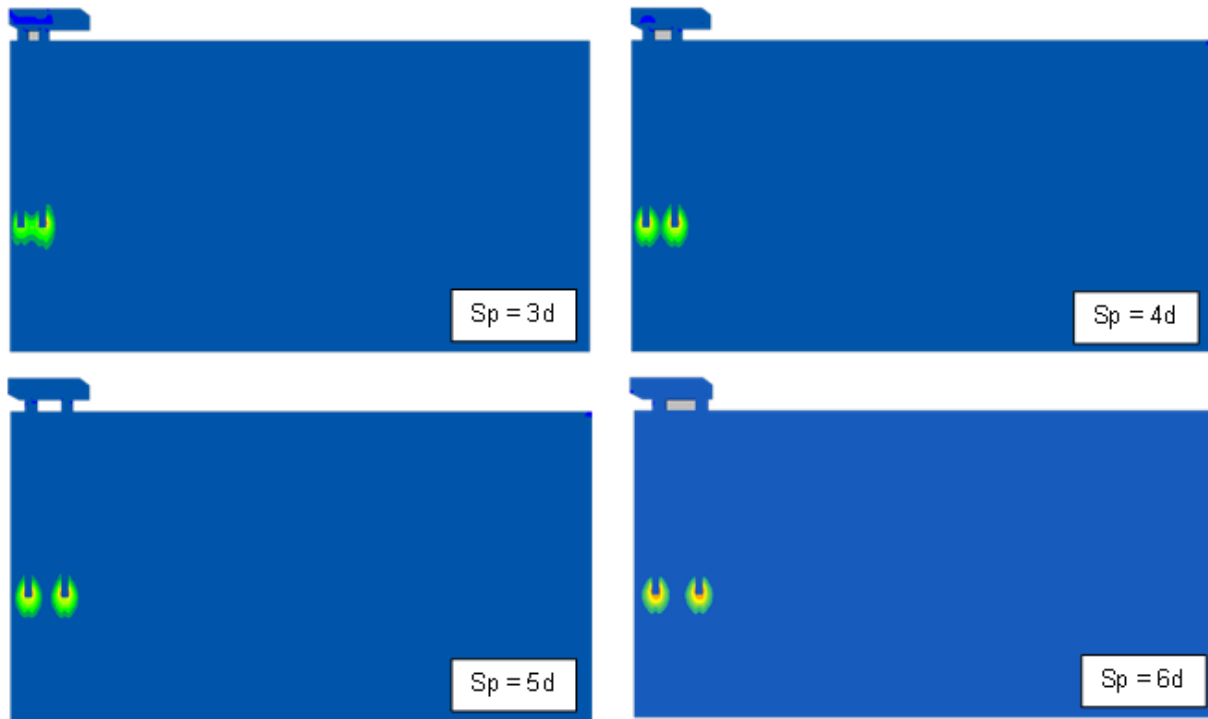


Figure 4.18 Distribution of maximum shear strain for GP with 16 piles and different pile spacing

The values of the pile group effect factor (C_g) were calculated (using Eq. 1.17 in chapter 1) and plotted in Table 4.6. The values of the C_g were lower than unity up to a certain settlement level, beyond which the C_g value became close to unity. However, this development depends on the number of piles and pile spacing. It should be noted that as settlement increases, the pile group effect becomes less pronounced presenting unnoticeable effects. This finding is in good agreement with the results of the centrifuge tests reported by Park and Lee (2015).

The value of C_g at the ultimate bearing capacity for all considered pile group configurations ($s = 10\% d$, which is equivalent to $s = 0.5\% Br$) varies from 0.58 to 1.02, with an average of approximately 0.88. It should be noted that in soft clays, the increase of S_p reduces the pile group effect at the initial settlement range. In contrast, the increase of n increases significantly the pile group effect. However, as the pile spacing increases as the effect of n on the GP performance becomes less significant. According to the results obtained (Table 4.6), It should be mentioned that the number of piles has a preponderant effect compared to pile spacing on the pile group effect.

Table 4.6 Values of χ_g for different n and S_p

s/Br (%)	$n = 25$		$n = 16$				$n = 9$				$n = 4$			
	$3d$	$4d$	$3d$	$4d$	$5d$	$6d$	$3d$	$4d$	$5d$	$6d$	$3d$	$4d$	$5d$	$6d$
0.1	0,13	0,17	0,17	0,21	0,26	0,31	0,27	0,31	0,36	0,40	0,48	0,53	0,58	0,62
0.2	0,27	0,35	0,35	0,43	0,50	0,58	0,51	0,59	0,67	0,74	0,83	0,89	0,94	0,96
0.3	0,39	0,49	0,49	0,59	0,68	0,75	0,69	0,78	0,86	0,90	0,94	0,96	0,97	0,98
0.4	0,49	0,60	0,61	0,72	0,80	0,86	0,82	0,89	0,92	0,94	0,97	0,99	1,00	1,01
0.5	0,58	0,70	0,70	0,81	0,89	0,92	0,88	0,92	0,95	0,97	0,99	1,01	1,01	1,02
0.6	0,65	0,77	0,78	0,89	0,93	0,95	0,92	0,95	0,97	0,98	1,00	1,02	1,02	1,02
0.75	0,74	0,86	0,87	0,93	0,96	0,97	0,95	0,97	0,98	1,00	1,02	1,02	1,03	1,03
1	0,84	0,92	0,93	0,97	0,99	1,00	0,98	1,00	1,00	1,01	1,03	1,04	1,03	1,04
1.25	0,89	0,95	0,97	0,99	1,01	1,00	1,00	1,01	1,02	1,02	1,04	1,04	1,04	1,04
1.5	0,92	0,97	0,99	1,01	1,02	1,02	1,02	1,02	1,02	1,03	1,05	1,04	1,05	1,04
1.75	0,93	0,99	1,00	1,02	1,03	1,03	1,02	1,03	1,03	1,03	1,05	1,05	1,05	1,05
2	0,95	1,00	1,01	1,03	1,03	1,03	1,03	1,04	1,03	1,03	1,05	1,05	1,05	1,04
4	1,02	1,05	1,06	1,07	1,06	1,04	1,04	1,05	1,05	1,04	1,03	1,05	1,05	1,04
6	1,05	1,07	1,10	1,07	1,05	1,02	1,04	1,05	1,04	1,03	1,00	1,03	1,03	1,03
8	1,08	1,08	1,11	1,07	1,04	1,00	1,03	1,03	1,03	1,03	0,98	1,01	1,02	1,01
10	1,09	1,08	1,11	1,06	1,04	0,99	1,02	1,02	1,03	1,02	0,96	1,00	1,00	1,00

• **Raft-Pile Interaction Effect**

Figure 4.19 illustrates the load-normalized settlement curves of GP and Ppr for the case of 25 piles with $S_p = 3d$ and $4d$. It can be observed that the load-normalized settlement curves of GP and Ppr are almost identical up to a certain settlement level of $s = 2\% Br$, beyond which the load-carrying capacity of Ppr becomes relatively greater than that of GP. At settlement level of $s = 10\% Br$, maximum differences of about 12% and 22% were observed for $S_p = 3d$ and $4d$ respectively. This finding indicates that no significant interaction effect occurs at the initial settlement range and some interaction effects appear with the increase of the settlement level. This is explained by the fact that at initial settlement the piles of a piled raft carried the almost of applied load with a minimal contribution of the raft, however with loading progress and after the full mobilization of the piles bearing capacity, the portion of the load carried by the raft increases and becomes more important, which increases the resistance by lateral friction of the pile due to the increase of the confinement of the soil between the piles. This is the raft-pile interaction effect.

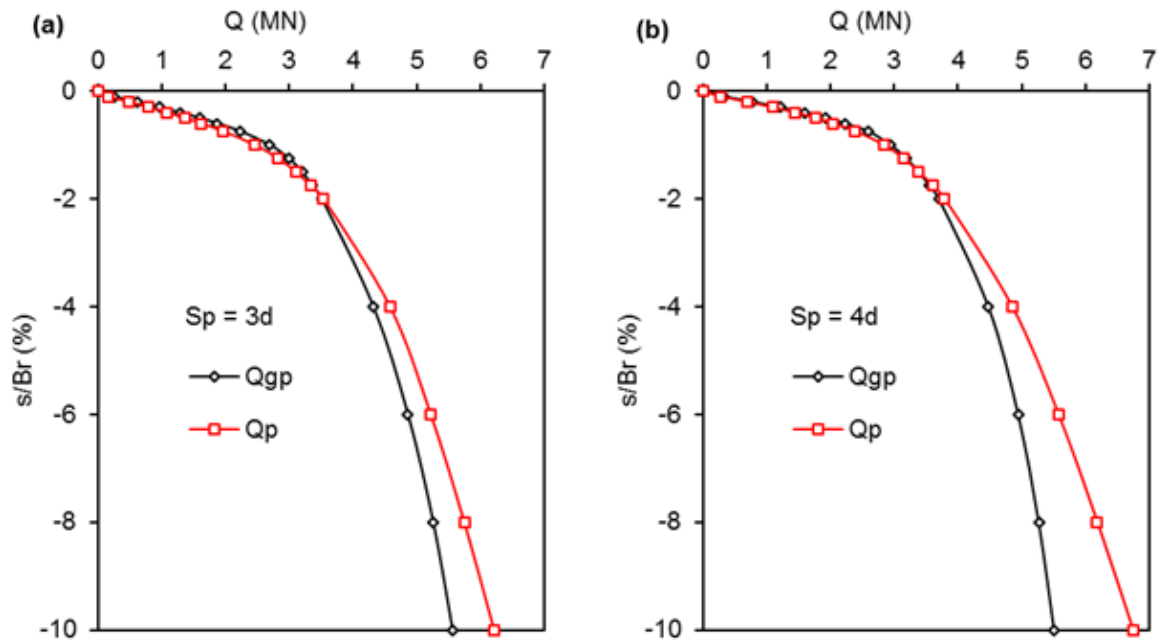


Figure 4.19 Load-normalized settlement curves of GP and Ppr, for the case of $n = 25$ piles, (a) $S_p = 3d$ and (b) $S_p = 4d$.

The load-carrying capacity of GP and Ppr of the case of 16 piles with different pile spacing is presented in Figure 4.20. It can be observed that GP exhibits a slightly greater load-carrying capacity than Ppr up to a certain settlement level of $s = 1.5\% Br$. A difference of about 25%, 17%, 11% and 4% at $s = 0.5\% Br$ is found for $S_p = 3d, 4d, 5d$ and $6d$, respectively. Nevertheless, with the increase of the settlement, the behavior is reversed. The load-carrying capacity of Ppr is significantly greater than of GP for different values of S_p . A difference of about 25%, 33%, 36% and 41% is noted at settlement level of $s = 10\% Br$ for $S_p = 3d, 4d, 5d$ and $6d$, respectively.

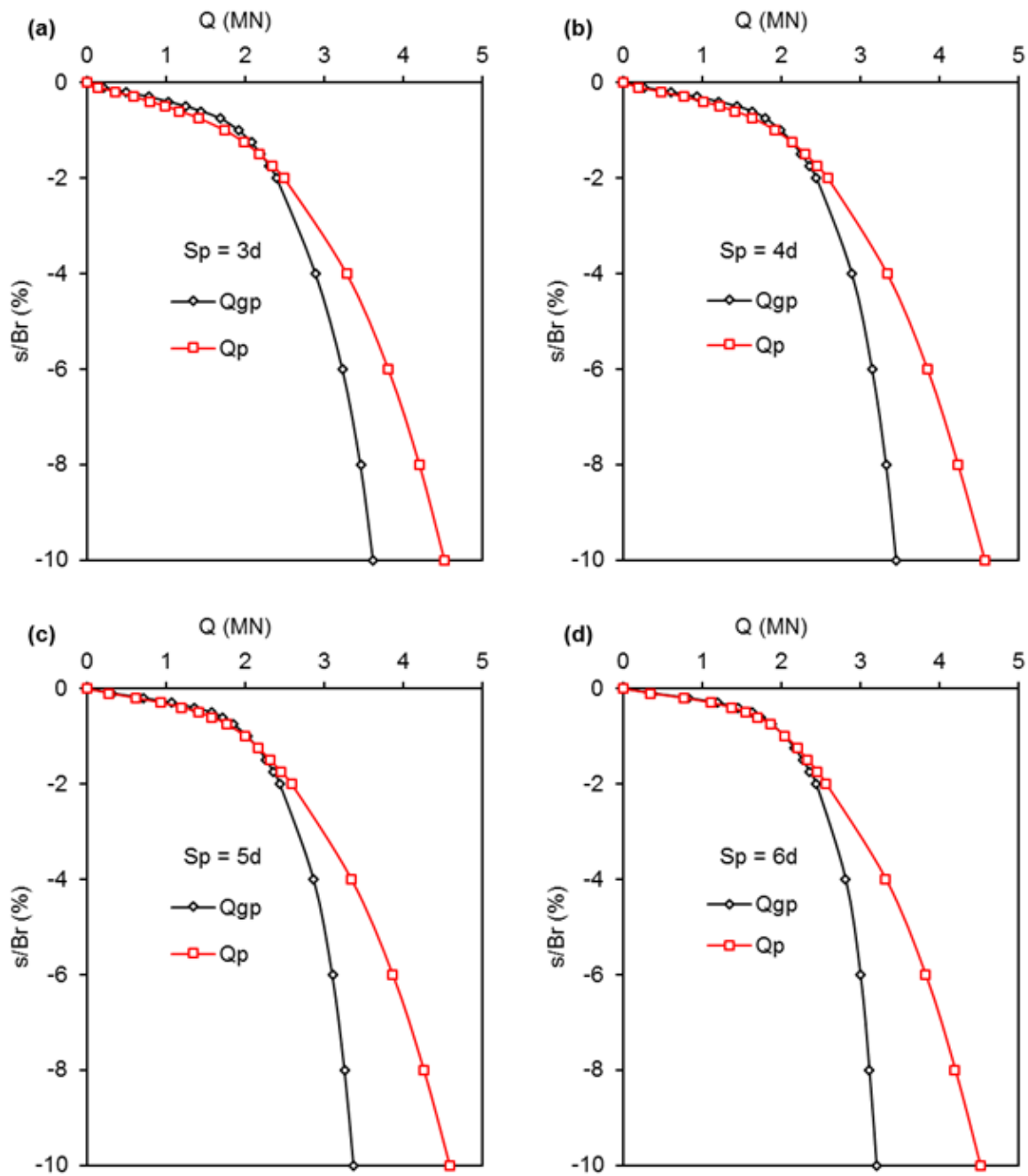


Figure 4.20 Load-normalized settlement curves of GP and Ppr, for the case of $n = 16$ piles with different S_p .

So, from the above-mentioned results, it can be concluded that at the initial loading stage, the difference between the load carried by GP and Ppr becomes negligible as much as pile spacing becomes more important. This finding reveals that for the small settlement level, the pile repartition on the whole raft area (area occupied by the piles almost equal to the area of the raft) decreases the contribution of the raft component. However, as the settlement level increases, the load-carrying capacity of Ppr becomes greater than that of the GP due to the

raft-pile interaction effect which depends on the S_p . Wherein; the pile repartition on the whole raft area increases the contribution of the raft component.

From Figures 5.19 and 5.20 it can be noted that the effect of pile spacing on the raft-pile interaction depends on piles number. As piles number decreases as the pile spacing effect becomes more significant. Similar results and trends were observed for cases of 9 and 4 piles.

de Sanctis and Mandolini (2006) conclude, $\eta_p = 1$, based on comparing the load-normalized settlement curves of GP and Ppr, which were tended to be approaching the same limiting value at a final settlement of $s = 25\% d$. The same observation is obvious in Figure 4.20a. Nevertheless, as explained earlier, when the settlement exceeds this limit ($s = 25\% d$), Q_p began to diverge from Q_{gp} (Q_p keeps increasing, while Q_{gp} remains almost constant). Consequently, the settlement level of $25\% d$ is not sufficient to judge and compare GP and Ppr.

Also, as an example, the load-carrying capacities of Ppr (Q_p) at the ultimate bearing state of the group of piles ($s = 10\% d$) markedly underestimate those at the ultimate bearing state of PR ($s = 10\% Br$) of about 356% and 282% for $S_p = 3d$ and $4d$, respectively for the case of 25 piles.

These results indicate that the piles components of piled raft system were fully overloaded due to their different component sizes. Therefore, η_p should be evaluated with caution. The failure interaction factor η_p should be the ratio of the load-carrying capacity of Ppr, obtained at a settlement level of $10\% Br$, to the ultimate load of GP, obtained at a settlement equal to $10\% d$, Eq. 1.25 (in chapter 1). In this context, most researchers go wrong when they estimate the failure interaction factor η_p because they compared $Q_{gp,ult}$ and Q_p at the same settlement level ($10\% Br$), without taking into account the different component sizes of PR system.

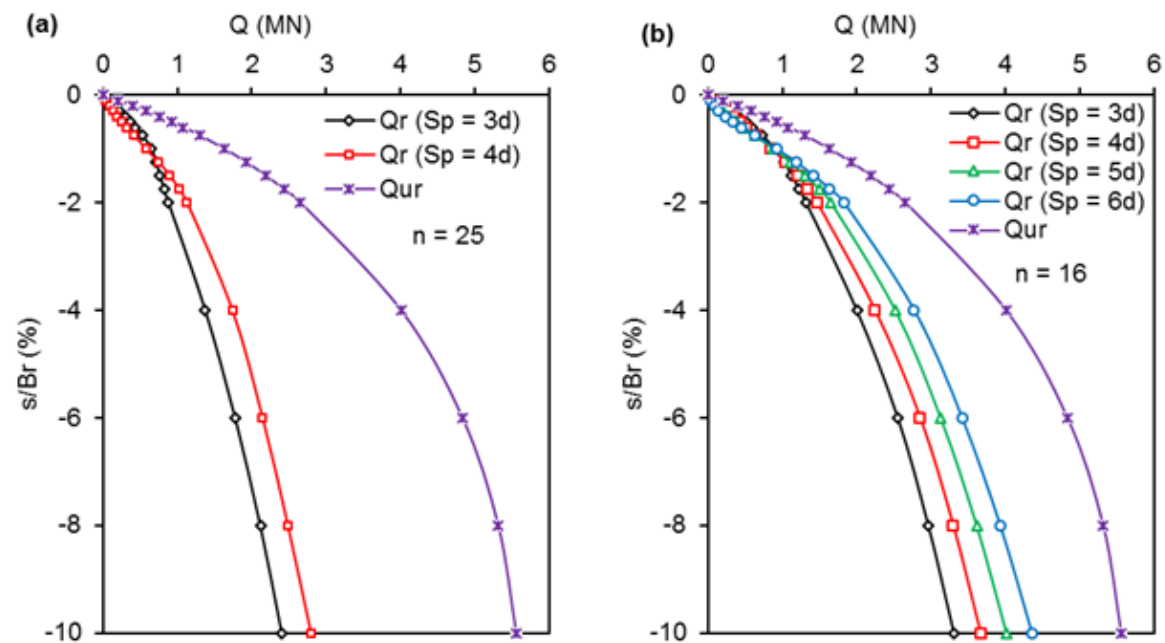
The values of the failure interaction factor η_p are summarized in Table 4.7. For all considered configurations, η_p varies from 2.77 to 3.89 with an average of approximately 3.0. It can be noted that increasing the S_p decreases the η_p value whatever the value of n , whereas η_p increases with the increase of piles number.

Table 4.7 η_r and η_p values at ultimate state

Case	n	S_p	Br	η_r	η_p
1	25	3d	10	0,434	3,890
2	25	4d	10	0,504	3,497
3	16	3d	10	0,596	3,617
4	16	4d	10	0,659	3,179
5	16	5d	10	0,722	2,911
6	16	6d	10	0,784	2,771
7	9	3d	10	0,804	3,102
8	9	4d	10	0,824	3,032
9	9	5d	10	0,844	2,957
10	9	6d	10	0,873	2,847
11	4	3d	10	0,951	2,914
12	4	4d	10	0,954	2,871
13	4	5d	10	0,953	2,838
14	4	6d	10	0,952	2,783

• **Pile-Raft Interaction Effect**

The load-normalized settlement curves of UR and Rpr, for different piles number and pile spacing are represented in Figure 4.21. It can be noted that, for the entire settlement range, the load-carrying capacity of Rpr is lower than that of UR for all n and S_p considered in this study. This finding indicates that adding even a limited number of piles to the raft can affect the performance of the raft.



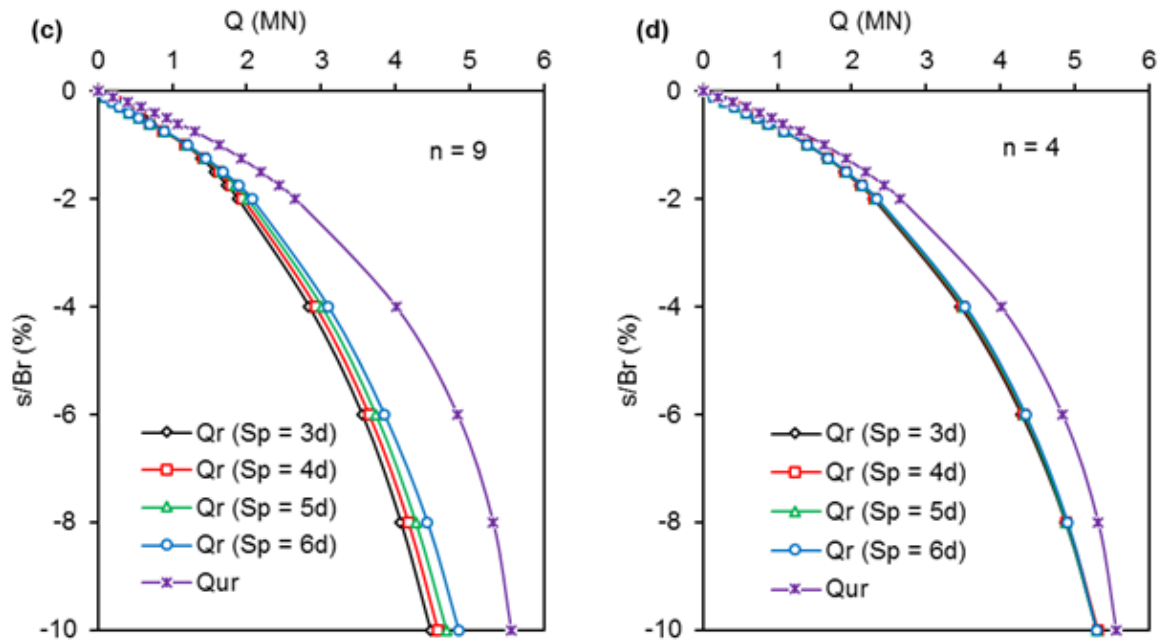


Figure 4.21 Load-normalized settlement curves of UR and Rpr, for different n and S_p

As an example, Figure 4.21a plots the load-normalized settlement curves of UR and Rpr for the case of $n = 25$ with $S_p = 3d$ and $4d$. The load-carrying capacity of Rpr for the case of $S_p = 3d$ is higher than that for the case of $S_p = 4d$ until a settlement level of $s = 1\% Br$. After this settlement limit, the raft behavior is inverted so the load-carrying capacity obtained from Rpr with $S_p = 4d$ overestimates that of Rpr with $S_p = 3d$. At ultimate state, a difference of about 16% was found. This means that, for a small settlement level, the area occupied by piles increases as the piles' contribution increases which inversely affects the performance of the raft. However, for a high settlement level, the behavior is reversed in which the bearing capacity of piles is fully mobilized because of the smaller pile foundation size. Besides, as piles beneath the raft become more spaced as the raft contribution increases by the fact of the raft-soil contact surface between piles became influential. Thus, the behavior of the raft is approaching to be similar to that of the unpiled raft as pile spacing increases.

Similar results and trends are observed for the case of $n = 16$ and 9 piles. While the pile spacing effect becomes unnoticeable for the case of $n = 4$. It can be seen that the increase of piles number considerably increases the piles' effect on the raft performance and as a result, the curve of Q_{ur} diverges more from that of Q_r . At the ultimate state and for the case of $S_p = 3d$, the load-carrying capacity of Rpr is smaller than that of UR of about 131%, 68%, 24%, and 5% for $n = 25, 16, 9,$ and 4 respectively. It can be concluded that S_p affected the piles' effect on the performance of the raft depending on settlement level and piles number.

The η_r values at the ultimate state are summarized in Table 4.7. The η_r values vary from 0.44 to 0.95, with an average of approximately 0.78. These results coincide perfectly with those reported by de Sanctis and Mandolini (2006). It can be noted that η_r is proportional with S_p , it rises as n increases. In contrast, η_r is inversely proportional to the pile number.

4.5 Summary

In this study, the load response of piled raft subjected to vertical loading in soft clay condition has been investigated using the FLAC^{3D} code considering all critical aspects of interactions between the soil, piles and raft. Based on previous works and the obtained results within the range of the parameters tested, the following conclusions and recommendations can be drawn:

- The computation results clearly show that the load carrying capacity of PR obtained by the sum of Q_{ur} and Q_{gp} , as reported by Lee et al. (2014), is significantly greater than Q_{pr} for the entire settlement range. Therefore, the neglect of these interaction effects could considerably overestimate the ultimate bearing capacity of PR system. Moreover, the interaction effects become more significant with the increase in the number of piles.
- The improvement of the load carrying capacity of PR with the increase in the number of piles is more pronounced with the increase of the pile spacing.
- For different pile spacing, the evolution of the load sharing coefficient α_p is divergent at low settlement levels ($s < 1\% B_r$) and then converges by increasing the settlement level. This behavior can be explained by that most of the applied loads are carried by the piles up a certain initial settlement beyond which the contribution of the raft increases progressively and the load portion carried by the raft becomes more important.
- The pile load distribution is affected by the pile position, pile spacing, and settlement level. At the initial settlement level, the part of the load carried by the piles is lower at the center and higher at the perimeter. However, at ultimate state the load is more distributed over all piles where the highest load portion is supported by the center pile.
- In the event of very limited settlement or that the increasing the number of piles poses a problem for economic reasons, the distribution of piles at the periphery rather than at the center of the raft will be a very effective alternative to improve the bearing capacity of the piled raft foundation.

- Since in the limit states approach, the ultimate capacity of the piled raft foundation system is mainly reached at a high level of movement, the pile group interaction effect can be negligible. Wherein, it was found less pronounced presenting unnoticeable effects. However, for a very less level of settlements (service limit), the pile group interaction effect was found significant depending on the number of piles and the pile spacing.
- At initial settlement the piles of a piled raft carried almost of applied load with a minimal contribution of the raft, therefore no significant raft-pile interaction effect arises at this range of settlement. However, with the increase of the settlement level, the raft-pile interaction effect occurs. This is because that after the full mobilization of the piles bearing capacity, the portion of the load carried by the raft increases and becomes more important, which increases the resistance by lateral friction of the pile due to the increase of the confinement of the soil between the piles.
- For the small settlement level, as piles constricted at the centered raft area as the contribution of the raft becomes more pronounced. However, as the settlement level increases, the load-carrying capacity of Ppr becomes greater than that of the GP due to the raft-pile interaction effect depending on the S_p . Wherein; the pile repartition on the whole raft area increases the contribution of the raft component.
- The piles components of piled raft system were fully overloaded due to their different component sizes. The failure interaction factor η_p should be the ratio of the load-carrying capacity of Ppr, obtained at a settlement level of 10% B_r , to the ultimate load of GP, obtained at a settlement equal to 10% d . Therefore, the direct comparison between $Q_{gp,ult}$, and Q_p at the same settlement level, without taking into account the different component sizes of the PR system is not recommended because it can make an error in estimating η_p .
- Increasing the pile spacing decreases the raft-pile interaction factor, while it increases with the increase of piles number.
- For a small settlement level, pile spacing increases as the piles contribution increases which inversely affects the performance of the raft. However, for a relatively high settlement level, the behavior is reversed in which the bearing capacity of piles is early mobilized because of the smaller pile size. Besides, the behavior of the raft is approaching to be similar to that of the unpiled raft as pile spacing increases by the fact of the raft-soil contact surface between piles became influential.

CONCLUSIONS AND RECOMMENDATIONS

Piled raft foundations were developed as an effective and economic mode compared to conventional foundations, which are a combination system of shallow foundation (raft) and deep foundation (piles). This results in a complex system and gives rise to significant raft-pile-soil interactions which affect the load response of piled raft foundations. The conventional design methods are based upon relatively conservative assumptions of raft-soil-pile interactions; as a result, they are in many cases inaccurate and unlikely to result in optimum design. Thus, resorting to numerical analyses seems to be the most reliable method, mainly because of the multiple interactions and the three-dimensional geometry. In this context, 3D finite-difference analyses were performed using FLAC^{3D} code to investigate the behavior of piled raft foundation in soft clays. The overall objective of the thesis focuses on the load response and the multiple interactions between piled raft components. For this purpose, several types of foundations were considered including piled raft, group of piles, unpiled raft, and single pile.

The modeling methodology carried out in this study is validated against the results from the popular analytical and experimental tests provided within the literature by comparing the results in the same geological conditions and similar subgrade-structure.

The performance of the piled raft foundation and the interactions behavior between the raft and piles in the system are also investigated by varying some parameters as piles number and pile spacing to provide further insight into the mechanical response of piled raft and aim at helping the engineers in taking a logical path in an iterative design process for a piled raft foundation. Four cases of uniformly pile arrangements of 2×2, 3×3, 4×4, and 5×5 were considered, corresponding to piles number of $n = 4, 9, 16,$ and 25 piles respectively. The foundation size was selected to allow for employing four commonly used pile spacing values (i.e. $3d, 4d, 5d,$ and $6d$) for $n = 4, 9,$ and 16 piles and two pile spacing values ($3d$ and $4d$) for n

Conclusions and recommendations

= 25 piles, with a pile diameter of 0.5 m, without changing the raft size. 16 pile configurations in total were considered in this 3D numerical parametric study

The material behavior of soil in this study is modeled with a linear elastic perfectly plastic constitutive law using the Mohr-Coulomb failure criterion. The Mohr-Coulomb model, widely used in the modeling of geotechnical works, has the advantage of requiring few soil parameters and that all these parameters can be obtained from the standard soil tests. Both raft and piles are made from reinforced concrete which is modeled as a linear elastic material. The foundation system is subjected to a vertical static load.

The results of this research were presented in the form of charts and tables, and the detailed conclusions for the pile group and piled raft foundations were presented at the end of chapters four and five, respectively. Nonetheless, it is useful to recall here the most important conclusions.

- The efficiency coefficient of the pile group was often lower than unity for different pile spacing and piles number due to interaction effects between piles. So a value of efficiency coefficient of unity for pile groups in clay could considerably overestimate the bearing capacity of group of piles essentially for cases of large piles number.
- Although the bearing capacity of the pile group increases with increasing number of piles, the efficiency of the pile group embedded in soft clay is very important in the case of a small number of piles. Whereas, the pile group bearing capacity can be improved simply by increasing the pile spacing without increasing the number of piles.
- Among all popular formulas considered in this research, the Los Angeles group action and Converse-Labarre methods lead to comparable C_g values to those obtained from present 3D numerical results. While, the method suggested by McCabe and Lehane would have required a higher number of piles to ensure the stability of the structure which requires more resources e.g. concrete, energy...
- Based on the present finite difference analysis results, a new efficiency coefficient formula was proposed as a function of pile spacing and the number of piles.
- The computation results clearly show that the load carrying capacity of piled raft foundation obtained by the sum of Q_{ur} and Q_{gp} , as reported by Lee et al. (2014), is significantly greater than Q_{pr} for the entire settlement range. Therefore, the neglect of these interaction effects could considerably overestimate the ultimate bearing capacity of piled

Conclusions and recommendations

raft foundation system. Moreover, the interaction effects become more significant with the increase in the number of piles.

- The improvement of the load carrying capacity of PR with the increase in the number of piles is more pronounced with the increase of the pile spacing.
- For different pile spacing, the evolution of the load sharing coefficient α_p is divergent at low settlement levels ($s < 1\% B_r$) and then converges by increasing the settlement level.
- The pile load distribution is affected by the pile position, pile spacing, and settlement level. At the initial settlement level, the part of the load carried by the piles is lower at the center and higher at the perimeter. However, at ultimate state the load is more distributed over all piles where the highest load portion is supported by the center pile.
- In the event of very limited settlement or that the increasing the number of piles poses a problem for economic reasons, the distribution of piles at the periphery rather than at the center of the raft will be a very effective alternative to improve the bearing capacity of the piled raft foundation.
- Since in the limit states approach, the ultimate capacity of the piled raft foundation system is mainly reached at a high level of movement, the pile group interaction effect can be negligent. Wherein, it was found less pronounced presenting unnoticeable effects. However, for a very less level of settlements (service limit), the pile group interaction effect was found significant depending on the number of piles and the pile spacing.
- For the small settlement level, as piles constricted at the centered raft area as the contribution of the raft becomes more pronounced. However, as the settlement level increases, the load-carrying capacity of piles in the piled raft foundation becomes greater than that of the freestanding pile group due to the raft-pile interaction effect depending on the pile spacing. Wherein; the pile repartition on the whole raft area increases the contribution of the raft component.
- The piles components of piled raft system were fully overloaded due to their different component sizes. The failure interaction factor η_p should be the ratio of the load-carrying capacity of in the piled raft foundation, obtained at a settlement level of $10\% B_r$, to the ultimate load of the freestanding pile group, obtained at a settlement equal to $10\% d$. Therefore, the direct comparison between $Q_{gp,ult}$, and Q_p at the same settlement level,

Conclusions and recommendations

without taking into account the different component sizes of the piled raft system is not recommended because it can make an error in estimating η_p .

- For a small settlement level, pile spacing increases as the piles contribution increases which inversely affects the performance of the raft. However, for a relatively high settlement level, the behavior is reversed in which the bearing capacity of piles is early mobilized because of the smaller pile size. Besides, the behavior of the raft is approaching to be similar to that of the unpiled raft as pile spacing increases by the fact of the raft-soil contact surface between piles became influential.
- Further 3D investigations will be carried out on more complex cases of piled raft under vertical and lateral loadings, especially on the influence of soil-structure interfaces parameters, the stiffness of materials, the number of piles and the piling configuration.

REFERENCES

1. Abdelrazaq, A., Poulos, H. G., Badelow, F., & Kim, S. H. (2011). Foundation Design and Pile Testing Program for the 151 Story Incheon Tower in Reclamation Area. In *Proceedings of the 7th International Conference on Tall Buildings, Incheon, Korea* (pp. 815-823).
2. Achmus, M., Kuo, Y. S., & Abdel-Rahman, K. (2009). Behavior of monopile foundations under cyclic lateral load. *Computers and Geotechnics*, 36(5), 725-735.
3. Akinmusuru, J. O. (1980). Interaction of piles and cap in piled footings. *Journal of the Geotechnical Engineering Division*, 106(11), 1263-1268.
4. Alnuaim, A. M., El Naggar, H., & El Naggar, M. H. (2017). Evaluation of piled raft performance using a verified 3D nonlinear numerical model. *Geotechnical and Geological Engineering*, 35(4), 1831-1845.
5. Alnuaim, A., El Naggar, H., & El Naggar, M. H. (2013). Performance of piled-raft system under axial load. In *18th International Conference on Soil Mechanics and Geotechnical Engineering* (pp. 2663-2666).
6. Alshenawy, A. O., Alrefeai, T. O., & Alsanabani, N. M. (2016). Analysis of piled raft coefficient and load-settlement on sandy soil. *Arabian Journal of Geosciences*, 9(6), 475.
7. Ata, A., Badrawi, E., & Nabil, M. (2015). Numerical analysis of unconnected piled raft with cushion. *Ain Shams Engineering Journal*, 6(2), 421-428.
8. Badelow, F., Kim, S., Poulos, H. G., & Abdelrazaq, A. (2009). Foundation design for a tall tower in a reclamation area. In *Proc. 7 th Int. Conf. Tall Buildings, Hong Kong, Ed. FTK Au, Research Publishing* (pp. 815-823).
9. Barden, L., & Monckton, M. F. (1970). Tests on model pile groups in soft and stiff clay. *Geotechnique*, 20(1), 94-96.
10. Basile, F. (2013). A practical method for the non-linear analysis of piled rafts. In *Proceedings of the 18th International Conference on Soil Mechanics and Geotechnical Engineering, Paris, France* (pp. 2-5).
11. Baziar, M. H., Ghorbani, A., & Katzenbach, R. (2009). Small-scale model test and three-dimensional analysis of pile-raft foundation on medium-dense sand. *International Journal of Civil Engineering* 7(3):170-175.

References

12. Bolin, H. W. (1941). The pile efficiency formula of the Uniform Building Code. *Building Standards Monthly*, 10(1), 4-5.
13. Borel, S. (2001). *Comportement et dimensionnement des fondations mixtes* (No. GT73), PhD thesis,
14. Laboratoire Central des Ponts et Chaussées.
15. Bowles, J. E. (1988). *Foundation analysis and design*, McGraw-Hill International Editions, Singapore.
16. Tomlinson M.J (1986) *Foundation Design and Construction*. Longman, 5rev edition. 856 pages.
17. Brand, E. W., Muktabhant, C., & Taechathummarak, A. (1972). Load tests on small foundations in soft clay. In *Performance of earth and earth-supported structures* (p. 903). ASCE.
18. Briaud, J. L., Tucker, L. M., & Ng, E. (1989). Axially loaded 5 pile group and single pile in sand. In *Congrès international de mécanique des sols et des travaux de fondations*. 12 (pp. 1121-1124).
19. Brown, P. T., & Wiesner, T. J. (1975). The behaviour of uniformly loaded piled strip footings. *Soils and foundations*, 15(4), 13-21.
20. Burland, J. B. (1995). Piles as settlement reducers. Keynote Address, 18th *Italian Congress on Soil Mechanics*, Pavia, Italy.
21. Butterfield, R., & Banerjee, P. K. (1971). The elastic analysis of compressible piles and pile groups. *Geotechnique*, 21(1), 43-60.
22. Cho, J., Lee, J. H., Jeong, S., & Lee, J. (2012). The settlement behavior of piled raft in clay soils. *Ocean Engineering*, 53, 153-163.
23. Clancy, P., & Randolph, M. F. (1996). Simple design tools for piled raft foundations. *Geotechnique*, 46(2), 313-328.
24. Clancy, P., & Randolph, M. F. (1993). An approximate analysis procedure for piled raft foundations. *International Journal for Numerical and Analytical Methods in Geomechanics*, 17(12), 849-869.
25. MELT-Ministère de l'Équipement, du logement et des transports (1993), "Règles techniques de conception et de calcul des fondations des ouvrages de génie civil (in french

References

- : technical rules for the design of foundations of civil engineering structures). Cahier des clauses techniques générales applicables aux marchés publics de travaux”, *FASCICULE No 62-Titre V, Textes Officiels* No. 93-3 T.O., p. 182.
26. Combarieu, O., & Evrard, H. (1979). Les fondations mixtes, semelle-pieux. *BULL LIAISON LAB PONTS CHAUSS*, (102).
 27. Combarieu, O. (1990). Fondations superficielles sur sol amélioré par inclusions rigides verticales. *Revue française de géotechnique*, (53), 33-44.
 28. Conte, G., Mandolini, A., & Randolph, M. (2003). Centrifuge modelling to investigate the performance of piled rafts. In *Centrifuge modelling to investigate the performance of piled rafts* (pp. 359-366). Millpress.
 29. Cooke, R. W. (1986). Piled raft foundations on stiff clays—a contribution to design philosophy. *Geotechnique*, 36(2), 169-203.
 30. Das, B. M. (2015). *Principles of foundation engineering*. Cengage learning.
 31. De Mello, V. F. B. (1969). ‘Foundations of Buildings on Clay. In *State of the Art Report, Proceedings, 7th International Congress on Soil Mechanics and Foundation Engineering* (Vol. 1, pp. 49-136).
 32. de Sanctis, L., & Mandolini, A. (2006). Bearing capacity of piled rafts on soft clay soils. *Journal of Geotechnical and Geoenvironmental Engineering*, 132(12), 1600-1610.
 33. de Sanctis, L., & Russo, G. (2008). Analysis and performance of piled rafts designed using innovative criteria. *Journal of geotechnical and geoenvironmental engineering*, 134(8), 1118-1128.
 34. Deb, P., & Pal, S. K. (2019). Analysis of load sharing response and prediction of interaction behaviour in piled raft foundation. *Arabian Journal for Science and Engineering*, 44(10), 8527-8543.
 35. Desai, C. S. (1974). Numerical design-analysis for piles in sands. *Journal of the Geotechnical Engineering Division*, 100(6), 613-635.
 36. Eurocode 7 (2004) Geotechnical design-part 1: General rules. *British Standards*, UK.
 37. Feld, J. (1943). Discussion on friction pile foundations. *Transactions of the American Society of Civil Engineers*, 108, 143-144.

References

38. Fioravante, V., Giretti, D., & Jamiolkowski, M. (2008). Physical modeling of raft on settlement reducing piles. *In from research to practice in geotechnical engineering* (pp. 206-229).
39. Fleming, W.G.K., Weltman, A.J., Randolph, M.F. and Elson, W.K. (1992). *Piling Engineering*. 2nd Ed., Surrey Univ. Press.
40. Frank, R. (1999). *Calcul des fondations superficielles et profondes* (p. 142). Techniques de l'Ingénieur et Presses de l'Ecole nationale des ponts et chaussées.
41. Taghavi Ghalesari, A., & Janalizadeh Choobbasti, A. (2018). Numerical analysis of settlement and bearing behaviour of piled raft in Babol clay. *European Journal of Environmental and Civil Engineering*, 22(8), 978-1003.
42. Ghalesari, A. T., Barari, A., Amini, P. F., & Ibsen, L. B. (2015). Development of optimum design from static response of pile–raft interaction. *Journal of Marine Science and Technology*, 20(2), 331-343.
43. Han, J., & Ye, S. L. (2006). A field study on the behavior of a foundation underpinned by micropiles. *Canadian geotechnical journal*, 43(1), 30-42.
44. Helmy, M. (2002). *Modeling pile group efficiency in cohesionless soil using artificial neural networks* (Doctoral dissertation, Concordia University).
45. Hooper, J. A. (1973). Observations on the behaviour of a pile-raft foundation on London Clay. *Proceedings of the institution of civil engineers*, 55(4), 855-877.
46. Horikoshi, K., & Randolph, M. F. (1997). On the definition of raft—soil stiffness ratio for rectangular rafts. *Géotechnique*, 47(5), 1055-1061.
47. Horikoshi, K., & Randolph, M. F. (1996). Centrifuge modelling of piled raft foundations on clay. *Geotechnique*, 46(4), 741-752.
48. Horikoshi, K., Matsumoto, T., Hashizume, Y., Watanabe, T., & Fukuyama, H. (2003). Performance of piled raft foundations subjected to static horizontal loads. *International Journal of Physical Modelling in Geotechnics*, 3(2), 37-50.
49. Houhou, M. N., Emeriault, F., & Belouar, A. (2019). Three-dimensional numerical back-analysis of a monitored deep excavation retained by strutted diaphragm walls. *Tunnelling and Underground Space Technology*, 83, 153-164.

References

50. Hussien, M. N., Ramadan, E. H., Hussein, M. H., Senoon, A. A., & Karray, M. (2016). Load sharing ratio of pile-raft system in loose sand: an experimental investigation. *International Journal of Geotechnical Engineering*, 11(5), 524-529.
51. Itasca Consulting Group Inc. FLAC3D, Version 5 (2013) *User's Guide Minneapolis, Minnesota*.
52. Jeong, S., Lee, J., & Lee, C. J. (2004). Slip effect at the pile–soil interface on dragload. *Computers and Geotechnics*, 31(2), 115-126.
53. Katzenbach, R., & Choudhury, D. (2013). ISSMGE Combined Pile-Raft Foundation Guideline. *Institute and Laboratory of Geotechnics. Technische Universität Darmstadt, Germany*.
54. Katzenbach, R., & Leppla, S. (2015). Realistic Modelling of Soil-Structure Interaction for High-Rise Buildings. *Procedia engineering*, 117, 162-171.
55. Katzenbach, R., Schmitt, A., & Turek, J. (2005). Assessing Settlement of High-Rise Structures by 3D Simulations. *Computer-Aided Civil and Infrastructure Engineering*, 20(3), 221-229.
56. Katzenbach, R., Leppla, S., Ramm, H., Seip, M., & Kuttig, H. (2013). Design and construction of deep foundation systems and retaining structures in urban areas in difficult soil and groundwater conditions. *Procedia Engineering*, 57, 540-548.
57. Katzenbach, R., Leppla, S., & Krajewski, W. (2014). Numerical analysis and verification of the soil-structure-interaction in the course of large construction projects in inner cities.
58. Katzenbach, R., Arslan, U., Moormann, C., & Reul, O. (2000). *Piled raft foundation projects in Germany* (Doctoral dissertation, Telford).
59. Kishida, H., & Meyerhof. (1965). Bearing Capacity of Pile Groups under Eccentric loads in sand. *In the Proceedings of the 6th International Conference on Soil Mechanics and Foundation Engineering*, (Vol. 2, pp. 270-274).
60. Kumar, A., & Choudhury, D. (2018). Development of new prediction model for capacity of combined pile-raft foundations. *Computers and Geotechnics*, 97, 62-68.
61. Lee, S. H., & Chung, C. K. (2005). An experimental study of the interaction of vertically loaded pile groups in sand. *Canadian Geotechnical Journal*, 42(5), 1485-1493.

References

62. Lee, J., & Salgado, R. (2005). Estimation of bearing capacity of circular footings on sands based on cone penetration test. *Journal of Geotechnical and Geoenvironmental Engineering*, 131(4), 442-452.
63. Lee, J., Kim, Y., & Jeong, S. (2010). Three-dimensional analysis of bearing behavior of piled raft on soft clay. *Computers and Geotechnics*, 37(1-2), 103-114.
64. Lee, J., Park, D., & Choi, K. (2014). Analysis of load sharing behavior for piled rafts using normalized load response model. *Computers and Geotechnics*, 57, 65-74.
65. Lee, J., Park, D., Park, D., & Park, K. (2015). Estimation of load-sharing ratios for piled rafts in sands that includes interaction effects. *Computers and Geotechnics*, 63, 306-314.
66. Liu, J. L., Yuan, Z. L., & Zhang, K. P. (1985). Cap-pile-soil interaction of bored pile groups. In *International conference on soil mechanics and foundation engineering*. 11 (pp. 1433-1436).
67. Luo, R., Yang, M., & Li, W. (2018). Normalized settlement of piled raft in homogeneous clay. *Computers and Geotechnics*, 103, 165-178.
68. Mali, S., & Singh, B. (2018). Behavior of large piled-raft foundation on clay soil. *Ocean Engineering*, 149, 205-216.
69. Mandolini, A. (2003). Design of piled raft foundations: practice and development. *Proceedings of Deep Foundations on Bored and Auger Piles—BAP IV, Ghent, Belgium*, 2-4.
70. Mandolini, A., & Viggiani, C. (1997). Settlement of piled foundations. *Géotechnique*, 47(4), 791-816.
71. Marti, J. (1982). Mixed discretization procedure for accurate solution of plasticity problems. *Int. Jour., Num. Methods & Analy. Methods in Geomech.*, 23-26.
72. Matsumoto, T., Fukumura, K., Pastsakorn, K., Horikoshi, K., & Oki, A. (2004). Experimental and analytical study on behaviour of model piled rafts in sand subjected to horizontal and moment loading. *International Journal of Physical Modelling in Geotechnics*, 4(3), 01-19.
73. Mayne, P. W., & Poulos, H. G. (1999). Approximate displacement influence factors for elastic shallow foundations. *Journal of Geotechnical and Geoenvironmental Engineering*, 125(6), 453-460.

References

74. McCabe, B. A., & Lehane, B. M. (2006). Behavior of axially loaded pile groups driven in clayey silt. *Journal of Geotechnical and Geoenvironmental Engineering*, 132(3), 401-410.
75. Nagtegaal, J. C., Parks, D. M., & Rice, J. R. (1974). On numerically accurate finite element solutions in the fully plastic range. *Computer methods in applied mechanics and engineering*, 4(2), 153-177.
76. Nguyen, N. T. (2008). *Modélisation du comportement des fondations profondes dans les argiles molles* (Doctoral dissertation, Laboratoire Sols, Solides, Structures-Risques ; IP Grenoble).
77. Nguyen, D. D. C., Kim, D. S., & Jo, S. B. (2013a). Settlement of piled rafts with different pile arrangement schemes via centrifuge tests. *Journal of Geotechnical and Geoenvironmental Engineering*, 139(10), 1690-1698.
78. Nguyen, D. D. C., Jo, S. B., & Kim, D. S. (2013b). Design method of piled-raft foundations under vertical load considering interaction effects. *Computers and Geotechnics*, 47, 16-27.
79. O'Neill, M. W., Hawkins, R. A., & Mahar, L. J. (1982). Load transfer mechanisms in piles and pile groups. *Journal of the Geotechnical Engineering Division*, 108(12), 1605-1623.
80. Park, D., & Lee, J. (2015). Comparative analysis of various interaction effects for piled rafts in sands using centrifuge tests. *Journal of Geotechnical and Geoenvironmental Engineering*, 141(1), 04014082.
81. Park, D., & Lee, J. (2015). Interaction effects on load-carrying behavior of piled rafts embedded in clay from centrifuge tests. *Canadian Geotechnical Journal*, 52(10), 1550-1561.
82. Park, D., Park, D., & Lee, J. (2016). Analyzing load response and load sharing behavior of piled rafts installed with driven piles in sands. *Computers and Geotechnics*, 78, 62-71.
83. Patil, J. D., Vasanvala, S. A., & Solanki, C. H. (2015). An experimental study on behaviour of piled raft foundation. *Indian Geotechnical Journal*, 46(1), 16-24.
84. Pells, P. J. N., & Turner, R. M. (1979). Elastic solutions for the design and analysis of rock-socketed piles. *Canadian Geotechnical Journal*, 16(3), 481-487.

References

85. Long, P. D. (1993). Footings with settlement-reducing piles in non-cohesive soil. Diss. University of Technology, Göteborg, Sweden.
86. Poulos, H. G. (1991). Analysis of piled strip foundations. In *International conference on computer methods and advances in geomechanics*. 7 (pp. 183-191).
87. Poulos, H. G. (1989). Pile behaviour—theory and application. *Geotechnique*, 39(3), 365-415.
88. Poulos, H. G., & Davis, E. H. (1980). *Pile foundation analysis and design*. Wiley, New York.
89. Poulos, H. G. (2001). Piled raft foundations: design and applications. *Geotechnique*, 51(2), 95-113.
90. Poulos, H. G. (2000). Practical design procedures for piled raft foundations. In *Design applications of raft foundations* (pp. 425-467). Thomas Telford Publishing.
91. Poulos, H. G. (1994). An approximate numerical analysis of pile–raft interaction. *International Journal for Numerical and Analytical Methods in Geomechanics*, 18(2), 73-92.
92. Poulos, H. G. (2016). Tall building foundations: design methods and applications. *Innovative Infrastructure Solutions*, 1(1), 1-51.
93. Poulos, H. G., & Bunce, G. (2008). Foundation design for the Burj Dubai—the world’s tallest building.
94. In: *Proceedings of 6th international conference on case histories in geotechnical engineering*, Arlington, VA, Paper 1.47, CD volume.
95. Poulos, H. G., Small, J. C., & Chow, H. (2011). Piled raft foundations for tall buildings. *Geotechnical Engineering Journal of the SEAGS & AGSSEA*, 42(2), 78-84.
96. Poulos, H. G., Small, J. C., & Chow, H. (2013). Foundation Design for High-Rise Tower in Karstic Ground. In *Foundation Engineering in the Face of Uncertainty: Honoring Fred H. Kulhawy* (pp. 720-731).
97. Poulos, H. G. (1993). Piled rafts in swelling or consolidating soils. *Journal of geotechnical engineering*, 119(2), 374-380.
98. Randolph, M. F. (1994). Design methods for pile groups and piled rafts. In *International conference on soil mechanics and foundation engineering* (pp. 61-82).

References

99. Randolph, M. F. (1983). Design of piled foundations. *Cambridge Univ. Eng. Dept., Res. Rep. Soils TR143*.
100. Randolph, M. F. (2003). Science and empiricism in pile foundation design. *Géotechnique*, 53(10), 847-875.
101. Reul, O., & Randolph, M. F. (2003). Piled rafts in overconsolidated clay: comparison of in situ measurements and numerical analyses. *Geotechnique*, 53(3), 301-315.
102. Reul, O. (2000). *In-situ-Messungen und numerische Studien zum Tragverhalten der kombinierten Pfahl-Plattengründung*. Inst. für Geotechnik.
103. Roscoe, K., & Burland, J. B. (1968). On the generalized stress-strain behaviour of wet clay. in *Engineering Plasticity*, J. Heyman and F. A. Leckie, Eds. Cambridge: Cambridge University Press, pp. 535-609.
104. Rose, A. V., Taylor, R. N., & El Naggar, M. H. (2013). Numerical modelling of perimeter pile groups in clay. *Canadian Geotechnical Journal*, 50(3), 250-258.
105. Russo, G. (1998). Numerical analysis of piled rafts. *International Journal for Numerical and Analytical Methods in Geomechanics*, 22(6), 477-493.
106. Russo, G., & Viggiani, C. (1998). Factors Controlling Soil-Structure Interaction for Piled Rafts. *Darmstadt Geotechnics, Darmstadt Univ. of Technology*, No. 4, 297-322.
107. Saffery, M. R., & Tate, A. P. K. (1961, July). Model tests on pile groups in a clay soil with particular reference to the behaviour of the group when it is loaded eccentrically. In *Proceedings of the Fifth Conference on Soil Mechanics and Foundation Engineering* (pp. 129-134).
108. Sales, M.M., Poulos, H.G., & Small, J.C. (2000). A New Approach for Analysis of Fully Mobilized Piles in Piled Rafts.
109. Sayed, S. M., & Bakeer, R. M. (1992). Efficiency formula for pile groups. *Journal of geotechnical engineering*, 118(2), 278-299.
110. Schofield, A., & Wroth, P. (1968). *Critical state soil mechanics*. McGraw-hill, London.
111. Seiler, J. F., & Keeney, W. D. (1944). The efficiency of piles in groups. *Wood Preserving News*, 22(11), 109-118.
112. Sheil, B. (2017). Numerical simulations of the reuse of piled raft foundations in clay. *Acta Geotechnica*, 12(5), 1047-1059.

References

113. Zeevaert, L. (1957). Compensated friction-pile foundation to reduce the settlement of buildings on the highly compressible volcanic clay of Mexico City. In *Proc. 4th Int. Conf. on SMFE* (Vol. 1, pp. 81-86).
114. Sinha, A. (2013). *3-D modeling of piled raft foundation* (Doctoral dissertation, Concordia University).
115. Sinha, J. (1997). *Piled raft foundations subjected to swelling and shrinking soils* (Doctoral dissertation, PhD Thesis, Univ. of Sydney, Australia).
116. Sinha, A., & Hanna, A. M. (2016). 3D numerical model for piled raft foundation. *International Journal of Geomechanics*, 17(2), 04016055.
117. Sönmez, N. (2013). *A study on design of Piled Raft Foundation Systems* (Master's thesis).
118. Ta, L. D. A., & Small, J. C. (1996). Analysis of piled raft systems in layered soil. *International Journal for Numerical and Analytical Methods in Geomechanics*, 20(1), 57-72.
119. Tradigo, F., Pisanò, F., Di Prisco, C., & Mussi, A. (2015). Non-linear soil–structure interaction in disconnected piled raft foundations. *Computers and Geotechnics*, 63, 121-134.
120. Van Impe, W.F., & Clerq, L. (1995). A Piled Raft Interaction Model. *Geotechnica*, No.73, 1-23.
121. Vermeer, P. A., & De Borst, R. (1984). Non-associated plasticity for soils, concrete and rock. *HERON*, 29 (3), 3-64.
122. Viggiani, C., Mandolini, A., & Russo, G. (2012). *Piles and piles foundations*. Taylor & Francis, London & New York.
123. Viggiani, C. (1998). Pile groups and piled rafts behaviour. In *Deep foundations on bored and auger piles BAP III* (pp. 77-91).
124. Whitaker, T. (1957). Experiments with model piles in groups. *Geotechnique*, 7(4), 147-167.
125. Wilkins, M. L. (1964). Fundamental methods in hydrodynamics. *Methods in Computational physics*, 3(1), 211-263.

References

126. Yamashita, K., Yamada, T., & Hamada, J. (2011). Investigation of settlement and load sharing on piled rafts by monitoring full-scale structures. *Soils and Foundations*, 51(3), 513-532.
127. Zhuang, G. M., & Lee, I. K. (1994). An elastic analysis of load distribution for raft-pile systems. *Finite elements in analysis and design*, 18(1-3), 259-272.

ANNEX

PRACTICAL ENGINEERING EXAMPLES (CASE STUDIES)

In the last decade, many high-rise buildings around the world are constructed which are supported by piled raft foundations in various soil profiles. Some of these tall buildings are briefly summarized in the following.

- **La Azteca building, Mexico**

This building exerted a total average load of approximately 118 kPa and was located on a soft and very deep clay which was also subjected to subsidence of the ground surface resulting from the extraction of groundwater. The case of the La Azteca building was described by Zeevaert (1957). The building was founded on a piled raft foundation, consisting of a 6 m deep excavation with a raft supported by 83 concrete piles of 0.4 m in diameter and 18 m in length. Figure A.1 shows the building of La Azteca.



Figure A.1 La Azteca building, Mexico (Poulos 2016)

Since the building was constructed before the development of numerical tools and computers, the challenges, in this case, were to design a foundation for a relatively tall building based on soft, very deep clay.

According to Poulos (2016), the measured settlements were about 20% lower than those calculated by Zeevaert (1957) but confirmed the predictions fairly well. Details of the piled raft foundation, soil profile, settlement calculated by Zeevaert (1957), and the measured settlement are shown in Figure A.2.

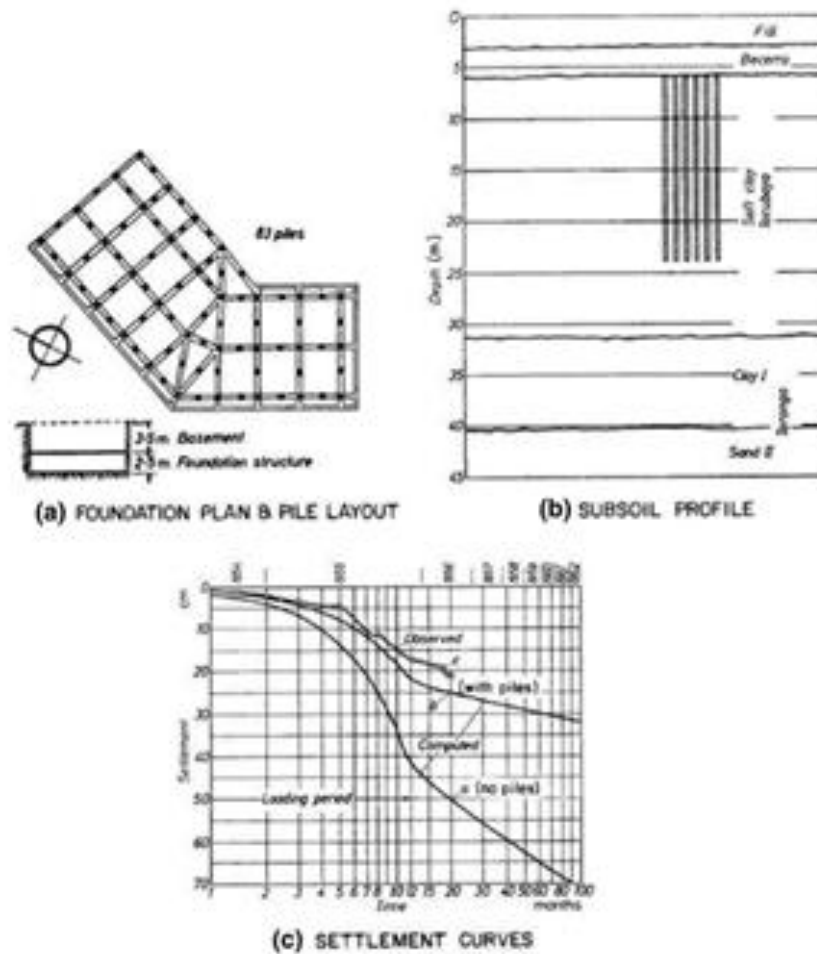


Figure A.2 Details of La Azteca foundation (Zeevaert 1957)

- **Burj Khalifa, Dubai**

The Burj Khalifa project consisted of a 160-story tower, with a podium development around the base of the tower, comprising a 4-6 story garage. Figure A.3 shows the Burj Khalifa building. The Burj Khalifa building is the tallest tower in the world with about 828 m. It is based on a 3.7 m thick raft supported by bored piles with 1.5 m in diameter and approximately

50 m in length. The Burj Khalifa is described in detail by Poulos and Bunce (2008), and/or Poulos (2016).

The main challenges, in this case, were to undertake an economic foundation design of the tallest building in the world, where the foundation conditions were relatively weak rocks and large wind loads had to be withstood (Poulos 2016).



Figure A.3 Burj Khalifa building (Poulos 2016)

A sensitivity analysis was performed by Poulos and Bunce (2008) using the finite element analysis model (ABAQUS) by applying the maximum nonlinear stress-strain relationships of soil strata. Figure A.4 shows the contours of the maximum axial load obtained from the numerical analysis. According to Poulos (2016), the maximum loads occur at the corners of the three 'wings' and were in the order of about 35 MN, while the minimum loads occur in the center of the group in the order of about 12- 13 MN.

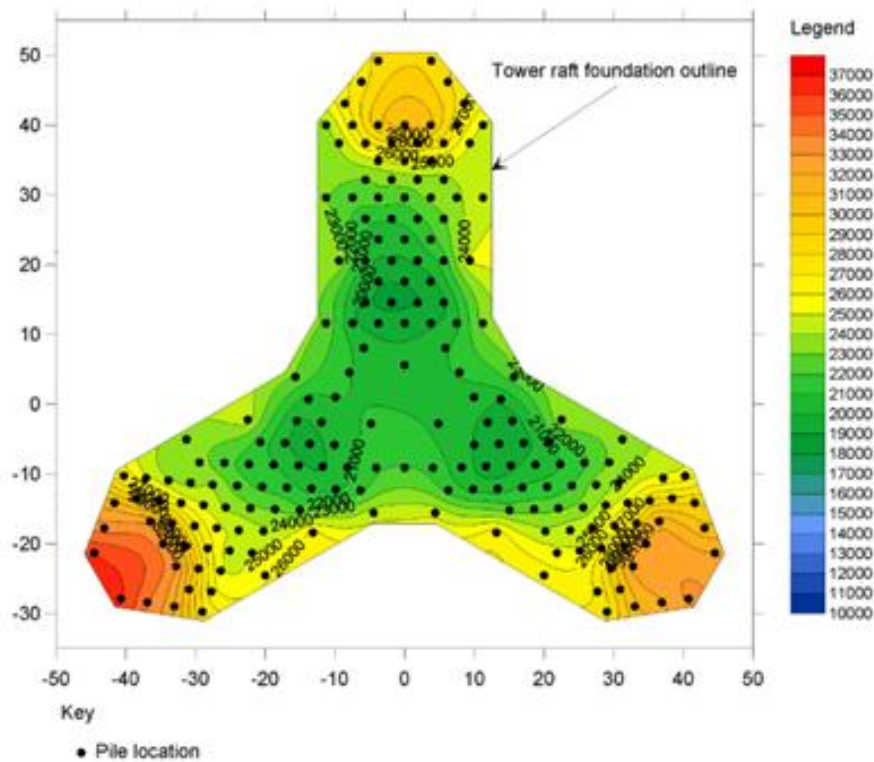


Figure A.4 Contours of the maximum axial load obtained from the numerical analysis
(Poulos 2016)

- **Incheon Tower, South Korea**

The Incheon building in Figure A.5 is described in detail by Badelow et al. (2009), Poulos et al. (2011) and Abdelrazaq et al. (2011). The 151-story Incheon tower, located on reclaimed land built on soft marine clay in Songdo, Korea. The piled raft foundation considered for the Incheon building comprises 172 bored piles with 2.5 m in diameter, indulged into the layer of soft rock and combined to a 5.5 m thick raft.



Figure A.5 Incheon tower, South Korea

The challenges, in this case, concern a very tall building, sensitive to differential settlement, and to be built on a site with very complex geological conditions. As reported by Poulos (2016), the number, arrangement, and size of piles were obtained from a series of experimental analyses through collaboration between the geotechnical engineer and the structural designer. The pile length was determined by the geotechnical engineer, taking into account the performance and capacity of the piles. Figure A.6 shows the plan view of the piled raft foundation.

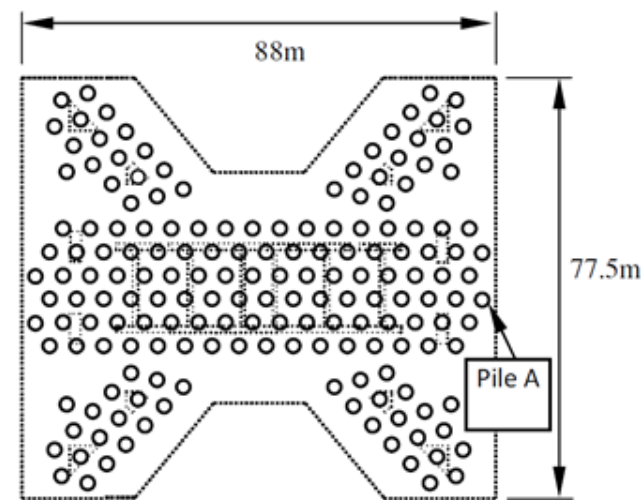


Figure A.6 Plan view of piles arrangement (Poulos et al. 2011)

- **Djeddah Tower , Saudi Arabia (Tower on karst limestone)**

Figure A.7 shows an architectural rendering of a high-rise project in Jeddah, Saudi Arabia, comprising a building over 390 m high. karstic conditions were found in certain areas of the site. The occurrence of cavities karstic in the ground can be followed by a decrease in the capacity of any piles in the group, thus setting up a raft can allow redistributing the load to the other piles in the group, and therefore a piled raft was considered for this building (Poulos 2016). The main challenges of this project were to assess whether the negative effects on the performance of the foundations of the limestone cavities would be within acceptable limits, or whether special treatment would be required to provide an adequate foundation system (Poulos et al. 2013; Poulos 2016).



Figure A.7 Architectural rendering of the Jeddah Tower, Saudi Arabia (Poulos 2016)

As reported by Poulos (2016), the piled raft foundation of the tower consisted of a 5.5 m thick raft, which was supported by 145 bored piles with 1.5 m in diameter. A pile length of about 40 m was assessed as necessary to support the declared service load of 22 MN per pile, based on a safety factor of approximately 2.4. Figure A.8 shows the plan view of the pile configuration.

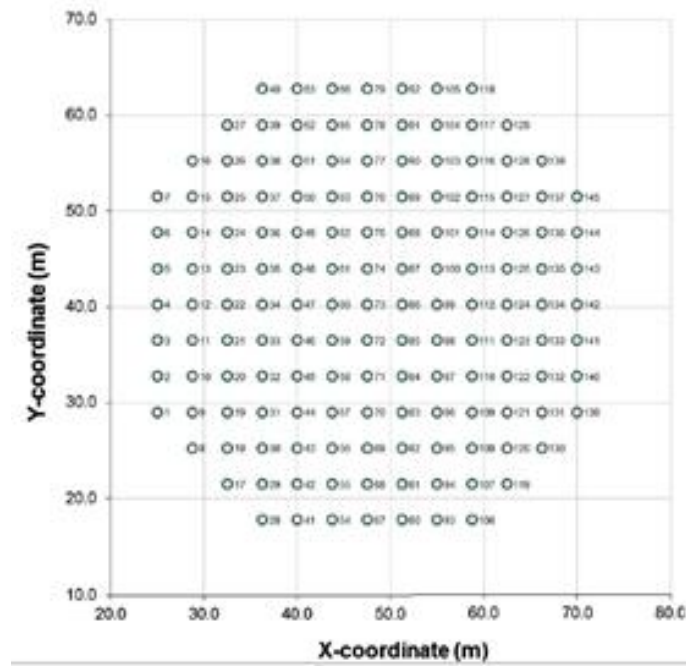


Figure A.8 Plan view of pile configuration (Poulos 2016)

- **Frankfurt Tower, Germany (Messeturm)**

The Messeturm tower of Frankfurt city in Germany is a tall building consisted of about 63 floors 257 m high. The Messeturm tower was built on piled raft foundation embedded in Frankfurt clay (Figure A.9). It is the second tallest building in Frankfurt, the second tallest building in Germany, and the third tallest building in the European Union. It was the tallest building in Europe from its achievement in 1991 until 1997 when it was overtaken by the Commerzbank Tower, also located in Frankfurt. The Messeturm tower foundation was a piled raft foundation consisted of a square raft of about 58.8 m in width, and a maximum thickness of 6 m in the centre, and a thickness of 3 m at the edges. The raft is located between 11 and 14 m below the ground surface, supported by 64 bored piles with a diameter of 1.3 m and a length of 34.9, 30.9, and 26.9 m in the inner, middle, and outer ring, respectively as shown in Figure A.10. More details on the Messeturm tower were reported in the research work of Katzenbach et al. (2000, 2005) and/or Reul (2000).



Figure A.9 Messeturm Tower of Frankfurt city, Germany (Katzenbach and Leppla 2015)

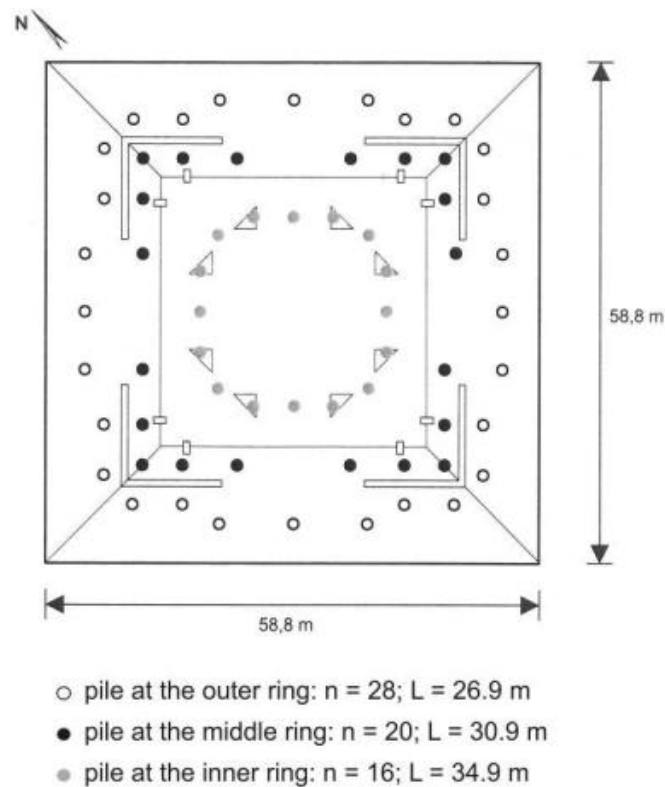


Figure A.10 Pile arrangement (Katzenbach et Leppla 2015)

According to Katzenbach et al. (2014), a pure piles foundation (a pile group) would have required 316 piles 30 m in length. Compared to the piled raft foundation of 64 piles and an

average length of about 30 m, a pile group foundation would have required more resources, e.g. concrete and energy, more time, and would require more than 3.9 million euros extra costs.

- **Mirax Plaza in Kyiv, Ukraine**

Figure A.11 presents a 3D architectural rendering of two buildings, each 192 m high (46 stories), as part of the Mirax Plaza project in Kyiv, Ukraine. The Mirax Plaza project is a shopping and amusement center and an underground car park, involving an area of about 294,000 m² cutting a natural slope of 30 m high. Figure A.12 illustrates a cross-section of the project. As reported by Katzenbach et al. (2013), the design of the foundation considers a piled raft foundation with 64 barrettes 33 m in length and a cross-section of 2.8 m × 0.8 m. The 3 m thick raft is located 10 m deep beneath the ground surface. The loads calculated on the barrettes were about 22.1 MN to 44.5 MN. The load on the outer barrettes was approximately 41.2 MN to 44.5 MN, which considerably exceeds the loads on the internal barrettes with a maximum value of about 30.7 MN. This behavior according to Katzenbach et al. (2013) is typical for a piled raft foundation.



Figure A.11 3D architectural rendering of Mirax Plaza in Kyiv, Ukraine

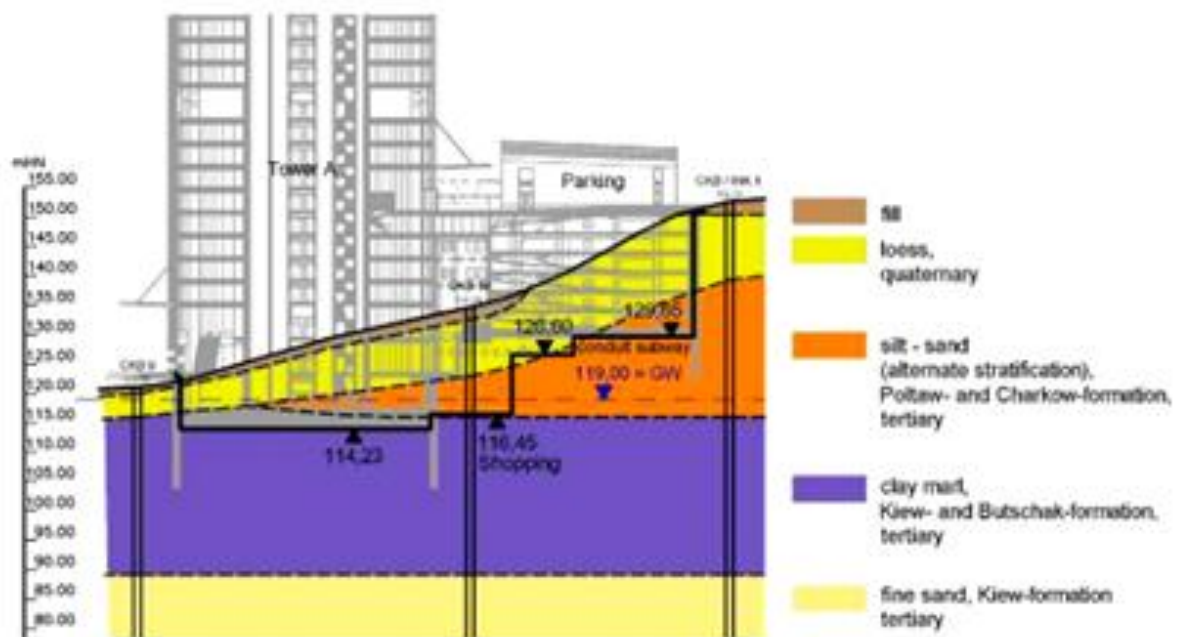


Figure A.12 Project cross-section (Katzenbach et al. 2013)

By using advanced optimization approaches and taking advantage of the benefits of the piled raft foundation, the number of barrettes could be reduced from 120 barrettes 40 m in length to 64 barrettes 33 m in length. Optimization of foundations results in a considerable reduction in the resources (construction materials, energy, etc.) and cost savings of around 3.3 million US dollars (Katzenbach et al. 2013).

- **Hyde Park Barracks, London**

The Hyde Park Barracks are in Knightsbridge in London center, on the southern edge of Hyde Park, and often were known as Knightsbridge Barracks. The building is 90 m high and has a two-story basement located 8.8 m below the ground surface. Figure A.13 presents the building of Hyde Park Barracks. The piled raft foundation is supported by 51 bored piles with a diameter of about 0.91 m and a length of about 24.8 m which are arranged symmetrically under a 1.5 m thick raft.



Figure A.13 Hyde Park Barracks building, London

Figure A.14 exposes the soil profile and the piles and raft properties as presented by Hooper (1973), as well as the pile configuration.

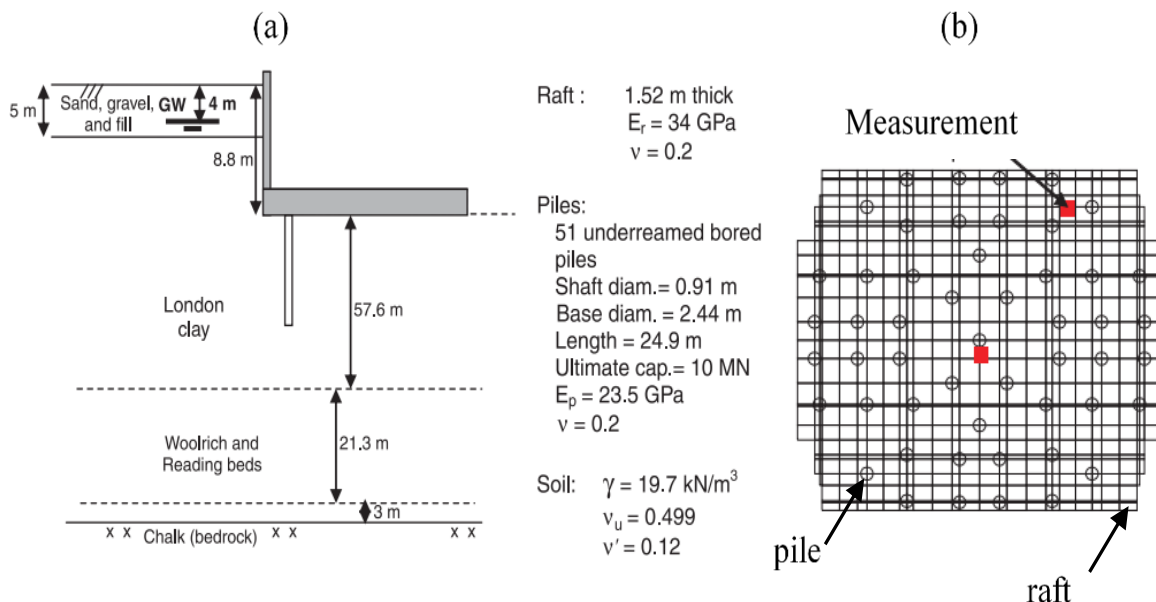


Figure A.14 Hyde Park Barracks Foundation Details (Hooper 1973)

• **Nineteen-story residential tower, Japan**

According to Yamashita et al. (2011), the geotechnical investigation of this project showed that the ground layer is composed of loose to medium sand of 63 m deep, underlain by a dense sand layer. Also, it was found that the water level was at a depth of 3 m from the ground surface. A piled raft foundation was suggested for this project to decrease total and differential settlements. The piled raft foundation consists of 28 bored piles 63 m in length. Figure A.15 presents the detail of the soil profile and foundation.

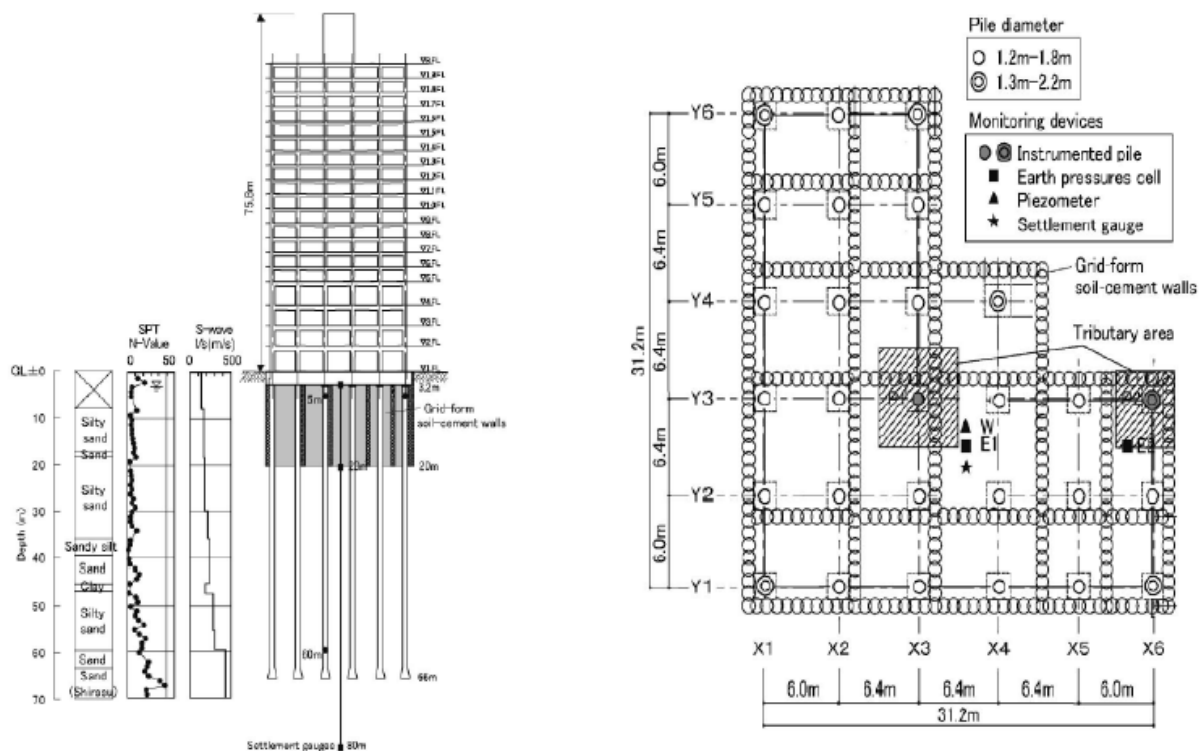


Figure A.15 Soil profile, foundation plan and elevation of nineteen-story residential tower (Yamashita et al. 2011)

• **Eleven-story building in Aichi Prefecture, Japan**

The building is 60.8 m in height, and located in Aichi Prefecture in Japan. Figure A.16 shows a schematic view of the building with the soil profile. The building occupies an area of 80 m by 43.5 m. The level of the foundation is mainly at a depth of 3.0 m, and partly at a depth of 3.6 m, from the ground surface. The water table appears about 17 m below the ground surface.

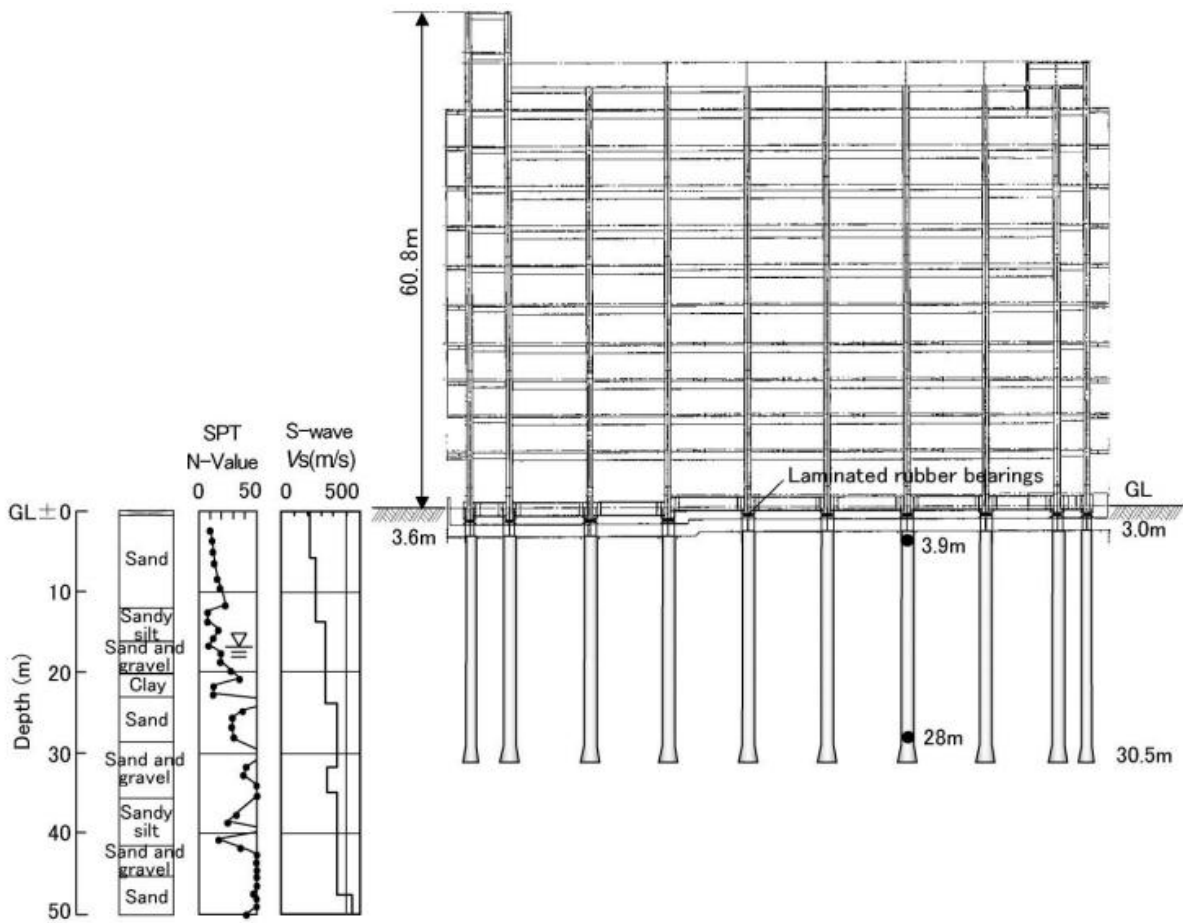


Figure A.16 Schematic view of the building with the soil profile (Yamashita et al. 2011)

In this project, a piled raft foundation of 40 piles was proposed to reduce the differential settlement of the raft to an acceptable level. The cast-in-place concrete piles are 27.5 m and 26.9 m in length. Various pile diameters were adopted varying with the depth. Figure A.17 illustrates the pile arrangement under the raft. More details are reported in the the research work of Yamashita et al. (2011).

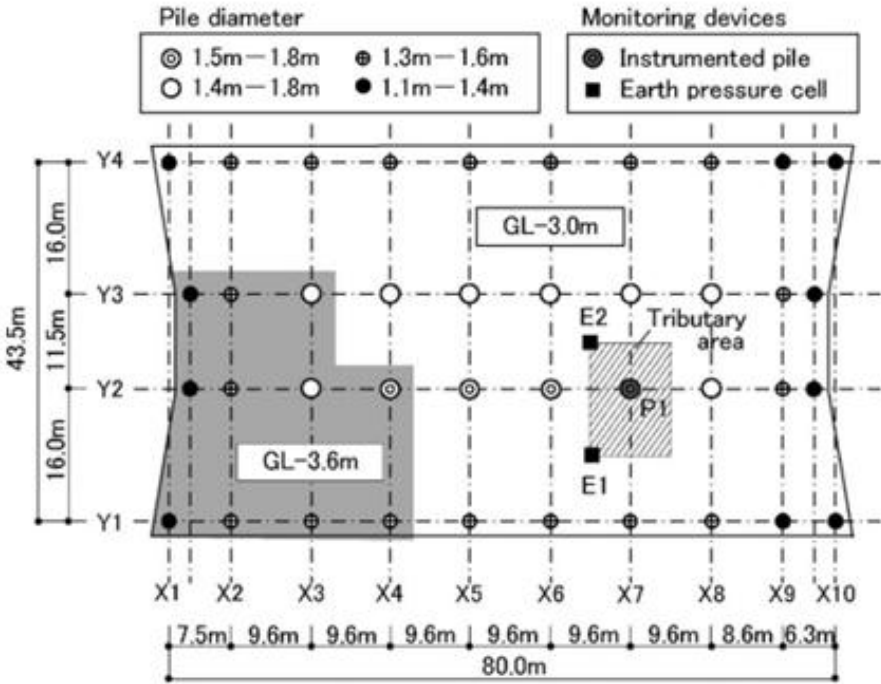


Figure A.17 Pile arrangement (Yamashita et al. 2011)

- **Osaka Hospital, Japan**

The hospital building is located in Osaka and consists of a thirteen-story high-rise section 51.3 m high above the ground surface and a four-story low-rise section. The building foundation level is at a depth of 6.4 m below the ground surface. The high-rise section is a steel-framed structure, and the low-rise section and the basement are reinforced concrete constructions. The hospital is built on an area of 55 m by 45 m. Figure A.18 shows a schematic view of the hospital construction. The hospital project is described in detail by Yamashita et al. (2011).

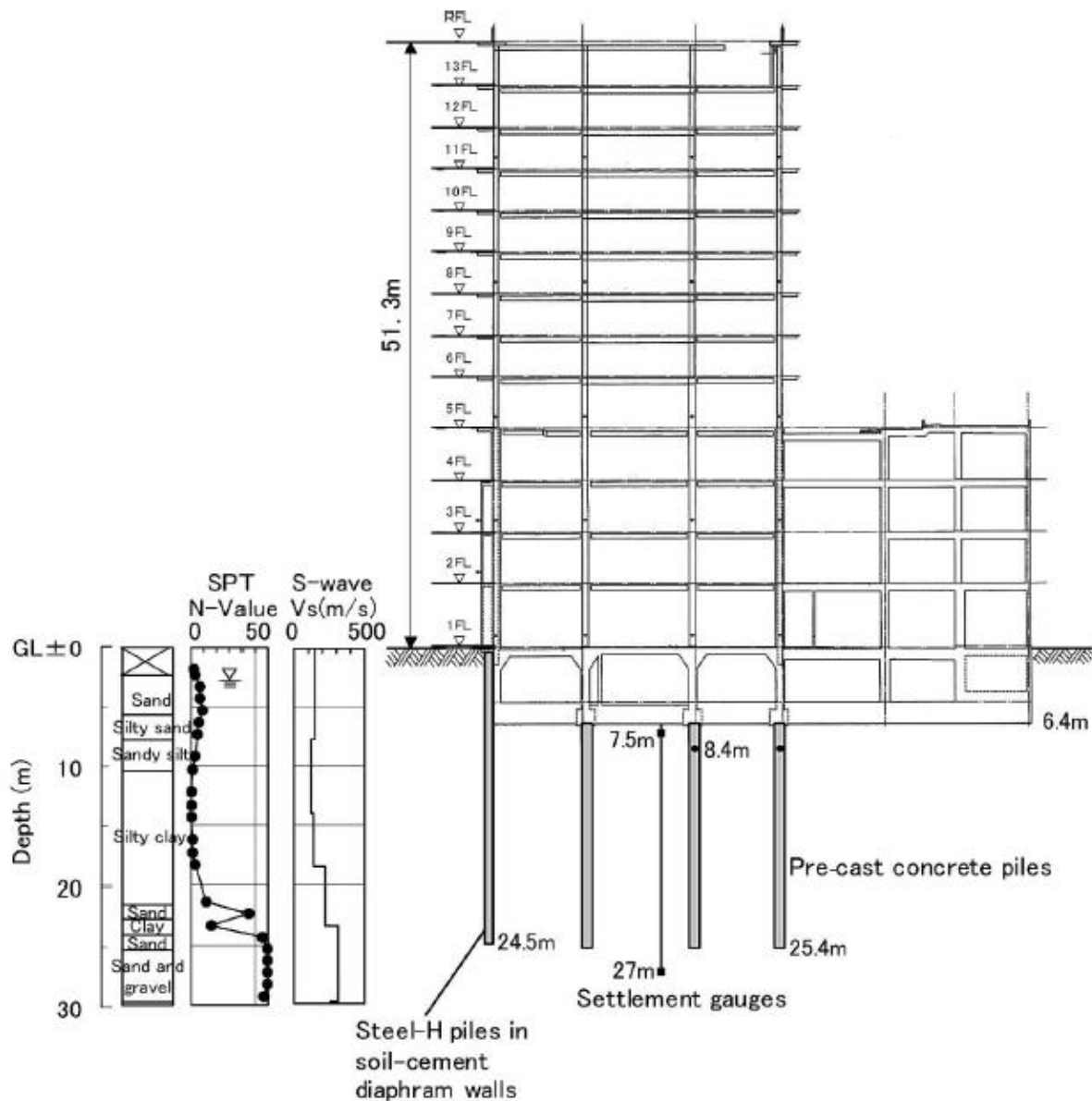


Figure A.18 Schematic view of the hospital construction with soil profile (Yamashita et al. 2011)

As reported by Yamashita et al. (2011), the average contact pressure on the raft was 196 kPa in the high section (13 stories) and 114 kPa in the low section (4 stories). Two foundation types were proposed for the hospital building, an unpiled raft and piled raft foundation in the low-rise section, and in the high-rise section, respectively. The piled raft foundation was proposed not to cause consolidation settlement and excessive differential settlement along with the interface between the high and low sections. Therefore, to reduce the consolidation and differential settlement, the proposed piled raft foundation is composed of 70 driven piles with a length of 19 m on the inside, and 198 H-steel piles built into diaphragm walls along the perimeter. Figure A.19 shows detail on the pile arrangement.

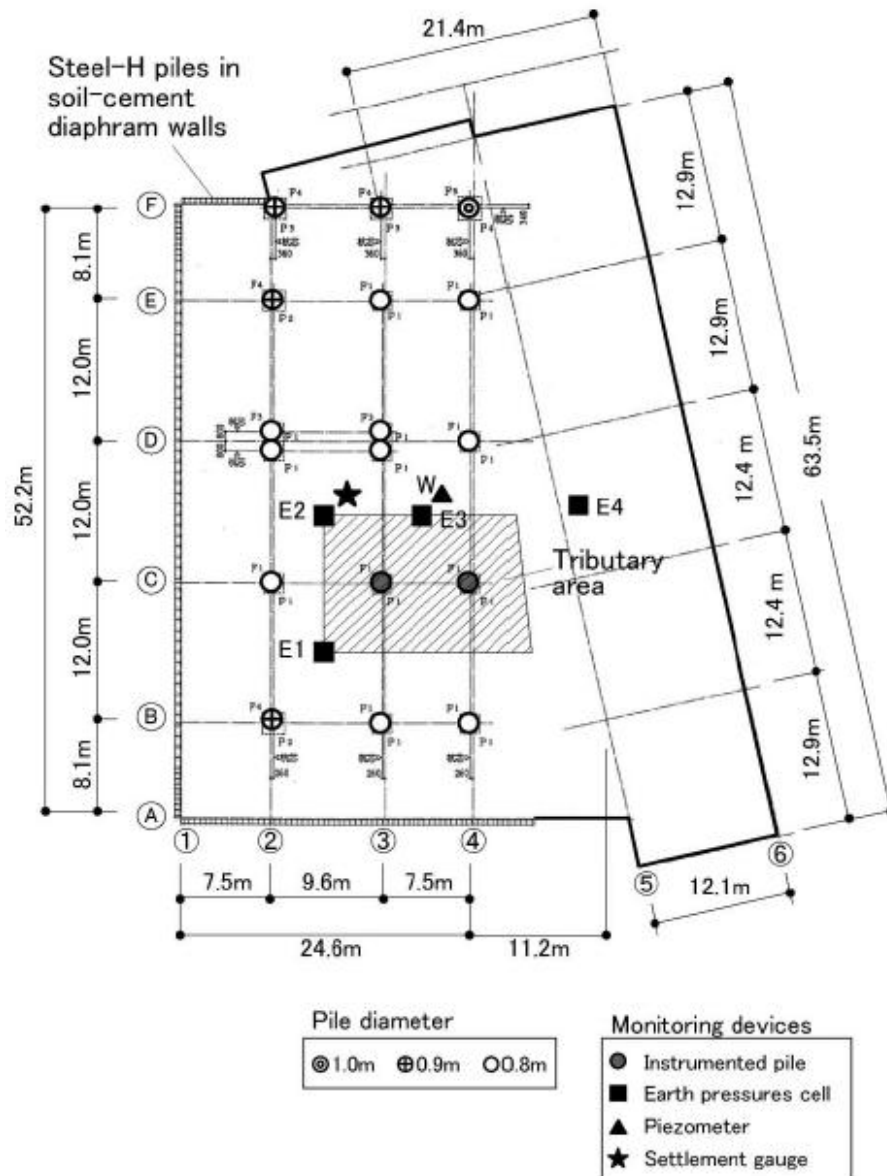


Figure A.19 Pile arrangement (Yamashita et al. 2011)

- **The forty-seven-story residential tower, Japan**

The 162 m high forty-seven-story residential tower is located in Nagoya, Aichi Prefecture. The building occupies an area of 50 m by 30 m. Figure A.20 (a) illustrates a schematic view of the building and the foundation with the soil profile. The building is a reinforced concrete structure with a base isolation system. The tower project is described in detail by Yamashita et al. (2011).

According to Yamashita et al. (2011), a piled raft foundation consists of a reinforced concrete raft, located 4.3 m below the ground surface, and 36 bored piles 50 m in length, is proposed. The foundation detail is shown schematically in Figure A.20(b).

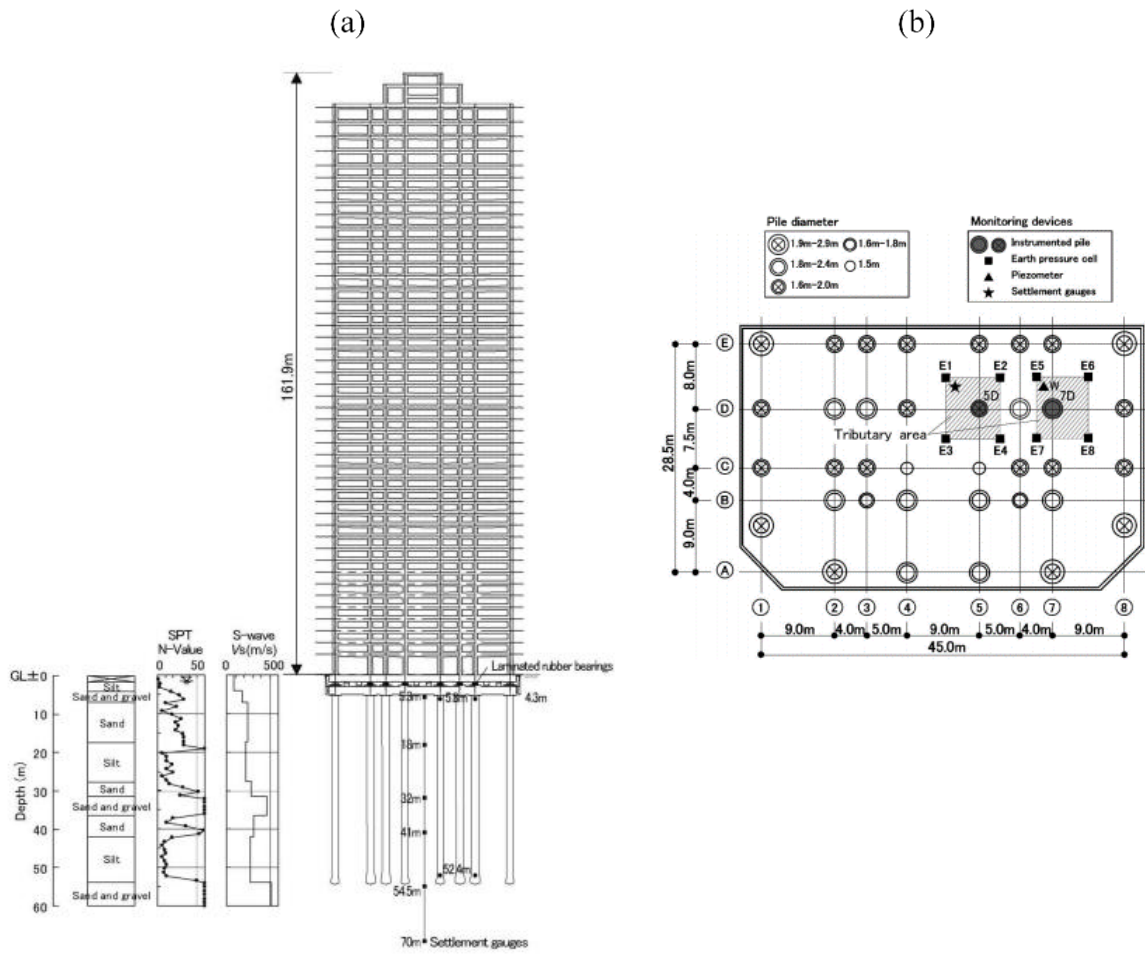


Figure A.20 Detail view of the building (a) Schematic view with soil profile (b) Pile arrangement (Yamashita et al. 2011)